Linear and H-Shaped Chiral Dimers for Applications in Photonic Liquid Crystals

Fiona Lucy Mackenzie

MSc by Research

Chemistry

December 2010

ACKNOWLEDGEMENTS

I am very grateful to Professor John Goodby for providing me with the opportunity to study for this MSc. I would like to express my sincerest appreciation towards him and thank him for his support throughout the project.

I wish to thank Dr. Stephen Cowling for his technical assistance and guidance during the year.

I would like to thank York Liquid Crystal Group, especially Edward Davis and Richard Mandle, for the discussions and advice on the synthetic problems.

I wish to express my appreciation to Professor John Goodby and the University of York for providing funding.

CONTENTS

1 ABSTRACT

The Optical Kerr effect in blue phases has recently been shown to be of practical use in fast switching display devices. This mode provides a linear response with respect to an applied electric field and thus grey-scale is possible. Fast responses are of prime interest in advanced display technologies for multiscreens and 3D displays. However, blue phases with wide temperature ranges of existence are almost unknown, and polymer stabilisation is used as the preferred option for creating room temperature blue phases, however, these are only kinetically stable. The objective of this study therefore was to seek new material design in the discovery of blue phase systems. The target design for exploration was dimers composed of two rod-like liquid crystal moieties that were either terminally or laterally attached to one another by aliphatic spacer units, in the belief that such systems would provide for low melting points.

Thus, two sets of chiral dimers were synthesized, using different length chiral spacers, in the attempt to produce blue phases. The linear dimers exhibited crystal B phases, while the H-shaped dimers exhibited low temperature chiral nematic phases. The odd-even effect was clearly observed in the transition temperatures for both dimers. Contact mixtures of the dimers in E7 showed induced chiral nematic phases with relatively short pitches, while pitch measurements and helical twisting power studies showed the helical twisting power values of both sets of dimers were much lower than needed in order to observe a blue phase.

2 INTRODUCTION

2.1 The Fourth State of Matter

Children are taught from an early age that there are three states of matter; solid, liquid and gas. They learn that solid objects are rigid and an atom or molecule in the structure is tightly bound to the neighbours surrounding it. Liquids flow to fill the shape of a container they are in and an atom or molecule in a liquid is relatively firmly bound but is free to move around. Gas atoms or molecules diffuse to fill the shape of the area they are in and are not bound together. The fourth state is always omitted from lessons. Liquid crystals, an intermediate stage between a liquid and a crystal solid, have the properties of both these states. The materials have some form of crystalline structure but the fluid properties of a liquid.

2.2 Introduction to Liquid Crystals

2.2.1 Liquid Crystal Systems

Molecules in a crystalline solid possess positional and orientational ordering, where their dynamic properties are restricted to oscillations and vibrations. Conversely, molecules in a liquid have a greater degree of freedom to move and rotate, and so have little positional or orientational ordering. The amount of positional and orientational ordering of molecules in a liquid crystal system is between that of a solid and a liquid [1], which is demonstrated in Figure 2.1. The orientation and position of the molecules, along with the defects formed in the system and the surface interactions gives each mesophase a characteristic optical texture when viewed through a polarised-optical microscope [1]. Polarising optical microscopy (POM) can be used to observe and identify the different liquid crystal phases.

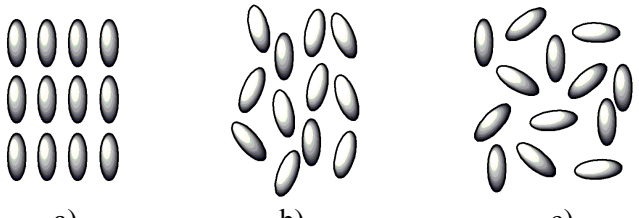

Figure 2.1: *Illustration showing the difference in positional and orientational ordering in* a) *a solid*; b) *a nematic liquid crystal*; c) *a liquid.*

The direction in which the molecules prefer to align is called the director and as a unit vector it is denoted by $\hat{n}$ [1]. In uniaxial nematic phases, the two possible horizontal vector directions are equivalent [2]. However, not all of the molecules present line up exactly with the director. The angle between the director and the position of the long molecular axis of a molecule, θ, determines the degree of orientational ordering in the system. If no orientational order is present, the order parameter S, used to describe the order of the system is 0. If all the molecules are orientated in exactly the same direction as the director and perfect orientational order is present, then S = 1 [1].

$$S = \left\langle \frac{3\cos^2\theta - 1}{2} \right\rangle \qquad \textbf{(Equation 2.1 [1, 2])}$$

Liquid crystals generally have order parameter values between 0.3 and 0.8. The order parameter is dependent on temperature. Usually, when the temperature of the liquid crystals is increased, S decreases [1, 2]. An illustration depicting the effect of temperature on S is shown in Figure 2.2.

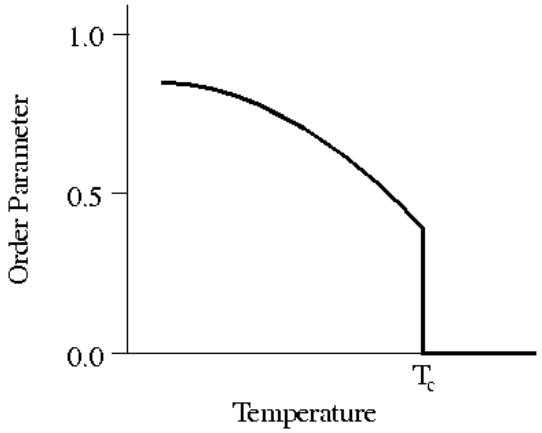

Figure 2.2: *Illustration showing the effect of temperature on the order parameter*, S *in a nematic liquid crystal* [3].

The simplest liquid crystal is the nematic phase, part of the calamitic liquid crystal group. The uniaxial molecules in the nematic phase have orientational ordering but no positional ordering [1], and possess a $D_{\infty h}$ symmetry [4]. Figure

2.3 shows the relationship between $\hat{n}$ and θ of the nematic phase. Calamitic liquid crystals with positional ordering are called smectic phases. The positional ordering of the molecules in a liquid crystal phase can be short range showing exponential decay or quasi-long range showing geometric decay [1, 2]. For example, in smectic/lamellar phases, the simplest way of looking at this is to assume the centres of mass of molecules are more likely to be in layers rather than between layers as you move in a direction parallel to the molecules. Smectic A and smectic C phases show such positioning. In both the short range and quasi-long range ordering, the orientation of the molecules in smectic phases can be tilted or orthogonal, with either a local hexagonal or rectangular packing matrix [1].

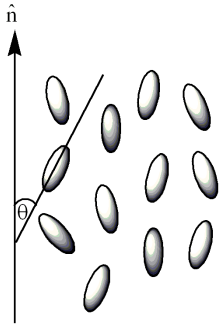

Figure 2.3: *Illustration showing molecules with orientational ordering with respect to the director,* $\hat{n}$*, in a nematic system.*

Not as commonly observed as the uniaxial nematic, is the biaxial nematic. Biaxial nematics have three optical axes, two of which are orthogonal [5], where the three directors are perpendicular to each other [6], with a D_{2h} symmetry [4]. The defects found in the biaxial nematic phase are similar to those in a chiral nematic phase [7]. Molecules that show biaxial nematic symmetry include bent-core molecules [5], an example of which is shown in Figure 2.4. Bent-core molecules are currently being investigated as compounds that may exhibit stabilized blue phases [4].

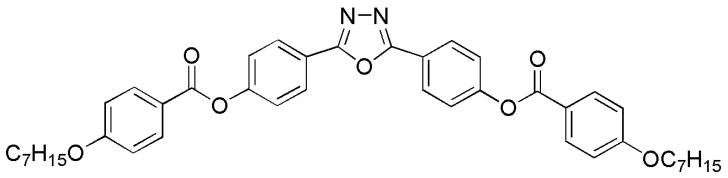

Figure 2.4: *Illustration showing a bent-core molecule* [4].

2.2.2 Classification of Liquid Crystals

There are three main groups of liquid crystals, thermotropic, lyotropic, and polymeric liquid crystals. Thermotropic liquid crystals are formed as a function of temperature. Liquid crystal phases are observed over certain defined temperature intervals. There are two types of thermotropic liquid crystals. The first are the calamitic liquid crystals, where the molecules have rod-like shapes with one molecular axis that is substantially longer than the other two axes. The second are the discotic liquid crystals, where the molecules have disc-like shapes with two of the molecular axes being much longer than the third axis [1].

Lyotropic liquid crystals are composed of a solid or thermotropic liquid crystal and a liquid (usually water) over a defined concentration and temperature range. Thus the molecular architectures of lyotropic liquid crystals generally have a hydrophilic head group attached to a hydrophobic tail. When these molecules are in water, the molecules can arrange into micelles, where the head groups form into a sphere, thereby forming a barrier between the tail groups and the water. If the lyotropic liquid crystals are surfactants, soaps or phospholipids, then when in water the solute molecules can form a bilayer organisation. In this instance, a lamellar structure forms, where the polar head groups form into back-to-back layers with their head in the water and the tails situated in between. When these molecules are placed in a non-polar solvent, reversed phases occur, with the hydrophilic head groups oriented towards the centre of the bilayer structure with the hydrophilic tails arranged on the outside [1].

Polymer liquid crystals effectively come in two types. Main chain polymers have rigid, so-called “mesogenic” units with flexible, hydrocarbon chains between. Liquid crystal positional and orientational ordering can be seen in the rigid units at certain temperatures. Side chain polymers on-the-other-hand have a flexible,

hydrocarbon backbone, onto which short hydrocarbon chains carrying "mesogenic units" are attached [1]. Illustrations of the different liquid crystal types can be seen in Figure 2.5.

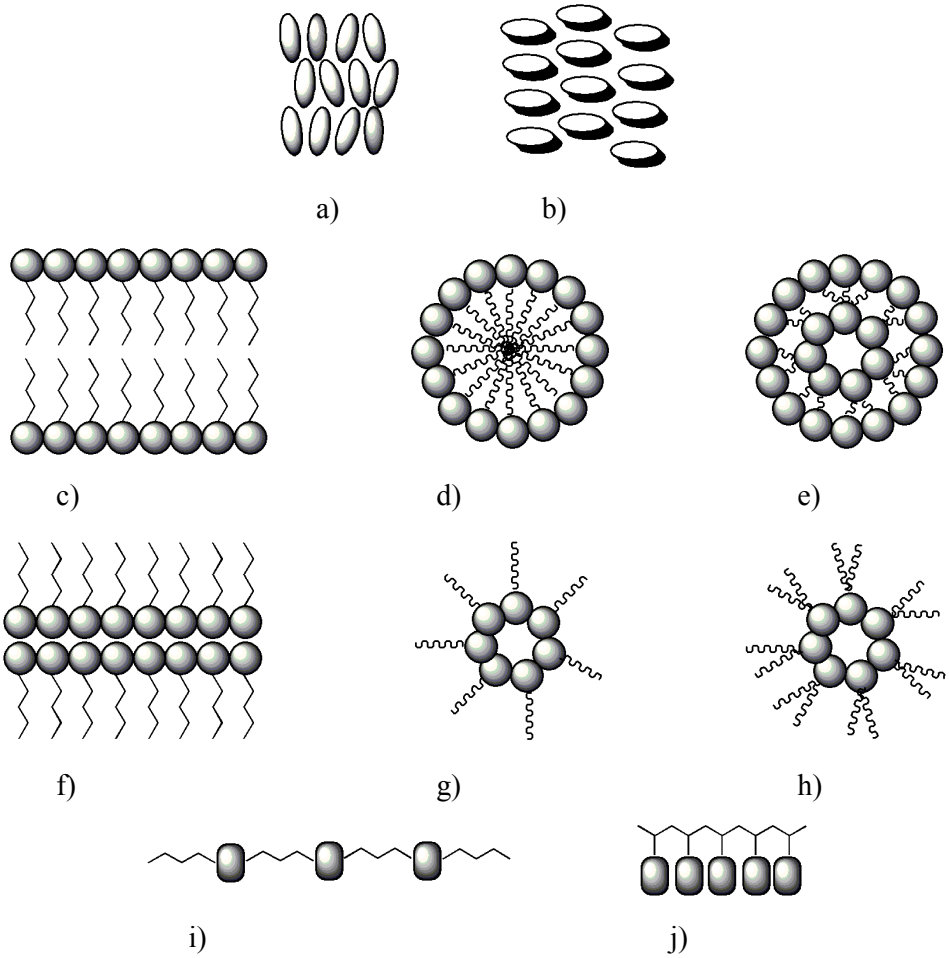

Figure 2.5: *Illustration showing the different types of liquid crystals*: a) *calamitic liquid crystals*; b) *discotic liquid crystals*; c) - e) *lyotropic liquid crystals*; f) - h) *revered phase lyotropic liquid crystals*; i) *main chain polymer*; j) *side chain polymer.*

2.2.3 Structure of Calamitic Liquid Crystals

Calamitic liquid crystal molecules can be thought of as being composed of sections. The choice of moieties in each section must be carefully considered with regard to the desired phase transitions and properties, such as dielectric anisotropy. The core ring system provides the structure with the rigidity needed for alignment and lateral interactions of the molecules The core is usually a

derivative of a two- or three-ring aromatic system but sometimes *trans*-1,4-cyclohexane rings are included. The linear zigzag shape of the *trans* conformation of the cyclohexane allows for efficient packing of the molecules. The c*is*-1,4-cyclohexane, on the other hand, has a bent conformation, which prevents efficient molecular packing thereby suppressing mesophase formation [1].

Terminal groups in liquid crystals are generally either small polar groups or saturated alkane chains. Polar groups, such as a cyano group, stabilize the orientation of the molecules through dipole-dipole interactions, which can be used under certain circumstances to stabilize nematic phases or to produce smectic phases with a stabilized lamellar arrangement [1]. The cyano group coupled to an aromatic ring produces a positive dielectric anisotropy for use in displays, such as the twisted nematic display [8]. Alkyl chains introduce flexibility into a rigid compound, reducing the melting point of a compound and stabilising the liquid crystal phases. Short hydrocarbon chains are found to produce nematic phase liquid crystals with high birefringence, while long hydrocarbon chains stabilize the smetic phase and give lower birefringence. If the flexibility of the molecule becomes too great by using very long terminal chains, the compound will become highly viscous due to the steric hindrance arising from the flexibility of chains. As a result the packing of the molecules will be disrupted, suppressing the liquid crystallinity of the compound [1].

Chirality also can be introduced into a liquid crystal system by having a branched alkyl chain. Branched chains interfere with the packing of the molecules in the system. The disruption causes liquid crystal phase instability and reduces the melting point of the compounds [1].

The effect of alkoxy groups on the system depends on the type of ring it is attached to. Next to an alicyclic ring the alkoxy group causes liquid crystal phase instabilities, but next to an aromatic ring the alkoxy the stabilizes the phases.

The presence of lateral substituents, such as fluorine, attached to the core can lead to a high negative dielectric anisotropy due to the dipole being perpendicular to the long axis of the molecule. Increasing the size of the lateral substituent however, could cause a decrease in (T_{N-I}) due to lateral repulsions. Conversely, if the lateral substituent is polar then the smetic phase can be stabilized [1].

Linking groups, such as an ester, join terminal groups to the core or connect different parts of the core together to aid synthesis or extend the length of the molecule. Linking groups must maintain the linearity of the molecule and must not separate areas of polarisibility. The ester linking group can be used to produce low melting points [1].

2.3 Chirality

Chirality is the non-superimposition of a compound onto its mirror image. Largely observed in nature, especially in amino acids, chirality is frequently seen in organic chemistry. Chiral molecules are generally four different ligands surrounding a carbon atom in a tetragonal shape. The non-superimposable molecules are enantiomers, and differentiated with the prefixes of (*S*)- and (*R*)- (Figure 2.6).

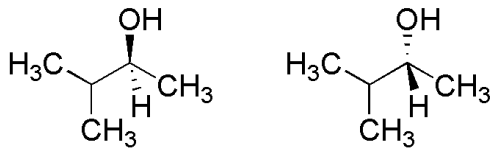

(a) (b)

Figure 2.6: *Illustration showing the non-superimposable enantiomers of 3-methyl butan-2-ol, where* (a) *is the (S)- enantiomer;* (b) *is the (R)- enantiomer.*

2.3.1 Chiral Systems

There are three ways in which chirality can be introduced into a self-organizing system. The most common method used in organic chemistry is through the inclusion of chiral moieties during the synthesis of a material. The second method involves doping achiral host compounds with chiral materials. The last, and not as common in liquid crystals, is through hydrogen bonding [9].

In a chiral system the incorporation of asymmetric molecules induces the formation of a helical structure. The director ($\hat{n}$) thus undergoes a small, slow rotation about an axis perpendicular to the director thereby forming a helix (Figure 2.7). The system possesses a helical twist direction, which depends on the absolute spatial configuration of enantiomer that is incorporated.

In the chiral nematic mesophases there is a temperature-dependency on the pitch, increasing the temperature makes the pitch tighter due to the increased fluctuations of the molecules. At higher temperatures, the molecules have more thermal energy than at lower temperatures, and the change in angle of the director is greater [1]. The pitch also differs between materials. Some materials give long helical pitches, while others give short pitch lengths [1].

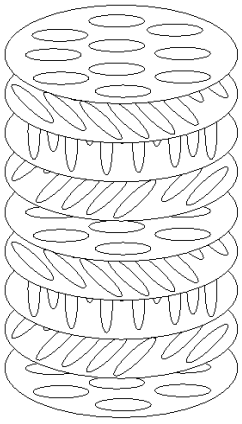

Figure 2.7: *Helical structure formed by chiral molecules*

2.4.2 Chiral Nematic Phase

The chiral nematic phase has local ordering that is similar to the nematic phase, where the molecules only have orientational ordering [1, 10]. The helices that form due to the asymmetry of the molecules then form a single twist along an axis perpendicular to the director. [1]. The helical structure can be oriented in three different ways, leading to three distinct defect textures. In the planar arrangement the helices are perpendicular to the surface, resulting in a texture that is described as the oily streak texture; in the polygonal defect texture the helices are parallel to the surface of the substrate, resulting in a finger print

texture; and the third texture is based on a focal conic arrangement where the helices parody the structure of the focal conic texture of the smectic A phase in that they radiate spherically from singularities [11].

2.4.3 Frustrated Chiral Liquid Crystal Phases

Frustrated liquid crystals phases occur when the local interactions of the molecules try to orient in a certain way, but they cannot maintain the orientation throughout the system because the bulk structure is dominant [1]. The most well known of the frustrated phases is the blue phase [12], which was first observed by Reinitzer in 1888 when he examined cholesteryl benzoate [13, 14] and later named by Coates and Gray in 1973 [13]. Another less well-known frustrated phase is the twist grain boundary phase (TGB phase) where the local twist competes with the formation of a bulk lamellar structure. Thus, in the TGB phase there is competition between the desire for the molecules for form a lamellar structure and the desire to form a helical structure. The molecules form in layers and blocks of the smectic A phase rotate with respect to each other and are separated by periodic screw disclinations that cause the director of each block to twist forming a quasi-helix [1].

2.4 Blue Phases Liquid Crystals

Blue phases are usually formed by chiral nematic liquid crystals of short pitch [15], and observed over a narrow temperature range [16, 17, 18] between the isotropic liquid and chiral nematic phase [12]. The blue phase has also been observed in conjunction with the smetic A phase [12]. Blue phases form in a similar way to the chiral nematic phase. The asymmetry of the molecules and their packing together leads to the formation of a helical structure. The helices can form along two axes that are perpendicular to one-another. This is known as double twist. However, it is not energetically favourable for more than two twists to form at once because they lead to a frustration in the molecular packing. As a consequence, the double twists align into cylindrical structures, which then form a frustrated three-dimensional cubic structure. It is not possible for the double twist cylinders to fill a three dimensional structure uniformly, where all the directors are the same and so disclinations form (Figure 2.8) in a highly frustrated structure [1, 4, 7 9, 12 and 15], stabilizing the structure [12, 15]. When

the periodicity of the defects is similar to the wavelength of visible light [19] selective reflection occurs [4, 20], thereby producing the colours and textures observed by polarised optical microscopy.

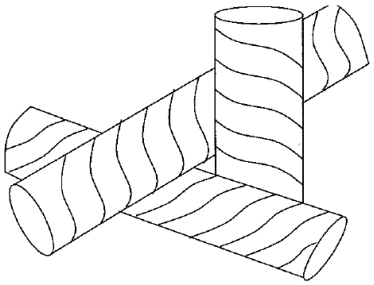

Figure 2.8: *Illustration showing the three double twist cylinders with a disclination at the core* [10].

There are three forms of blue phases, which are known as BP I, BP II and BP III [7, 21], where BP III is the higher temperature form. BP I has a body-centred cubic structure with an O_8 symmetry [15, 19, 20]. BP II has just a cubic structure with an O_2 symmetry [7, 21, 22]. The structure of BP III, which is sometimes called the 'Fog Phase', is not as well known, but it is believed it has a similar symmetry as the isotropic liquid, with arbitrary orientation [7, 21, 22]. BPI and II show platelet textures, while BPIII shows a cloudy texture. Figure 2.9 shows the structures and defect textures of BP I and BP II, and the texture of BP III.

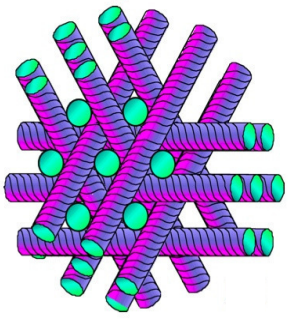

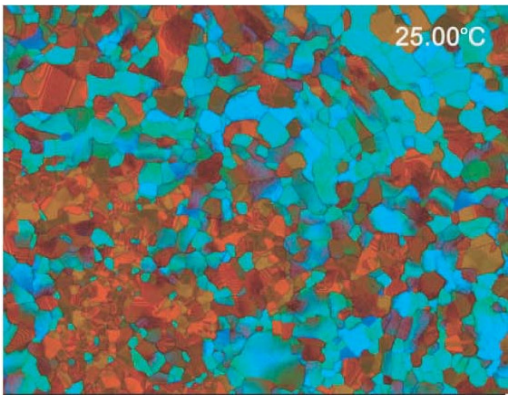

(a)

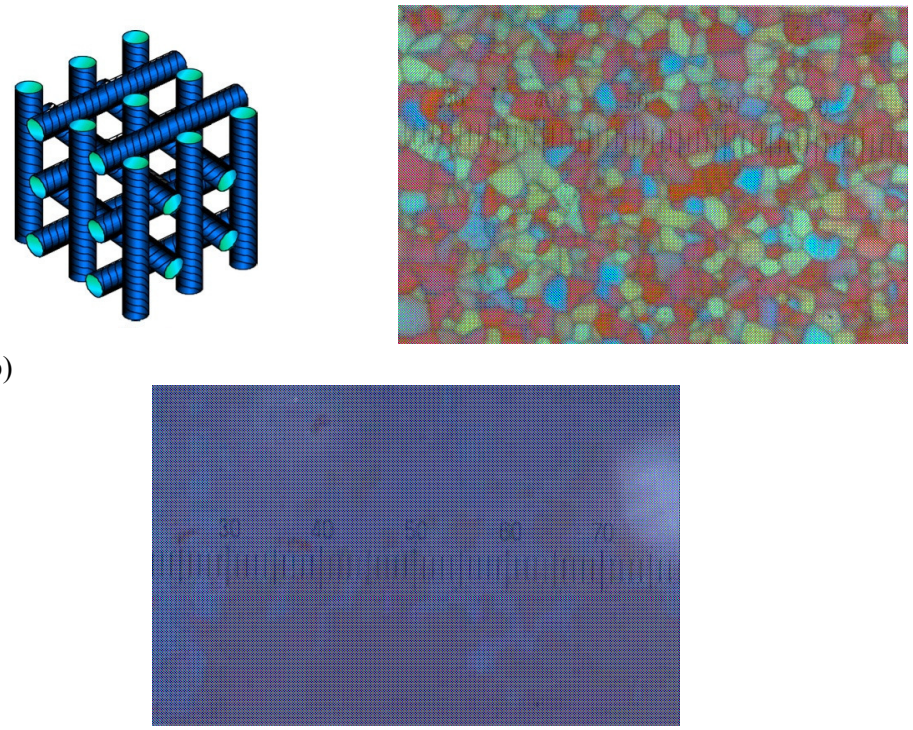

(b)

(c)

Figure 2.9: *The structures and textures of* (a) *BPI;* (b) *BPII* [10]; (c) *BPIII* [10];

Under an applied electric field, the blue phases can undergo three transformations. These are caused by a local reorientation of molecules; a distortion of the lattice, also known as electrorestriction; and phase transitions to lower symmetry phases [4, 23].

2.5 Optical Display Devices and the Use of Blue Phase Compounds

Liquid crystals are extensively used in display devices, such as calculators and television displays [8]. Optical displays generally consist of the components shown in Figure 2.10, the orientation of the liquid crystal is dependent on the type of liquid crystal device. There are different modes of operation for display devices such as twisted nematic, TN (mainly calculators and watches), in-plane switching, IPS (Samsung televisions) and vertically aligned nematic, VAN (television). The TN and IPS devices require the liquid crystal to possess positive dielectric anisotropy while the liquid crystal is required to possess negative dielectric anisotropy for the VAN display. Two glass substrates, generally coated with indium-tin oxide to act as a transparent electrode, are covered with a

polymeric alignment layer. The alignment layer encourages the liquid crystal molecules between the glass substrates to align in a preferred orientation. On the outer side of the glass substrates are the polarisers. The polarisers are usually arranged perpendicular to each other. Across the two substrates an electric field is applied [8].

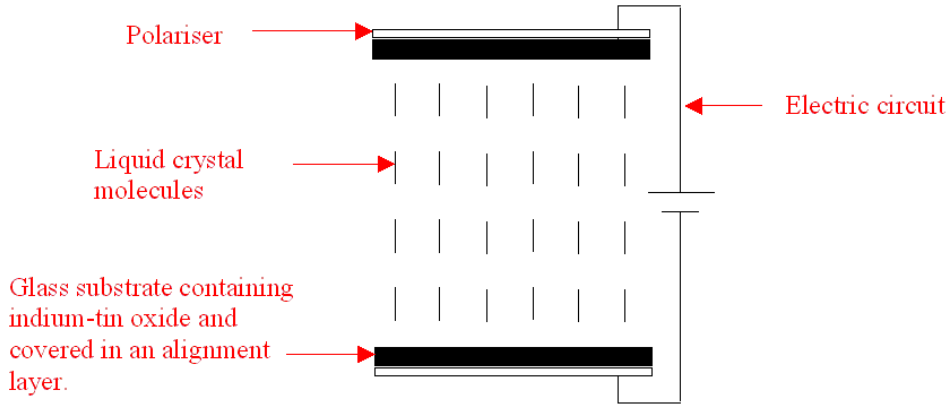

Figure 2.10: *Illustration showing the component parts of a liquid crystal display.*

The dielectric anisotropy of liquid crystals is vital for their use in displays. Each liquid crystal phase has a degree of relative permittivities due to the polarity and polarisibility parallel to the director ($\varepsilon_{\parallel}$), and perpendicular to the director ($\varepsilon_{\perp}$). The difference between $\varepsilon_{\parallel}$ and $\varepsilon_{\perp}$ gives the dielectric anisotropy ($\Delta\varepsilon$) of the system. The equation for dielectric anisotropy is shown in Equation 2.2 [1].

$$\Delta\varepsilon = \varepsilon_{\parallel} - \varepsilon_{\perp} \qquad \textbf{Equation 2.2.} [1]$$

Depending on the structure of the molecule, the dielectric anisotropy can either be positive or negative. Materials with strongly polar terminal groups have a greater $\varepsilon_{\parallel}$ than $\varepsilon_{\perp}$ and so will have a positive dielectric anisotropy. Materials with polar lateral groups have a greater $\varepsilon_{\perp}$ than $\varepsilon_{\parallel}$ and so will possess a negative dielectric anisotropy [1, 24]. Examples of compounds with positive and negative dielectric anisotropy can be seen in Figure 2.11.

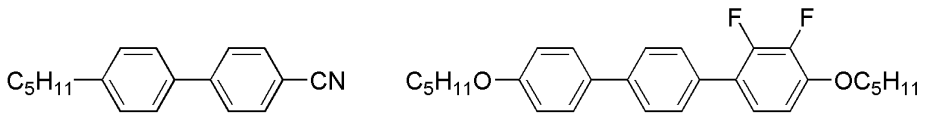

(a) (b)

Figure 2.11: *Illustration showing* (a) *a material with positive dielectric anisotropy* (b) *a material with negative dielectric anisotropy.*

Whether materials with positive or negative dielectric anisotropy are used in a display device depends on the type of device. Table 2.1 shows a selection of display modes using nematic liquid crystals, and the dielectric anisotropy required for device operation.

Display	Dielectric Anisotropy ($\Delta\varepsilon$)
Twisted Nematic	Positive
Vertically Aligned Nematic	Negative
In-Plane Switching	Positive
Polymer Dispersed Liquid Crystal	Either

Table 2.1: *The dielectric anisotropy of a number of display modes* [8]

The molecules in a display align in such a way that the greatest dipole, and hence induced polarisibility, is parallel to the electrodes. An electric field is then applied, causing the molecules to switch orientation. Taking vertically aligned nematic (VAN) displays as an example, the liquid crystal molecules used are those that have a value of $\varepsilon_{\perp}$ that is larger than $\varepsilon_{\parallel}$. In the device the molecules align so that the dipole/polarisibility representing $\varepsilon_{\perp}$ is parallel to the electrodes and the director of the molecules is perpendicular to the electrodes. Applying an electrical field across the electrodes causes the molecules to switch so that they are parallel to the electric field, and when the field is switched-off they realign to become perpendicular to the electrodes [8] (see Figure 2.12). Typically in nematic display devices the switching time for the molecules is in the order of 10s milliseconds for the on time while the off-time is dictated by the elastic constants of the liquid crystal and as such it is generally slow at 30-50 milliseconds. These switching times limit the nematic display device for high speed display applications and can cause for image blur to occur in displays.

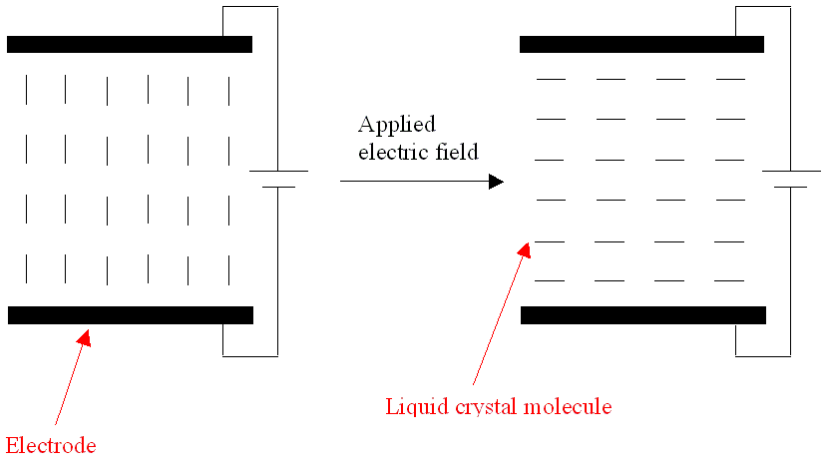

Figure 2.12: *Illustration showing the alignment of molecules in VAN display.*

The blue phase has many advantages over the nematic phase for use in displays [25, 26, 27]. Due to the optically isotropic three-dimensional cubic structure there is no need for the aligning or switching of the molecules to obtained a desired orientation [19 and 26, 27]. Due to the Bragg reflection of visible light, blue phases reflect light and there is no need for coloured filters [24]. There is growing interest in using BP liquid crystals in applications such as display technologies. The appeal of the blue phases is the isotropic cubic structure and the three-dimensional self-assembled photonic band-gaps and electrically controllable Bragg diffraction of visible light [21], which makes blue phase LCs additionally suitable for applications in optical devices [28], tunable photonic crystals [17, 29, 30, 31] and fast light modulators [17, 29].

2.6 Research into Stabilizing Blue Phase Liquid Crystals

The narrow 1 $^{\circ}$C temperature range of the blue phase [16, 17, 18] limits its uses in application considerably [18, 32]. In order to make use of the blue phase, methods in which the phase could be stabilized and the temperature range increased are currently being reviewed.

2.6.1 Polymer Stabilized Liquid Crystals

The earliest attempt at increasing the temperature range was through polymer stabilization [21, 33]. The method generally involves a cross-linking polymer

network dispersed in a liquid crystal in order to stabilize the desired orientation of the liquid crystal directors [21, 33].

H.-S. Kitzerow *et. al.* attained a stable blue phase through polymer stabilization by the photopolymerization of diacrylates, which led to the formation of cross-linked polymers [34]. A chiral diacrylate and non-chiral diacrylate [34], all based on C6M derivatives (commercial diacrylate prepared by Philips Research Laboratories) [35] were synthesized. Binary mixtures of the chiral diacrylate and a non-chiral diacrylate exhibited blue phases. The microscope studies showed that the blue phases (BPI, BPII, BPIII) appeared close to the clearing point and only for a very short temperature range. It was discovered that the clearing point temperature had a linear relationship with concentration, where concentration was the ratio of chiral diacrylate to non-chiral diacrylate. From this, the concentrations were estimated which would lead to the appearance of blue phases. A photoinitiator, α, α-dimethoxydeoxybenzoin, was subsequently added to the mixtures, and the mixtures then subjected to UV light from a high pressure mercury lamp for a short amount of time, where the light intensity was around 10 mW cm^{-2} at 366 nm, and the temperature was kept constant. This caused the diacrylates to polymerize. The blue phases present before polymerization were also present after polymerization. When the heat source was removed from the polyacrylates, the blue phases did not disappear. The polymerization of the diacrylates caused polymer networks to form, while a blue phase was occurring. The networks stabilized the phase and allowed it to be stable at room temperature.

Conversely, non-conventional polymer stabilization was carried out by Kukuchi *et. al.* [21]. Coexistence between the polymer and an equilibrium phase resulted in thermodynamic stability. In order to produce the liquid crystal-polymer composites a 1:1 molar ratio of two liquid crystals, JC-1041XX and 5CB, were mixed with a chiral dopant to induce a blue phase, a diacrylate monomer, acrylate monomers and a photo-initiator. The acrylate monomers used were varied in proportion to produce a number of different mixtures. The *in situ* photopolymerization was achieved using a metal halide light source that irradiated UV light of 1.5 mW cm^{-2} at 365 nm. The temperature of the composite

mixture was subjected to during the initial polymerisation was at a range where a blue phase would be expected to appear. When the acrylate monomer EHA was used in the mixture, the blue phase that was observed possessed a temperature range that lasted for over 66 °C. In order to achieve this range, between 3.99 mol % and 6.81 mol % of EHA was used. Figure 2.13 shows the texture of the blue phase observed in a mixture of 3.99 mol % EHA. Less than 3.99 mol % stabilized the blue phase over a range of less than 10 °C. The monomer TMHA also successfully increased the blue phase temperature range to over 66.0 °C. However, the monomers HA and 6CBA did not increase the temperature range by any more the 1 °C. It is understood that the branched side groups that are present in EHA and TMHA but not HA are the reason for BP stabilization. 6CBA is a mesogenic monomer, and when poly(6CBA) is mixed with the blue phase induced liquid crystal mixture, the polymer becomes homogenously dispersed in a blue phase region, and as a result cannot stabilize the phase. The dispersion does not occur with respect to poly(EHA) and poly(TMHA) as these two acrylates have a lower miscibility in liquid crystals than poly(6CBA). It was noted that the Bragg reflection of the liquid crystal did not change upon polymerization. As a result it was thought that the lattice structure of the blue phase was not destroyed during polymerization and the polymer chains formed random coils along the disclination lines of the liquid crystal structure. This was expected to lead to the blue phase being more thermodynamically stable at a lower temperature below the transition temperature from isotropic liquid to blue phase, than is usually seen. It seems that the polymer chains stabilized the disclination lines [21], which usually have detrimental affects on the stability of the cubic structure. The electro-optical performance response times of the 3.99 mol % EHA composite was found to be 100 μs at room temperature [21].

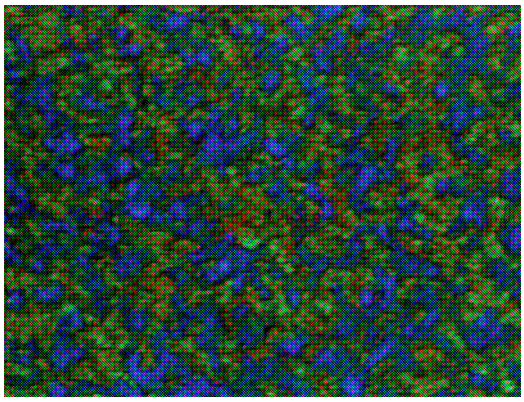

Figure 2.13: *Polarised optical micrograph showing the BPI texture of a sample containing 3.99 mol % of EHA at 46.3 °C* [21].

Samsung have reported a prototype blue phase liquid crystal display. Although not confirmed, it is believed that a 50 °C temperature range of the blue phase was achieved through polymer stabilization. Applying an electric field to the optically isotropic system results in optical anisotropy (Figure 2.14) due to the optical Kerr effect. The device has not been perfected yet as "stains" were observed in the display which is believed to be due to orientational defects of the blue phase structure [36].

(a)

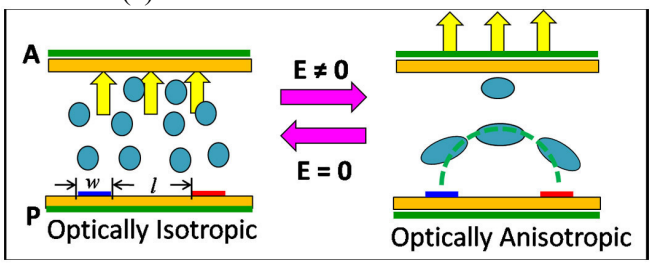

(b)

Figure 2.14: *Illustration showing* (a) *Samsung's blue phase LCD;* (b) *the organisation of a blue phase in a device with parallel electrodes with no voltage applied (left) and with application of an electric field (right)* [27, 37].

Polymer-stabilized blue phase liquid crystals have a number of advantages over traditional nematic phase liquid crystals. The cubic structure of the phase means that the switching of the molecules is not needed. Motion-image blur is reduced due to the fast response times (range of less than a millisecond). If a LED backlight is used in the device colour filters are not needed. The device has a better optical efficiency, device resolution, and a lower cost of producing the display. As the dark state of the display is optically isotropic the viewing angle can be wide and there is a possibility that optical retardation films are not required [26, 27].

2.6.2 Non-Polymer Stabilized Liquid Crystals

While stabilizing the blue phase using polymer networks has proved successful [13, 33, 34], if blue phases are to be used in future applications, other issues in addition to the stabilization of the phase need to be resolved. These include long-term stability, hysteresis, operating voltage and residual birefringence [25]. There is also a need for blue phases to exhibit a large Kerr Effect [26]. Additionally, there has been mention of the polymers affecting the properties and optical nature of the phase. The polymers act like an external alignment. From a production perspective, to have a required amount of stabilized blue phase liquid crystals for displays, a large amount of polymer is needed. This will generate a large volume of composite, increasing the size of the display needed and the cost. As a result, research into stabilising the blue phase without using polymers has begun.

2.6.2.1 Linear Dimers

Early work on linear dimers involved the synthesis of symmetric and non-symmetric bimesogens [38]. Linear bimesogens consist of mesogenic moieties linked with alkyl spacers, see Figure 2.15 where the alkyl spacer possesses 7, 9 or 11 methylene groups. These homologous systems were mixed together, along with BDH1281, which is a high helical twisting power dopant, and produced a phase sequence that included the three blue phases and an unidentified chiral smetic phase. The blue phase sequence had a temperature range of over 41 $^{\circ}$C, where the BPI temperature itself had a temperature range of over 40 $^{\circ}$C, see Figure 2.16. The BPI phase was shown to be stable at room temperature over a

four-month period, with different sample thicknesses, as the phase maintained its texture during this time. Also confirmed was the specular lattice reflections that gave rise to the reflected colours. The reflected colour was found to change with the concentration of BDH1281. Due to the molecular chirality, the change in concentration affected the pitch of the system and so red, blue and green reflected colours were seen for BPI. When an alternating electric field of 14 V μm^{-1} was applied to the liquid crystal mixture at room 25 $^{\circ}C$ and then increased to 18 V μm^{-1}, the reflected colour changed from red/orange to green/blue, corresponding to a wavelength change of 572 nm to 506 nm. Removing the electric field caused the reflected colour to change back to red/orange. This shows the reflected colour of the mixture can be changed at room temperature to an alternative colour. The colour change occurs because the electric field causes the defect lattice in the blue phase structure to deform and the reflectance band is thus switched linearly. A switching time of the electro-optical response was determined to be 10 – 40 ms, with relaxation times of 1 – 10 ms. The switching time range was dependant on the temperature. It was believed that properties of the mixtures would make them useful in liquid crystal displays [38].

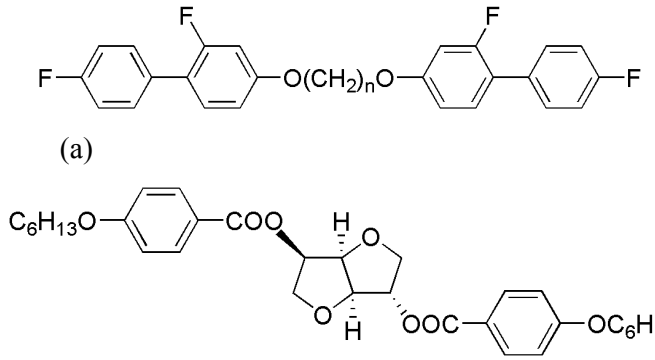

Figure 2.15: *Illustration showing* (a) *the generic structure of the linear bimesogen that was used in a doping mixture to induce a blue phase with a wide temperature range* [38]; (b) *structure of the high helical twisting power dopant,* BDH1281 [38, 39].

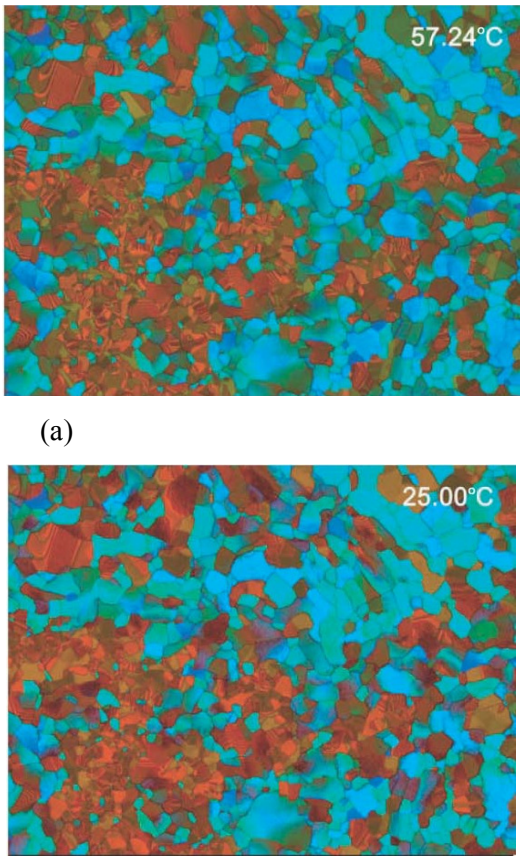

Figure 2.16: *Polarised optical micrograph showing the BPI phase at* (a) *57.24 ^{o}C and* (b) *25.00 ^{o}C, showing the phase is stable over a wide temperature and at room temperature* [38].

2.6.2.2 T-shaped Dimers

Stabilization of the blue phase through doping is dependant on the exact concentration of the chiral dopant. Using a single compound that exhibits a blue phase would lead to less potential error and cost less in manufacturing the display. In order to have a compound exhibit a blue phase, the compound must form highly frustrated structures and have suitable interactions to allow for chiral transfer between the molecules. Sato *et. al.* synthesized T-shaped molecules with a chiral group in a terminal chain. The molecules had different length alkyl chains, as seen in Figure 2.17. The widest blue phase temperature range produced by these T-shaped molecules was of 13 $^{\circ}$C for a compound called **T-1 (10,8),** which possessed ten carbons in its central alkyl chain and eight carbons in its terminal alkyl chain [12].

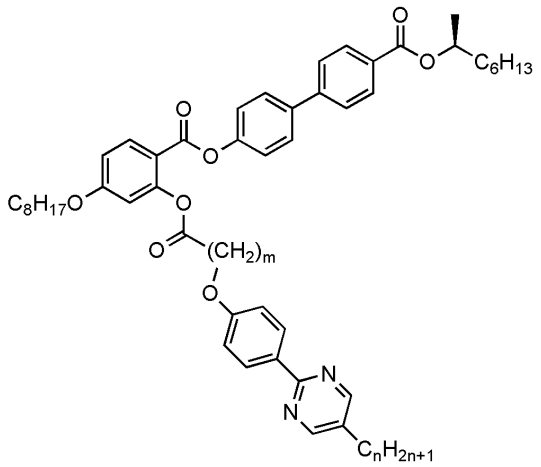

Figure 2.17: *Illustration showing a generic structure of the chiral T-shaped molecules* **T-1 (m,n)** *produced by Sato et. al., which exhibited a wide temperature range blue phase* [12].

Yoshizawa and Iwamochi then moved onto creating binary mixtures containing a T-shaped molecule and a chiral dopant [32] to investigate if a T-shaped molecule could lead to a wide temperature range blue phase. The mixtures contained between 30 % w/w and 60 % w/w of the chiral dopant, S811 (Figure 2.18). A mixture containing 60 % w/w of chiral dopant showed a room temperature blue phase with a phase sequence of isotropic liquid 36 $^{\circ}$C BPIII 28 ^{o}C N*. Electro-optic studies of the mixture showed an 85 % transmittance through a cell when an electric field was applied. The response times of the switching were found to be independent of temperature, except near the BPIII – N* transition. The rise and decay times were found to be 1.6 ms and 3.9 ms respectively. When the percentage of S811 was lowered to 40 % w/w, the clearing point and the blue phase were observed at a much higher temperature (Iso 74.5 $^{\circ}$C BPII 70.5 $^{\circ}$C N*).

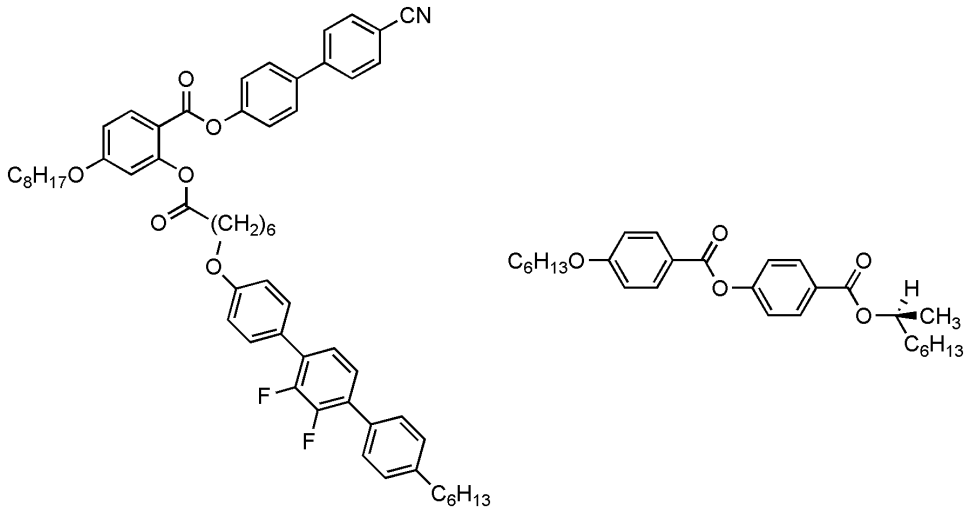

(a) (b)

Figure 2.18: *Illustration showing* (a) *a chiral T-shaped molecule synthesized by Iwamochi and Yoshizawa, which when mixed with* (b) *a chiral smectic liquid crystal,* S811*, exhibits a blue phase with a temperature range near room temperature* [32].

2.6.2.3 Binaphthyls

Some materials, despite not possessing asymmetric molecular structures, show signs of chirality. For example, materials such as binaphthyl derivatives possess axial chirality [29]. Theoretical work in which molecules with axial chirality are used to stabilize the blue phase determined that biaxiality is significant to the process of stabilization [29, 40]. Experimental work was carried out to explore this theory. Thus, a homologous series of U-shaped binaphthyl dimers, **(*R*)-n**, see Figure 2.19, each with axial chirality was synthesized [15]. When polarising optical microscopy was carried out on the dimers that possessed of an odd number of methylene units in the chain, **(*R*)-7**, **(*R*)-9**, **(*R*)-11**, a blue phase and smectic A phase was observed. The widest temperature range observed was of 9 $^{\circ}$C. Compounds **(*R*)-6**, **(*R*)-8**, **(*R*)-10**, **(*R*)-12,** did not show a blue phase. Instead, **(*R*)-6**, **(*R*)-8**, **(*R*)-10** showed a chiral nematic phase and a smectic A phase, while **(*R*)-12** only showed a SmA phase. The difference in the phase sequence observed is due to the odd-even effect. The increased stability of the SmA phase was caused by the increase in the chain length. When each dimer was doped into a host nematic liquid crystal a helical structure was induced. The compounds

with an even chain length were found to have a twisting power higher than the compounds with an odd chain length. Compounds **(*R*)-6**, **(*R*)-7**, **(*R*)-8**, and **(*R*)-9** were found to have a right-handed twist, while **(*R*)-10**, **(*R*)-11** and **(*R*)-12** had a left-handed twist. The more stable conformation of the **(*R*)-n** dimer was found to be the *cis*-conformer. Modelling work of the compounds suggests that the dimer with an odd methylene spacer length has a stronger twisting power than the even chain length dimer. It is thought that the axial chirality of the dimer and the twisted structure is the cause is the stabilization of the blue phase This work shows that axial chirality from compounds, such as binaphthyls, can stabilize the blue phase, up to a range of 9 °C. The odd-even effect is clearly seen in this series of compounds, and has a pronounced effect on the phase transitions of the materials. The odd chain length dimers are believed to have fairly twisted molecular architectures, more so than the even chain length dimers, and this coupled with the axial chirality is thought to be the main reasons the blue phase is stabilized [15].

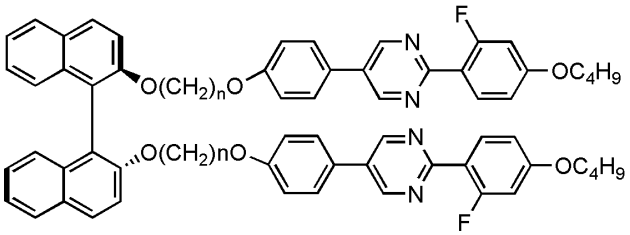

Figure 2.19: *Illustration of the general structure of the U-shaped binaphthyl derivate that was synthesized to have a stabilized blue phase* [15].

Subsequent experimental work showed that bimesogenic binaphthyl derivatives have two origins of twisting power units [41]. Following this research, a binaphthyl derivative containing two 2,3-difluoro-1,4-diphenylbenzene units, Figure 2.20, was synthesized [29]. The dimeric nature of this compound gives it axial chirality and hence biaxiality which can stabilize the blue phase, without needing a polymer framework or doping. It is thought that the binaphthyl compound favours the *cis*-conformation and the two origins of the twisting power of the compound results from the asymmetry and twist present. A reported blue phase temperature range of 30 °C is given. The DSC thermogram shows the initial heating cycle of the compound has a blue phase temperature range of 10

°C, while the cooling cycle and subsequent heat shows a reported temperature range of 30 °C [29]. The subsequent heating cycle showed a temperature range of 30 °C for the blue phase, however, it was noticed that if the compound was left for any length of time, the stronger crystal properties reappeared and so as with the first heat, a blue phase temperature range of 10 °C was observed. This is not a practical property for use in a device. Electrooptic analyses showed that a bright state was obtained upon an applied electric field of 14 V μm^{-1}. The switching times were found to be very long, 18 s for the rise time alone. The large hysteresis for the switching times [29] makes this compound unappealing for use in display devices.

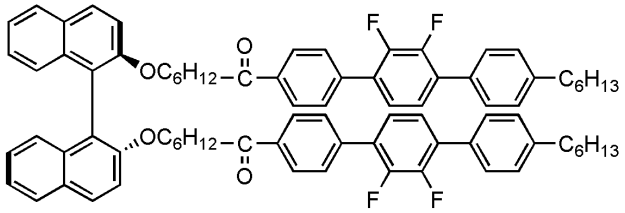

Figure 2.20: *Illustration showing the structure of the binaphthyl compound* [29].

2.6.2.4 Bent Core Molecules

It has already been shown experimentally [29] and theoretically [4, 40] that biaxiality in a system can lead to wide temperature range blue phases. It is not only binaphthyls that possess molecular biaxiality. Bent-core molecules also have this property and are being used to widen blue phase temperature ranges [4]. One study looked at mixing a chiral dopant with a bent-core nematogen [4], see Figure 2.21. The bent-core oxadiazole derivative, which has a dipole bisecting the N-N bond and the oxygen [42] resulting in a negative dielectric anisotropy, makes the system ideal for vertically aligned displays [8]. Before the chiral dopant was added, the bent-core nematogen exhibited a phase sequence of Iso $\rightarrow$ N $\rightarrow$ SmX $\rightarrow$ SmY $\rightarrow$ Cr. A mixture containing 8 % w/w of the chiral dopant showed the presence of BPIII and BPI, before transforming to a N* phase. When the concentration of chiral dopant was increased from 5 % w/w to 8 % w/w, the wavelength of the selective reflection became shorter, and the colours in the platelets of the blue phases texture changed accordingly (Figure 2.22). The sizes of the platelets also increased. This case is unusual as BPI is

generally only stabilized by uniaxial molecular systems when mixed with a chiral dopant. It was found that increasing the chirality also increased the blue phase temperature range. When 10 % w/w of the chiral dopant was mixed with the bent-core system, the temperature range of the blue phase that was observed was found to be 15 $^{\circ}$C. It is stated that this temperature range is larger than for uniaxial rod-like mesogens, suggesting that the interaction between biaxiality and chirality of the molecular systems stabilizes the blue phase structure. Electrooptic analyses of a 10 % w/w mixture showed that applying an electric field of 8 V μm^{-1} caused a dark state of BPI to switch to a bright state. Removing the electric field caused a switch back to the dark state. The switching took around 10 ms to occur. The analysis could only be carried out at low temperatures and low electric fields as the bent-core material was found to decompose at high temperatures and high applied electric fields. It was proved that the results seen were due to the Kerr effect, with a combination of the materials undergoing a local reorientation and lattice distortion. The third blue phase transformation, due to the presence of an applied electric field, of a phase transition to lower symmetry phases, was not believed to contribute to the electrooptic effects seen. The Kerr constant was found to be more than 100 times greater than traditional materials displaying the Kerr effect, however a high temperature dependence of the Kerr effect on BPI was found. The research successfully stabilized the temperature range of the blue phase, resulting in a phase that was observed over 15 $^{\circ}$C. The technique used to stabilize the phase was the doping of a bent-core oxadiazole derivative with a high-twist dopant [4].

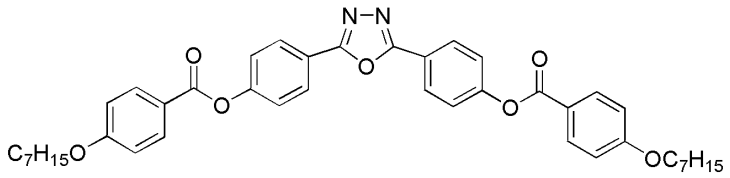

(a)

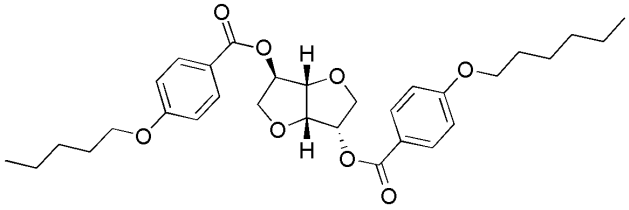

(b)

Figure 2.21: *Illustration showing the structure of* (a) *the bent-core oxadiazole derivative;* (b) *the chiral dopant used in the mixtures* [4].

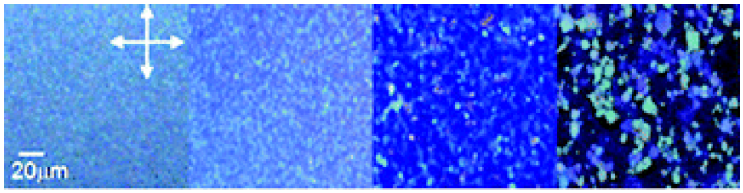

5 wt% **6 wt%** **7 wt%** **8 wt%**

Figure 2.22: *Polarising optical micrograph showing the observational change of the blue phase due to increasing the concentration of chiral dopant* [4].

2.6.2.5 Metal complexes

Usually blue phases are only found in chiral organic systems but Seshadri and Haupt reported the first observed blue phase in a metallomesogen. A ferrocene molecule was added to a chiral Schiff's base derivative to form the compound seen in Figure 2.23. The phase sequence of the compound showed Iso → BP → N* → TGBA → SmA → SmC. This is additionally the first metallomesogen to exhibit a TGBA phase [43].

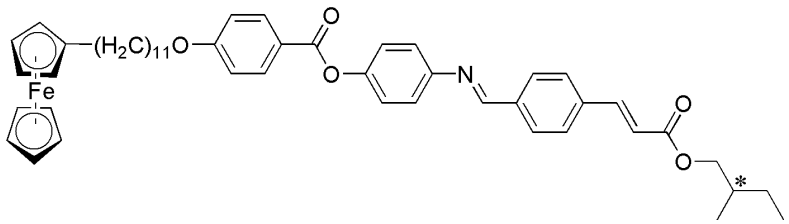

Figure 2.23: *Illustration of the ferrocene-Schiff based derivative that exhibited a blue phase* [43].

Palladium complexes have also been found to exhibit blue phases [20]. The ortho-palladated complexes, synthesized from imines [44, 45] were found to have high helical twisting powers when mixture with a nematic host, although in their pure form one complex was found only to have a blue phase temperature range of 4 °C [20].

2.6.2.6 Self-assembled hydrogen-bonded complexes

As previously mentioned, a third way of incorporating chirality into a liquid crystal system is through hydrogen bonding [9]. A recent study involving hydrogen bonding self-assembly reported the presence of a blue phase [9]. The self-assembled complexes consist of a chiral moiety, SFBA, and an achiral moiety, PPI mixed in different molar ratios. Figure 2.24 shows the structures of the moieties. The chiral moiety acted as the hydrogen donor, while the achiral moiety acted as the hydrogen acceptor. Separately, the moieties did not exhibit any phases, but after self-assembly occurs, phases were observed. This showed that a mesogenic unit was created through hydrogen bonding. Mesogenic complexes with different molar ratios of SFBA to PPI were made. A number of these mixtures exhibited blue phases. The complex of 2:1 molar ratio of SFBA to PPI was found to show a BPII phase, with a temperature range of 23 °C. This was found to be the widest temperature range exhibited by the mixtures. To compare the affects on blue phase stabilization through hydrogen bonding with other means, a mixture of 1:1 molar ratio of SFBA to PPI and chiral dopant, S811, Figure 2.23, was made. A BPII phase was again observed. The temperature range of the mixture, according to the binary phase diagram, was around 10 °C. The blue phase textures from both mixtures are displayed in Figure 2.25. No birefringence was seen from the blue phases, verifying that the phase had a cubic

structure. It is believed that the complexes in this experiments help stabilize the blue phase in a number of ways. The first is through the presence of SFBA-PPI and acid dimers, which are formed during the reaction when there is an excess of SFBA. These molecules fill the double twist cylinder and the increase in chiral dopant increases the chiral twisting power, which stabilizes the blue phase structure and widening the temperature range. Secondly, the relatively weak hydrogen bonding, with respect to covalent bonding, results in the mesogenic complex being quiet flexible. With this flexibility, attaining blue phases is easier, regardless of a low twisting force. Therefore, the blue phase is stabilized and the temperature range is widened. The third suggestion is that fluorine atom on the SFBA moiety stabilizes the blue phase as the fluorine atom creates another weak hydrogen bond in the complex. Fluorine, as a small, electronegative atom, reduces the electron density of the aromatic ring [9]. Better packing of the molecules in the phase then ensues. The effect of the fluorine atom was observed when complexes of a non-fluorinated chiral moiety and achiral moiety was analysed [9].

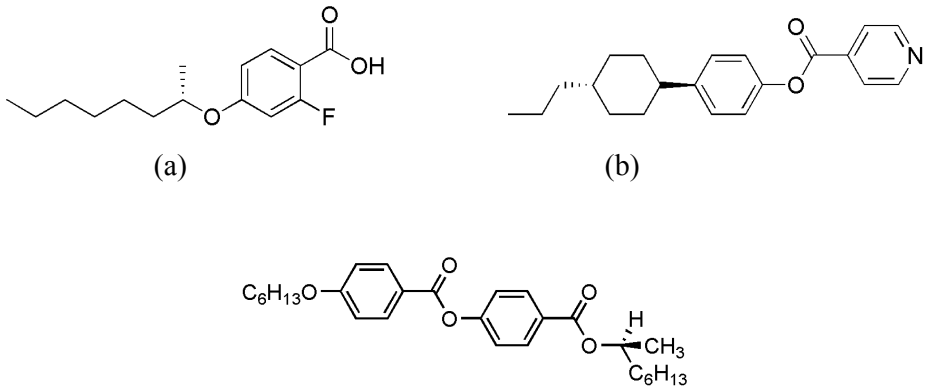

Figure 2.24: *Illustration showing the structure of* (a) *the chiral moiety, SFBA, used to produce the hydrogen-bonded self-assembled complex;* (b) *the achiral moiety, PPI, hydrogen-bonded self-assembled complex* [9]; (c) *chiral dopant S811* [32, 46]

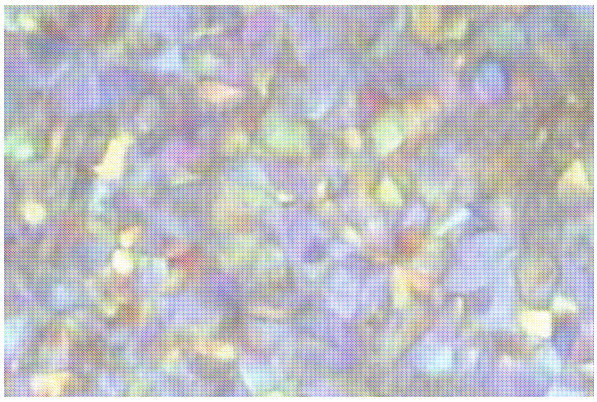

(a)

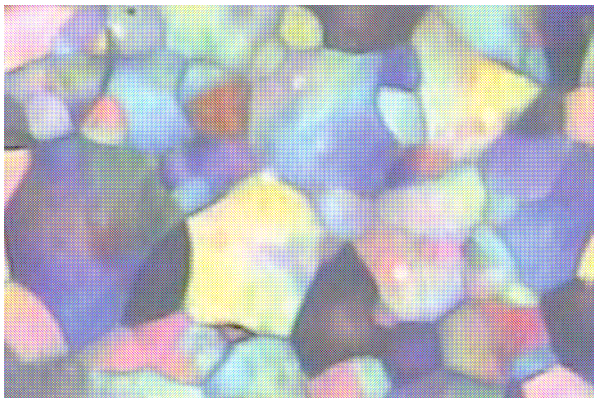

(b)

Plate 2.25: *Polarising optical micrograph showing blue phase (BPII) textures of* (a) *complex of 2:1 molar ratio of SFBA to PPI at 78.3 °C;* (b) *complex of 1:1 molar ratio of SFBA to PPI mixed with a chiral dopant at 102.0 °C* [9].

2.6.3 Achievements of Blue Phase Stabilization

The research has shown that is possible to stabilize the blue phase through a number of methods. The most successful methods were through polymer stabilization, synthesizing chiral molecules and through chiral dopants [12, 21, 32, 38]. The temperature range of the blue phase was stabilized up to 66 °C in one case [21]. Once the blue phase has been stabilized and the electrooptic properties of the phase found to be suitable for use in displays [25, 26], there is no reason to prevent the use of blue phase liquid crystals from being widely used in applications.

2.7 Introduction References

[1] P. J. Collings and M. Hird, *Introduction to Liquid Crystals*, Eds.: G. W Gray, J. W. Goodby and A. Fukuda, Taylor and Francis, London and New York, 1997, p 1, 2, 5, 7 – 10, 48, 50, 52, 56, 61, 62, 67, 71, 113, 125, 126, 196.

[2] P. J. Collings, *Liquid Crystals: Nature's Delicate Phase of Matter*, Adam Hilger, Bristol, 1990, p 8, 9, 10.

[3] Stefan Agamanolis, *Liquid Crystal Displays: Past, Present, and Future*, uploaded 18 May 1995, accessed 11 Nov 2010, http://web.media.mit.edu/~stefan/liquid-crystals/node2.html

[4] M. Lee, S.-T. Hur, H. Higuchi, K. Song, S.-W. Choi and H. Kikuchi, *J. Mater. Chem*., 2010, **20**, 5813.

[5] L. A. Madsen, T. J. Dingemans, M. Nakata, and E.T. Samulski, *Phys. Rev. Letts.,* 2004, **92** ,14, 145505.

[6] D. Demus, J. W. Goodby, G. W. Gray, H.-W. Spiess, V. Vil, *Handbook of Liquid Crystals,* Wiley VCH, Weinham, 1998, Vol 2B, p 993.

[7] Edt. H-S. Kitzerow and C. Bahr, *Chirality in Liquid Crystals*, Springer-Verlag, New York, 2001, p 115, 124, 125, 188, 189, 199

[8] K. Takatoh, M. Hasegawa, M. Koden, N. Itoh, R.Hasegawa and M. Sakamoto, *Alignment Technologies and Applications of Liquid Crystal Devices*, The Liquid Crystal Book Series, Eds. G. W. Gray, J. W. Goodby and A. Fukuda, Taylor and Francis, Oxfordshire and New York, 2005, p 99, 101.

[9] W. He, G. Pan, Z. Yang, D. Zhao, G Niu, W. Huang, X. Yuan, J. Guo, H. Cao and H. Yang, *Adv. Mater*., 2009, **21**, 2050.

[10] I. Dierking, *Textures of Liquid Crystals*, Wiley VCH, Germany, 2003, p.45, 168.

11] R. Eelkema, Thesis: *Liquid Crystals as Amplifiers of Molecular Chirality*, 1978, p 15.

[12] M. Sato, A. Yoshizawa and F. Ogasawara, *Mol. Cryst. and Liq. Cryst.*, 2007, **475**, 99.

[13] T. Kato and J. E. Bara, L*iquid crystalline functional assemblies and their supramolecular structures,* Springer-Verlag Berlin Heidelberg, p 101.

[14] P. J. Collings, *Liquid Crystal: Nature's Delicate Phase of Matter,* 2nd edition, Princeton University Press, New Jersey and Oxfordshire, p 12.

[15] J. Rokunohe and A. Yoshizawa, *J. Mater. Chem*., 2005, **15**, 275.

[16] M. Sato and A. Yoshizawa, *Adv. Mater*, 2007, **19**, 4145.

[17] A. Yoshizawa, M. Sato and J. Rokunohe, *J. Mater. Chem.*, 2005, **15**, 3285.

[18] A. Yoshizawa, *J. SID*, 2008, **16**, 1189.

[19] Y. Hisakado, H. Kikuchi, T. Nagamura, T. Kajiyama, *Adv. Mater.,* 2005, **17**, 1, 96.

[20] J. Buey, P. Espinet, H.-S. Kitzerow and J. Strauss, *Chem. Commun*., 1999, Issue 5, 441.

[21] H. Kikuchi, M. Yokota, Y. Hisakado, H. Yang and T. Kajiyama, *Nature*, 2002, **1**, 64.

[22] P. E. Cladis, T. Garel and P. Pieranski, *Phys. Rev. Letts*., 1986, 57, 2841.

[23] J.-I. Fukuda, M. Yoneya, and H. Yokoyama, *Phys. Rev. E,* 2009, **80**, 031706

[24] J.-H Lee, D. N. Liu and S.-T. Wu, *Introduction to Flat Panel Displays,* John Wiley and Sons Ltd, West Sussex, 2008, p 60, 64.

[25] K.-M. Chen, S. Gauza, H. Xianyu and S.-T. Wu, *J. Display Technology*, 2010, **6**, 318.

[26] L. Rao, Z. Ge, S. Gauza, K.-M. Chen and S.-T. Wu, *Mol. Cryst. and Liq. Cryst*., 2010, **527**, 30/[186].

[27] L. Rao nad S.-T. Wu, *Emerging Blue Phase LCDs*, SPIE Newsroom, uploaded July 2010, accessed October 2010, http://spie.org/x41180.xml?ArticleID=x41180

[28] H. Coles, M. Pivnenko, J. Hannington, 2009, US Patent US2009115957.

[29] A. Yoshzawa, Y. Kogawa, K. Kobayashi, Y. Takanishi and J. Yamamoto, *J. Mater. Chem.*, 2009, **19**, 5759.

[30] P. Schewe, J. Riordon and B. Stein, *AIP*, 2003, 633.

[31] W. Cao, A. Muñoz, P. Palffy-Muhoray and B. Taheri, *N. Mat.,* 2001, **1**, 111.

[32] H. Iwamochi and A. Yoshizawa, *Appl. Phys. Express*, 2008, **1**, 11180.

[33] R. A. M. Hikmet, *J. Appl. Phys.,* 1990, **68**, 4406.

[34] H.-S. Kitzerow, H. Shmid, A. Ranft, G. Heppke, R. A. M. Hikmet and J. Lub, *Liq. Cryst.,* 1993, **14**, 911.

[35] R. A. M. Hikmet, *Liq. Cryst*., 1991, **9**, 405.

[36] Naoki Tanaka, *[SID] Blue Phase: Samsung's 'Revolutionary' LCD Discussed*, Nikkei Electronics, Nikkei Business Publications, Inc, 2008, accessed December 2010, http://techon.nikkeibp.co.jp/english/NEWS_EN/20080527/152422/

[37] Samsung, *Samsung Develops Worlds First "Blue Phase" Technology to Achieve 240 Hz Driving Speed for High-Speed Video*, Samsung Press Release, May 2008, http://www.samsung.com/us/aboutsamsung/news/newsIrRead.do?news_ctgry=irnewsrelease&news_seq=8351

[38] H. Coles and M. Pivnenko, *Nat. Letts*., 2005, **436**, 997.

[39] H. Coles, M. Pivnenko and J. Hannington, 2009, US Patent US0115957.

[40] D. C. Wright and N. D. Mermin, *Rev. Mod. Phys*., 1989, **61**, 385.

[41] K. Kobayashi and A. Yoshizawa, *Liq. Cryst.*, 2007, **34**, 1455.

[42] B. R. Acharya, A. Primak and S. Kumar, *Phys. Rev. Letts.,* 2004, **92**, 145506.

[43] T. Seshadri and H.-J. Haupt, *Chem. Comm*., 1998, 735.

[44] J. Buey and P. Espinet, *J. Organomet. Chem*., 1996, **507**, 137.

[45] M. J. Baena, J. Buey, P. Espinet, H.-S. Kitzerow and G. Heppke, *Angew. Chem. Int. Ed. Engl*., 1993, **32**, 1201.

[46] S. Kurihara, S. Nomiyama and T. Nonaka, *Chem. Mater.,* 2000, **12**, 9.

3 PROJECT AIMS

3.1 Previous Research

As mentioned in the previous chapter (Introduction, Section 2.6), blue phase liquid crystals have the potential to be used in many applications due to their macroscopic cubic arrangement and interesting electrooptical response properties [1]. However, practical applications of blue phase liquid crystals have been hindered, as the phase usually only exists in a narrow temperature range of 1 $^{\circ}$C [2, 3, 4]. Recently, a great deal of research has been directed towards the stabilization of the blue phase *via* various methods, one of which includes polymer stabilization [5, 6].

Polymer stabilization of the blue phase has proven to be a particularly successful method of increasing the blue phase temperature range. Indeed, Samsung have demonstrated a Blue Phase LCD panel capable of operating at room temperature. The blue phase is stabilized through a polymer and liquid crystal matrix that produced a phase with a temperate range of 50 $^{\circ}$C [7]. Although the use of polymers to stabilise the phase seems promising [5,6], there are still some issues to be dealt with [8, 9]. For instance, the Samsung mode has orientation defects affecting the picture quality that need to be resolved before mass production can be considered [7]. The amount of polymer needed for the device affects the optical properties of the display, compared to a display that does not require a polymer matrix. Additional work that examining the long-term stability of the matrix and maintaining a switching time with a small hysteresis is required before polymer stabilization can be deemed the best way to stabilize the blue phase for applications [8]. In addition to this approach, a great deal of recent research has been targeted towards synthesising compounds that have wide temperature range blue phases [10, 11] including room temperature [12]. The focal point of current research is in the area of synthesising dimers and bimesogens [2, 12, 13, 14, 15 and 16], and this approach is yielding some promising results.

3.1.1 Achiral Linear Dimers

The earliest example of a wide temperature range of a blue phase without polymer stabilization was reported by Coles and Pivnenko [15]. A number of linear bimesogens were prepared, where the mesogenic moieties were linked *via* a simple alkyl spacer. The series of bimesogens were mixed with each other and with BDH1281, a strong twisting power dopant from Merck Chemicals. The general structure of the linear bimesogen and BDH1281 can be seen in Figure 3.1. The reported mixture contained bimesogens with an alkyl spacer of 7, 9 and 11 methylene units. The phases and transition temperatures shown by the mixture were Iso 57.72 °C BP III* 57.58 °C BP II* 57.22 °C BP I* 16.5 °C SmX* - 28.0 °C glass, where SmX* was an unidentified smectic phase [15].

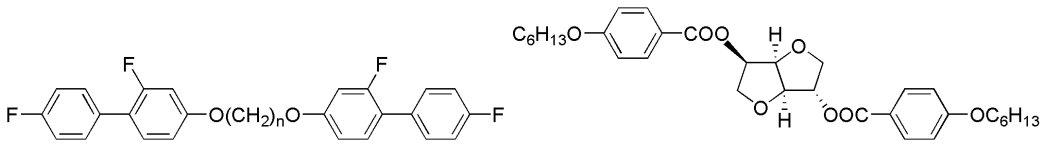

(a) (b)

Figure 3.1: *Illustration showing* (a) *the generic structure of the linear bimesogen of H. Coles and M. Pivnenko that was used in a doping mixture to induce a blue phase with a wide temperature range* [15]*;* (b) *the structure of the high helical twisting power dopant,* BDH1281 [15, 17].

3.1.2 Chiral T-shaped Dimers

The effect of structure and position of coupling was investigated and this lead to research involving T-shaped molecules [18]. Sato *et. al.* synthesised chiral T-shaped molecules attached to an alkyl spacer by ester and ether linkages. Four **T-1(m, n)** dimers were produced, where m represents the number of methylene units in the central alkyl chain and n represents the number of carbon atoms in the terminal alkyl chain. The generic structure of the **T-1(m, n)** dimers is given in Figure 3.2. All of the **T-1(m, n)** compounds, upon cooling, showed the phase sequence Iso $\rightarrow$ BP $\rightarrow$ N*. The texture of blue phase observed was indicative of BP III. The blue phase existed between 25 °C and 32 °C, [16], showing that it is possible to obtain a blue phase at room temperature. The widest temperature range blue phase produced by the **T-1(m, n)** dimer was 13 °C for **T-1(10,8)** [16].

Sato *et. al.* also produced a dimer with an extended core in one of the mesogenic units. The structure of the extended dimer **(T-2(10, 6))** is shown in Figure 3.2. **T-2(10, 6)**, and the material still exhibited the phase sequence of Iso $\rightarrow$ BP $\rightarrow$ N*. The clearing point was increased to 77 $^{\circ}$C and the blue phase only existed over a 5 $^{\circ}$C temperature range.

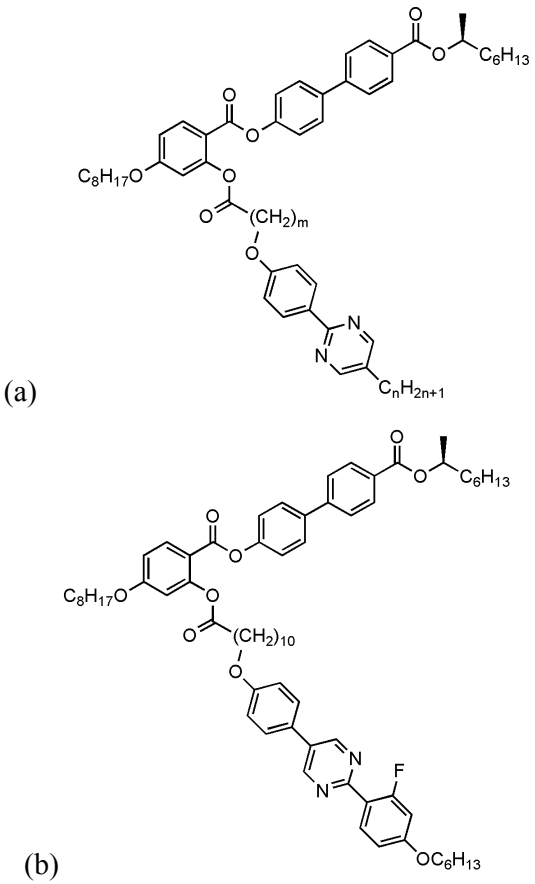

Figure 3.2: *Illustration showing* (a) *the generic structure of the chiral T-shaped* **T-1(m, n)** *dimers;* (b) *the structure of the chiral T-shaped* **T-2(10, 6)** *dimer, which showed an extended blue phase temperature range, both produced by Sato et al* [16].

A similar material, **T-3** shown in Figure 3.3, was also synthesized that showed the following phase sequence: Iso 49 $^{\circ}$C BPIII 41 $^{\circ}$C N* - 10 $^{\circ}$C glass with a melting point of 61 $^{\circ}$C. It was proposed that the temperature range of the blue phase had been widened due to the biaxiality of the dimer and the chirality of the terminal group [2].

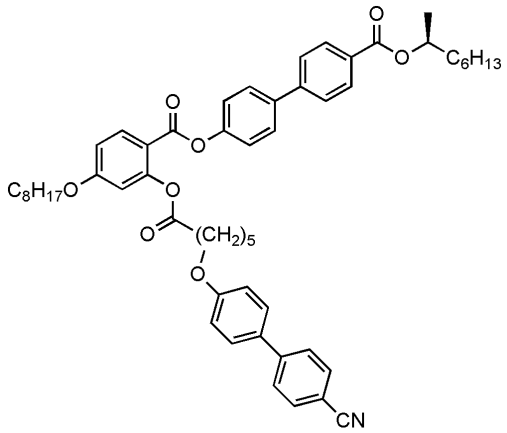

Figure 3.3: *Illustration showing the chiral T-shaped molecule,* **T-3** [2].

3.1.3 Achiral T-shaped Dimers

An alternative approach to produce a wide range blue phase has involved doping achiral molecules with high helical twisting power dopants. A number of binary mixtures containing a T-shaped dimer and a chiral smectic liquid crystal, S811, have been reported by Iwamochi and Yoshizawa [12]. The structure of the achiral T-shaped dimer and S811 are shown in Figure 3.4. A BPIII existing over an 8 $^{\circ}$C range was observed in a binary mixture containing 40 % w/w of the dimer and 60 % w/w of S811. The blue phase was observed around room temperature [12], but the temperature range needs to be increased significantly for use in display applications.

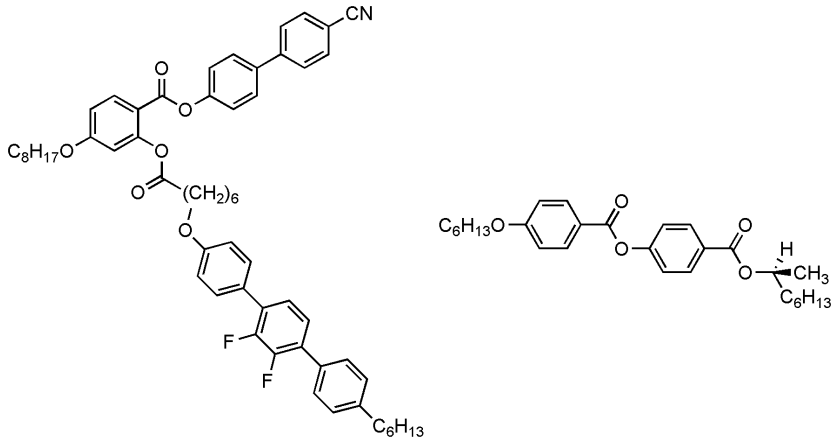

(a) (b)

Figure 3.4: *Illustration showing* (a) *an achiral T-shaped molecule,* **T-4***, which when mixed with* (b) *a chiral smectic liquid crystal,* S811*, exhibits a blue phase with a wide temperature range near room temperature* [12].

3.1.4 Summary of Liquid Crystal Dimer Strategies

Liquid crystal dimers are of immense interest in the search for wide temperature blue phases for display applications. Doping dimers with chiral materials as produced blue phases that exist over temperature ranges of 8 – 40 °C. Chiral dimers have yielded blue phases over 13 – 50 °C temperature ranges, which include room temperature. This shows the viability of this approach.

3.2 Project Aims

The aim of the project is to prepare chiral dimeric liquid crystals in the search for wide temperature blue phases. The project involves the synthesis and characterization of two series' of chiral dimers. These will be investigated to determine if they exhibit blue phases or will be useful as dopants to induce blue phases in mixtures.

The main focus of this project is to produce a series of dimers, which are composed of achiral mesogens coupled together using chiral spacers. This approach has not been attempted previously. The first series are linear dimers, where the monomers are to be terminally attached to a central chiral spacer. The second series of dimers to be targeted are H-shaped, where the mesogens are laterally attached to a central chiral spacer.

3.2.1 Linear Dimers

Research has showed that doping linear dimers with a chiral dopant can produce a blue phase [15]. This project will synthesize linear dimers from a phenolic compound (see Figure 3.5) and a chiral dicarboxylic acid. It is hoped that the chiral acid in the centre of the dimer will provide the frustration needed to produce blue phase without the need for doping.

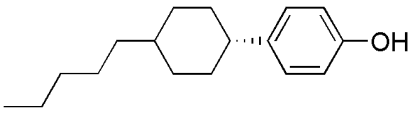

Figure 3.5: *Illustration showing PCH-5-phenol, the monomeric unit for the linear dimers.*

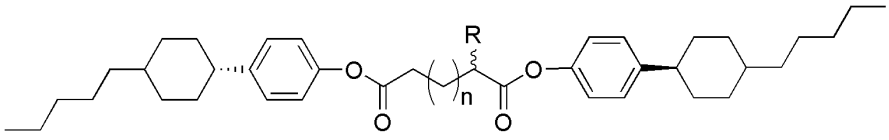

n = 0, R = CH_3, (*S*)-
n = 0, R = CH_3, (*R*)-
n = 1, R = CH_3, (*S*)-
n = 1, R = CH_3, (*R*)-
n = 0, R = Ph, (*S*)-

Figure 3.6: *Illustration showing the proposed structure of the linear dimers.*

Five dicarboxylic acid spacers are to be used [(*S*)-(–)-methylsuccinic acid, (*R*)-(+)-methylsuccinic acid, (S)-(+)-2-methylglutaric acid, (*R*)-(–)-2-methylglutaric acid and (*S*)-(+)-phenylsuccinic acid] to produce five linear dimers (see Figure 3.6 for the structure). The succinic acids are based on 4 carbon atoms and the glutaric acids are based on five carbon atoms. Differences in the phase types formed and the transition temperature observed between the dimers synthesized from the two spacer lengths will be studied and discussed.

3.2.2 H-Shaped Dimers

It has been determined previously, that H-shaped dimers exhibit mesophases, including the nematic phase [19], coupled with low melting properties. It is believed that if packing frustrations can be introduced into these dimer systems then blue phases might be observed.

The aim was to couple a chiral dicarboxylic acid spacer between two synthesised mesogenic monomers in such a way as shown in Figure 3.7.

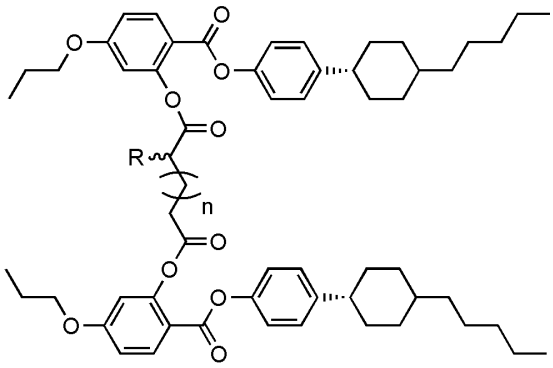

Figure 3.7: *Illustration showing the proposed structure of the H-shaped dimers*.

As with the linear dimers dicarboxylic acids of different lengths will be used, i.e., [(*S*)-(–)-methylsuccinic acid, (*R*)-(+)-methylsuccinic acid, (S)-(+)-2-methylglutaric acid, (*R*)-(–)-2-methylglutaric acid and (*S*)-(+)-phenylsuccinic acid], and the effects of the spacer length on mesophase formation and associated transition temperatures are to be investigated.

3.2.3 Analysis of the Dimers

Once the dimers have been synthesised, the structures will be confirmed through a number of standard techniques. Characterization of the liquid crystal properties (mesophases identification, transition temperatures and enthalpies of transition) will be carried out using polarising optical microscopy and differential scanning calorimetry.

3.2.4 Mixture Work

If the dimers do not exhibit a blue phase, the compounds will be mixed with a nematic host in the attempt to induce the phase. Initially, contact preparations will be carried out with a host liquid crystal, followed by an investigation at fixed concentrations to determine if the dimers can induce blue phases through

chirality transfer. This approach is similar to the one reported by Coles *et. al.* who used a chiral dopant with achiral dimers as the host [15].

Subsequent work will involve determining the helical twisting powers of the target materials. Each of the dimers will be doped into a nematic host at varying concentrations in order to determine their helical twisting powers. The pitch, and as a consequence the helical twisting power, of each dimer synthesised will be determined using the Grandjean-Cano wedge method.

3.3 References

[1] Z. Ge, S. Gauza, M. Jiao, H. Xianyu and S.-T. Wu, *Appl. Phys. Letts.*, 2009, **94**, 101104.

[2] M. Sato and A. Yoshizawa, *Adv. Mater.*, 2007, **19**, 4145.

[3] A. Yoshizawa, M. Sato and J. Rokunohe, *J. Mater. Chem.*, 2005, **15**, 3285.

[4] A. Yoshizawa, *J. SID*, 2008, **16**, 1189.

[5] H. Kikuchi, M. Yokota, Y. Hisakado, H. Yang and T. Kajiyama, *Nature*, 2002, **1**, 64.

[6] S.-Y. Lu and L.-C. Chien, *Appl. Phys. Lett.,* 2007, **91**, 131119.

[7] Naoki Tanaka, *[SID] Blue Phase: Samsung's 'Revolutionary' LCD Discussed*,
Nikkei Electronics, Nikkei Business Publications, Inc, 2008,
http://techon.nikkeibp.co.jp/english/NEWS_EN/20080527/152422/

[8] K.-M. Chen, S. Gauza, H. Xianyu and S.-T. Wu, *J. Display Technology*, 2010, **6**, 318.

[9] L. Rao, Z. Ge, S. Gauza, K.-M. Chen and S.-T. Wu, *Mol. Cryst. Liq. Cryst.*, 2010,
527, 30/[186].

[10] M. Lee, S.-T. Hur, H. Higuchi, K. Song, S.-W. Choi and H. Kikuchi, *J. Mater. Chem.*, 2010, **20**, 5813.

[11] W. He, G. Pan, Z. Yang, D. Zhao, G Niu, W. Huang, X. Yuan, J. Guo, H. Cao and H. Yang, *Adv. Mater.*, 2009, **21**, 2050.

[12] H. Iwamochi and A. Yoshizawa, *Appl. Phys. Express*, 2008, **1**, 111801.

[13] J. Rokunohe and A. Yoshizawa, *J. Mater. Chem.*, 2005, **15**, 275.

[14] A. Yoshzawa, Y. Kogawa, K. Kobayashi, Y. Takanishi and J. Yamamoto, *J. Mater. Chem.*, 2009, **19**, 5759.

[15] H. Coles and M. Pivnenko, *Nat. Letts*., 2005, **436**, 997.

[16] M. Sato, A. Yoshizawa and F. Ogasawara, *Mol. Cryst. Liq. Cryst.*, 2007, **475**, 99.

[17] H. Coles, M. Pivnenko and J. Hannington, 2009, US Patent US0115957.

[18] C. Imrie and P. Henderson, *Current Opinion in Colloid and Interface Science*, 7 2002, **7**, 298.

[19] W.-S. Bae; J.-W. Lee; J.-I. Jin, *Liq. Cryst.,* 2001, **28,** 59.

4 ABBREVIATIONS

4.1 Chemical Abbreviations

PCH-5-Phenol – 4-(4-pentylcyclohexyl)phenol

EDAC – *N*-(3-dimethylaminopropyl)-*N′*-ethylcarbodiimide hydrochloride

DMAP – 4-(dimethylamino)pyridine

DCM – dichloromethane

THF – tetrahydrofuran

$CDCl_3$ – deuterated chloroform

D_6-DMSO – deuterated dimethyl sulfoxide

K_2CO_3 – potassium carbonate

DCC – *N*,*N′*-dicyclohexylcarbodiimide

4.2 Unit Abbreviations

g – grams

mmol – 1×10^{-3} moles (millimoles)

mol – moles

ml – 1×10^{-3} Litres (millilitres)

L – Litres

eq. – equivalent

v/v – volume by volume

^{o} C – degree Centigrade

MHz – 1×10^{6} Hertz (mega Hertz), where Hertz = s^{-1}

kJ mol^{-1} – 1×10^{3} Joules per mole (kilojoules per mole)

m/z – mass-to-charge ratio

μm^{-1} – 1×10^{-6} metres (micrometres)

mm – 1×10^{-3} metres (millimetres)

cm – 1×10^{-2} metres (centimetres)

MP – megapixels

4.3 Analysis Abbreviations

^{1}H NMR – proton nuclear magnetic resonance

^{13}C NMR – carbon-13 nuclear magnetic resonance

IR – infrared

MS – mass spectrometry

ESI – electrospray ionisation

M^+ – parent ion

GC – gas chromatography

UV-Vis – ultraviolet-visible

UV - ultraviolet

HPLC – high performance liquid chromatography

TLC – thin layer chromatography

DSC – differential scanning calorimetry

4.4 ^{1}H and ^{13}C NMR Abbreviations

s – singlet

d – doublet

t – triplet

q – quartet

quint – quintet

sext – sextet

m – multiplet

Ar – aromatic ring

ArH – hydrogen atom on an aromatic ring

Cy – cyclohexyl ring

4.5 Liquid Crystal Phase Abbreviations

Iso – isotropic liquid

Cr – crystal

N – nematic

SmA – smectic A

B – crystal B

N* – chiral nematic

BP – blue phase

5 EXPERIMENTAL

5.1 Chemical Analysis and Purification

The following analysis techniques were used to confirm the structures and purities of the materials synthesised.

5.1.1 Nuclear Magnetic Resonance Spectroscopy

^{1}H NMR spectra were obtained *via* the use of a JEOL EX400 NMR Spectrometer operating at 400 MHz. ^{13}C NMR spectra were obtained via the use of a JEOL EX400 NMR Spectrometer operating at 100.6 MHz. The δ_H values were recorded in ppm and the coupling constants are reported in Hertz.

5.1.2 Infrared Spectroscopy

Infrared spectral analyses were carried out on a Shimadzu IR Prestige-21 FTIR Spectrometer in conjunction with a Specac 'Golden Gate' ATR crystal adaptor.

5.1.3 Mass Spectrometry

The mass of each of the materials was determined by mass spectrometry using a Bruker microTOF-MS ESI.

5.1.4 Elemental Analysis

An elemental analysis was carried out using an Exeter Analytical Inc. CE-440 Elemental Analyser in conjunction with a Sartorius SE2 analytical balance.

5.1.5 Gas Chromatography

Gas chromatographic analyses were carried out using a Shimadzu 2014 gas chromatogram, fitted with an AOC-20i auto sampler, using a HP-5 column and hydrogen carrier gas.

5.1.6 UV-Vis Spectroscopy

The UV-Vis absorption spectra of the materials were recorded *via* the use of a dual beam Shimadzu UV 2401PC UV-Vis spectrophotometer, using index-

matched Quartz cuvettes with a 1 cm pathlength. Dichloromethane was used as the solvent for each analysis.

5.1.7 HPLC

In order to determine the purity of the mesogenic compounds, HPLC analysis was carried out on a Shimadzu Prominence HPLC with a DGC-20AS degasser, LC 20AT liquid chromatograph, SIL-20A auto sampler, CBM-20A communications bus module, CTO-20A column oven, SPD-20 UV/Vis detector and FRC-10A fraction collector. Preparative HPLC was carried out using the same equipment.

5.1.8 Column Chromatography

Column Chromatography, used to purify the materials, was carried out using Fluka Silica Gel 60 with a 220 – 440 mesh.

5.1.9 Thin Layer Chromatography

Merck TLC Silica Gel 60 F_{254}, Aluminium Sheets were used for thin layer chromatography. TLC plates were visualised with UV light or by oxidation using iodine or permanganate solution.

5.2 Characterisation and Evaluation of Liquid Crystals

5.2.1 Polarised Optical Microscopy

A Zeiss AXIOSKOP 40 polarised light microscope with a Mettler Toledo FP82HT hot-stage in conjunction with a Mettler FP90 central processor was used to investigate the mesomorphic behaviour of the final compounds, intermediates and mixtures. Images of defect textures were captured using an InfinityX 21 MP digital camera with Infinity Capture Software. An Olympus BX40 polarised light microscope, with Linkam stage THM 600 in conjunction with a Linkam 93 temperature control unit equipped with liquid nitrogen cooling and a Linkam LNP power unit,§ was used to investigate the sub-ambient temperature mesomorphic behaviour of the final H-shaped compounds. Photomicrographs were captured using a PixeLINK digital camera with PixeLINK Capture SE Software.

5.2.2 Differential Scanning Calorimetry

A Mettler Toledo DSC 822e equipped with an autosampler and operating with Star^{e} software was used to determine phase transitions and the associated enthalpies. The instrument was calibrated using Indium as a reference with an onset temperature of 156.55 ± 0.2 ^{o} C, ΔH 28.45 ± 0.4 J g^{-1} [1].

5.3 Synthesis

5.3.1 Reagents

PCH-5-Phenol (**1**) was purchased from Merck and the starting materials for the chiral spacers (**2** – **6**) were purchased from TCI Europe. Methyl 2,4-dihydroxybenzoate (**12**) was purchased from Sigma. The solvents were purchased from Fisher Scientific. All were used without further purification.

5.3.2 Synthetic Pathway 1

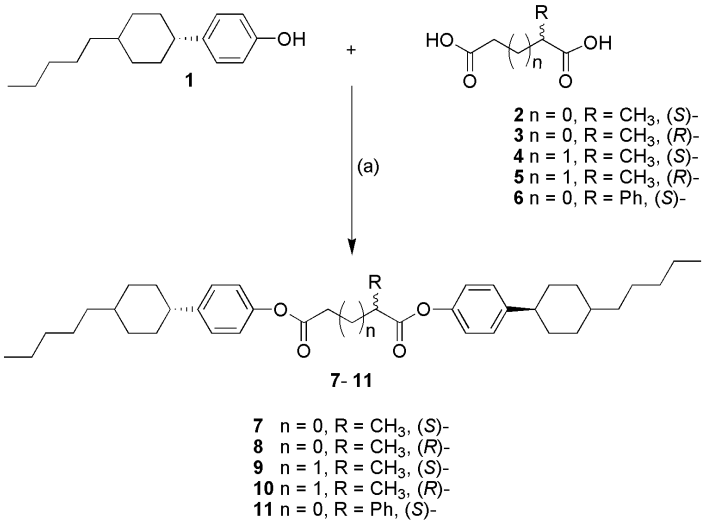

Scheme 5.1: *Synthetic pathway 1 for the synthesis of dimers* **7 – 11**.

Synthesis of (*S*)-*Bis*-[4-(4-pentylcyclohexyl)phenyl]-2-methylsuccinate (7)

(*S*)-(–)-methylsuccinic acid, **2** (0.10 g, 0.76 mmol), PCH-5-phenol, **1** (4 eq., 0.75 g, 3.03 mmol), EDAC (4 eq., 0.58 g, 3.03 mmol) and DMAP (0.8 eq., 0.08 g, 0.61 mmol) were dissolved in DCM (60 ml) and stirred for 5 days at room temperature. The solution was then washed with water (3 x 25 ml) and dried over anhydrous magnesium sulphate (30 min) [2]. The crude product was purified by column chromatography over silica gel (hexane/DCM 2:1 v/v as eluent). The product was recrystallised from ethanol and isolated as colourless crystals.

Yield: 0.33 g (74 %)

^{1}H NMR (400 MHz, $CDCl_3$): δ 7.16 – 7.18 (4H, m, 2 x ArH), 6.97 (4H, d, J = 8.2, 2 x ArH), 3.19 – 3.28 (1H, m, CH), 3.01 (1H, dd, J = 16.8, 8.5, CH), 2.77 (1H, dd, J = 16.8, 5.8, CH), 2.43 (2H, tt, 2 x CH Cy), 1.82 – 1.88 (8H, m, 4 x CH_2 Cy), 1.44 (3H, d, J = 7.0, CH_3) 1.17 – 1.42 (22H, m, 6 x CH_2, 4 x CH_2 Cy, 2 x CH Cy), 0.96 – 1.06 (4H, m, 2 x CH_2), 0.87 (6H, t, 2 x CH_3) ppm.

^{13}C NMR (100.6 MHz, $CDCl_3$): δ 173.85 (carboxylic acid next to chiral spacer), 170.46 (carboxylic acid in spacer), 148.58 (ArO), 148.42 (ArO), 145.50 (Ar Cy), 145.43 (Ar Cy), 127.71 (4 x Ar CH), 121.06 (4 x Ar CH), 44.04 (2 x Ar CH Cy), 37.70 (CH_2 next to chiral centre), 37.34 (2 x CH_2), 37.24 (2 x Cy CH alk) 36.04, (chiral CH), 34.36 (4 x CH_2 Cy), 33.53 (4 x CH_2 Cy), 32.19 (2 x CH_2), 26.63 (2 x CH_2) 22.70 (2 x CH_2), 16.99 (chiral CH_3), 14.12 (2 x CH_3) ppm.

IR (neat) $\tilde{\nu}_{max}$: 2916, 2847, 1751, 1605, 1504, 1450, 1381, 1296, 1196, 1165, 1126, 1057, 1018, 957, 841, 725, 664, 540 cm^{-1}.

MS m/z: 606.45 ($M^+ + NH_4^+$)

Elemental analysis: Calculated analysis for $C_{39}H_{56}O_4$: C 79.55, H 9.59. Found: C, 79.72, H, 9.61.

Synthesis of (*R*)-*Bis*-[4-(4-pentylcyclohexyl)phenyl]-2-methylsuccinate (8)

The synthesis of compound **8** was similar to the one used for the preparation of **7**. The following quantities were used: (*R*)-(+)-methylsuccinic acid, **3** (0.10 g, 0.76 mmol), PCH-5-phenol, **1** (4 eq., 0.75 g, 3.03 mmol), EDAC (4 eq., 0.58 g, 3.03 mmol) and DMAP (0.8 eq., 0.075 g, 0.61 mmol) were dissolved in DCM (60 ml).

Yield: 0.24 g (54 %)

^{1}H NMR (400 MHz, $CDCl_3$): δ 7.15 – 7.19 (4H, m, ArH), 6.97 (4H, d, J = 8.5, 2 x ArH), 3.20 – 3.28 (1H, m, CH), 3.06 (1H, dd, J = 16.8, 8.5, CH), 2.77 (1H, dd, J = 16.8, 5.5, CH), 2.44 (2H, tt, 2 x CH Cy), 1.82 – 1.88 (8H, m, 4 x CH_2 Cy), 1.43 (3H, d, J = 7.0, CH_3), 1.17 – 1.42 (22 H, m, 6 x CH_2, 4 x CH_2 Cy, 2 x CH Cy), 0.96 – 1.06 (4H, m, 2 x CH_2), 0.88 (6H, t, 2 x CH_3) ppm.

^{13}C NMR (100.6 MHz, $CDCl_3$): δ 173.85 (carboxylic acid next to chiral centre), 170.46 (carboxylic acid in spacer), 148.58 (ArO), 148.40 (ArO), 145.49 (Ar Cy), 145.42 (Ar Cy), 127.70 (4 x Ar CH), 121.06 (4 x Ar CH), 44.03 (2 x Ar CH Cy), 37.69 (CH_2 next to chiral centre), 37.33 (2 x CH_2) 37.23 (2 x Cy CH alk), 36.03 (chiral CH), 34.35 (4 x CH_2 Cy), 33.52 (4 x CH_2 Cy), 32.18 (2 x CH_2), 26.62, (2 x CH_2), 22.70 (2 x CH_2) 16.99 (chiral CH_3), 14.12 (2 x CH_3) ppm.

IR (neat) $\widetilde{\nu}_{max}$: 2916, 2847, 1751, 1605, 1504, 1450, 1381, 1296, 1196, 1500, 1126, 1057, 1018, 957, 910, 841, 725, 664, 540 cm^{-1}.

MS m/z: 606.45 ($M^+ + NH_4^+$)

Elemental analysis: Calculated analysis for $C_{39}H_{56}O_4$: C 79.55, H 9.59. Found: C 79.62, H 9.57.

Synthesis of (*S*)-*Bis*-[4-(4-pentylcyclohexyl)phenyl]-2-methylpentanedioate (9)

The methodology used for compound **9** was similar to the one used for the preparation of **7**, except that the reaction mixture was stirred for only 1 day and the eluent used was hexane/DCM 1:1 v/v. The following quantities were used: (*S*)-(+)-2-methylglutaric acid, **4** (0.10 g, 0.68 mmol), PCH-5-phenol, **1** (4 eq., 0.68 g, 2.74 mmol), EDAC (4 eq., 0.53 g, 2.74 mmol) and DMAP (0.8 eq., 0.067 g, 0.55 mmol) were dissolved in DCM (60 ml).

Yield: 0.21 g (51 %)

^{1}H NMR (400 MHz, $CDCl_3$): δ 7.17 – 7.20 (4H, m, ArH), 6.95 – 6.99 (4H, m, ArH) 2.76 – 2.85 (1H, m, CH), 2.66 – 2.70 (2H, m, CH_2), 2.44 (2H, tq, 2 x CH Cy), 2.15 – 2.24 (1H, m, CH), 1.96 – 2.05 (1H, m, CH), 1.82 – 1.88 (8H, m, 4 x CH_2 Cy), 1.35 (3H, d, J = 7.0, CH_3), 1.17 – 1.45 (22H, m, 6 x CH_2, 4 x CH_2 Cy, 2 x CH Cy), 0.94 – 1.09 (4H, m, 2 x CH_2), 0.88 (6H, t, 2 x CH_3) ppm.

^{13}C NMR (100.6 MHz, $CDCl_3$): δ 174.58 (carboxylic acid next to chiral centre), 171.71 (carboxylic acid in spacer), 148.49 (2 x ArO), 145.41 (2 x Ar Cy), 127.70

(4 x Ar CH), 121.07 (4 x Ar CH), 44.04 (2 x Ar CH Cy), 38.80 (chiral CH), 37.34 (2 x CH_2) 37.25 (2 x CH_2 Cy alk), 34.37 (4 x CH_2 Cy), 33.53 (4 x CH_2 Cy), 32.19 (2 x CH_2), 31.94 (CH_2 next to carboxylic acid in spacer), 28.49 (middle CH_2 in spacer), 26.63 (2 x CH_2), 22.70 (2 x CH_2), 17.14 (chiral CH_3), 14.11 (2 x CH_3) ppm.

IR (neat) $\widetilde{\nu}_{max}$: 2916, 2847, 1751, 1605, 1504, 1450, 1381, 1319, 1196, 1141, 1103, 1049, 1010, 964, 918, 841, 725, 625, 532 cm^{-1}.

MS m/z: 620.47 ($M^+ + NH_4^+$)

Elemental analysis: Calculated analysis for $C_{40}H_{58}O_4$: C 79.69, H 9.70. Found: C 79.59, H 9.74.

Synthesis of (*R*)-*Bis*-[4-(4-pentylcyclohexyl)phenyl]-2-methylpentanedioate (10)

The methodology used for the synthesis of compound **10** was similar to the one used for the preparation of **9**. The following quantities were used: (*R*)-(–)-2-methylglutaric acid, **5** (0.10 g, 0.68 mmol), PCH-5-phenol, **1** (4 eq., 0.68 g, 2.74 mmol), EDAC (4 eq., 0.53 g, 2.74 mmol) and DMAP (0.8 eq., 0.067 g, 0.55 mmol) were dissolved in DCM (60 ml).

Yield: 0.34 g (82 %)

^{1}H NMR (400 MHz, $CDCl_3$): δ 7.10 – 7.14 (4H, m, ArH), 6.89 – 6.94 (4H, m, ArH) 2.75 (1H, sext, J = 7.0, CH), 2.60 – 2.64 (2H, m, CH_2), 2.34 – 2.43 (2H, tq, 2 x CH Cy), 2.20 (1H, sext, J = 7.6, CH), 1.91 – 2.00 (1H, m, CH), 1.77 – 1.83 (8H, m, 4 x CH_2 Cy), 1.29 (3H, d, J = 7.0, CH_3), 1.19 – 1.39 (22H, m, 6 x CH_2, 4 x CH_2 Cy, 2 x CH Cy), 0.91 – 1.01 (4H, m, 2 x CH_2), 0.82 (6H, t, 2 x CH_3) ppm.

^{13}C NMR (100.6 MHz, $CDCl_3$): δ 174.58 (carboxylic acid next to chiral spacer), 171.72 (carboxylic acid in spacer), 148.50 (2 x ArO), 145.39 (2 x Ar Cy), 127.68 (4 x Ar CH), 121.06 (4 x Ar CH), 44.02 (2 x Ar CH Cy), 38.78 (chiral CH), 37.33 (2 x CH_2), 37.23 (2 x Cy CH alk), 34.36 (4 x CH_2 Cy), 33.52 (4 x CH_2 Cy), 32.18 (2 x CH_2) 31.92 (CH_2 next to carboxylic acid in spacer), 28.48 (middle CH_2 in spacer), 26.62 (2 x CH_2), 22.69 (2 x CH_2), 17.13 (chiral CH_3), 14.11 (2 x CH_3) ppm.

IR (neat) $\widetilde{\nu}_{max}$: 2917, 2847, 1751, 1504, 1450, 1381, 1319, 1196, 1142, 1103, 1057, 1018, 964, 918, 841, 725, 540 cm^{-1}.

MS m/z: 620.47 ($M^+ + NH_4^+$)

Elemental analysis: Calculated analysis for $C_{40}H_{58}O_4$: C 79.69, H 9.70. Found: C 79.50, H 9.67.

Synthesis of (*S*)-*Bis*-[4-(4-pentylcyclohexyl)phenyl]-2-phenylsuccinate (11)

The methodology used for compound **11** was similar to the one used for the preparation of **7**. The following quantities were used: (*S*)-(+)-phenylsuccinic acid, **6** (0.10g, 0.51 mmol), PCH-5-phenol, **1** (4 eq., 0.51 g, 2.06 mmol), EDAC (4 eq., 0.39 g, 2.06 mmol) and DMAP (0.8 eq., 0.05 g, 0.41 mmol) were dissolved in DCM (60 ml).

Yield: 0.13 g (39 %)

^{1}H NMR (400 MHz, $CDCl_3$): δ 7.30 – 7.43 (5H, m, 5 x ArH), 7.15 (4H, dd, *J* = 16.8 8.5, 4 x ArH), 6.86 – 6.94 (4H, m, 4 x ArH), 4.38 (1H, dd, *J* = 10.1, 5.2, CH), 3.50 (1H, dd, *J* = 17.1, 10.1, CH), 2.99 (1H, dd, *J* = 17.1, 5.5, CH) 2.37 – 2.47 (2H, m, 2 x CH Cy), 1.81 – 1.88 (8H, m, 4 x CH_2 Cy) 1.17 – 1.44 (22H, m, 6 x CH_2, 4 x CH_2 Cy, 2 x CH Cy), 0.95 – 1.07 (4H, m, 2 x CH_2), 0.86 – 0.90 (6H, m, CH_3) ppm.

^{13}C NMR (100.6 MHz, $CDCl_3$): δ 171.52 (carboxylic acid next to chiral centre), 170.24 (carboxylic acid in spacer), 148.60 (2 x ArO), 145.55 (2 x Ar Cy), 137.01 (chiral Ar), 129.07 (2 x Ar CH), 127.96 (Ar CH), 127.89 (2 x Ar CH), 127.67 (4 x Ar CH), 120.97 (4 x Ar CH), 47.36 (chiral CH), 44.04 (2 x Ar CHCy), 37.99 (CH_2 next to chiral centre), 37.33 (2 x CH_2), 37.24 (2 x Cy CH alk), 34.35 (4 x CH_2 Cy), 33.52 (4 x CH_2 Cy), 32.18 (2 x CH_2), 26.62 (2 x CH_2), 22.70 (2 x CH_2), 14.11 (2 x CH_3) ppm.

IR (neat) $\tilde{\nu}_{max}$: 2917, 2847, 1751, 1705, 1597, 1504, 1450, 1404, 1358, 1327, 1204, 1150, 1134, 1018, 949, 833, 702, 640, 532 cm^{-1}.

MS m/z: 668.47 ($M^+ + NH_4^+$)

Elemental analysis: Calculated analysis for $C_{44}H_{58}O_4$: C 81.19, H 8.95. Found: C 80.96, H 9.03.

5.3.3 Synthetic Pathway 2

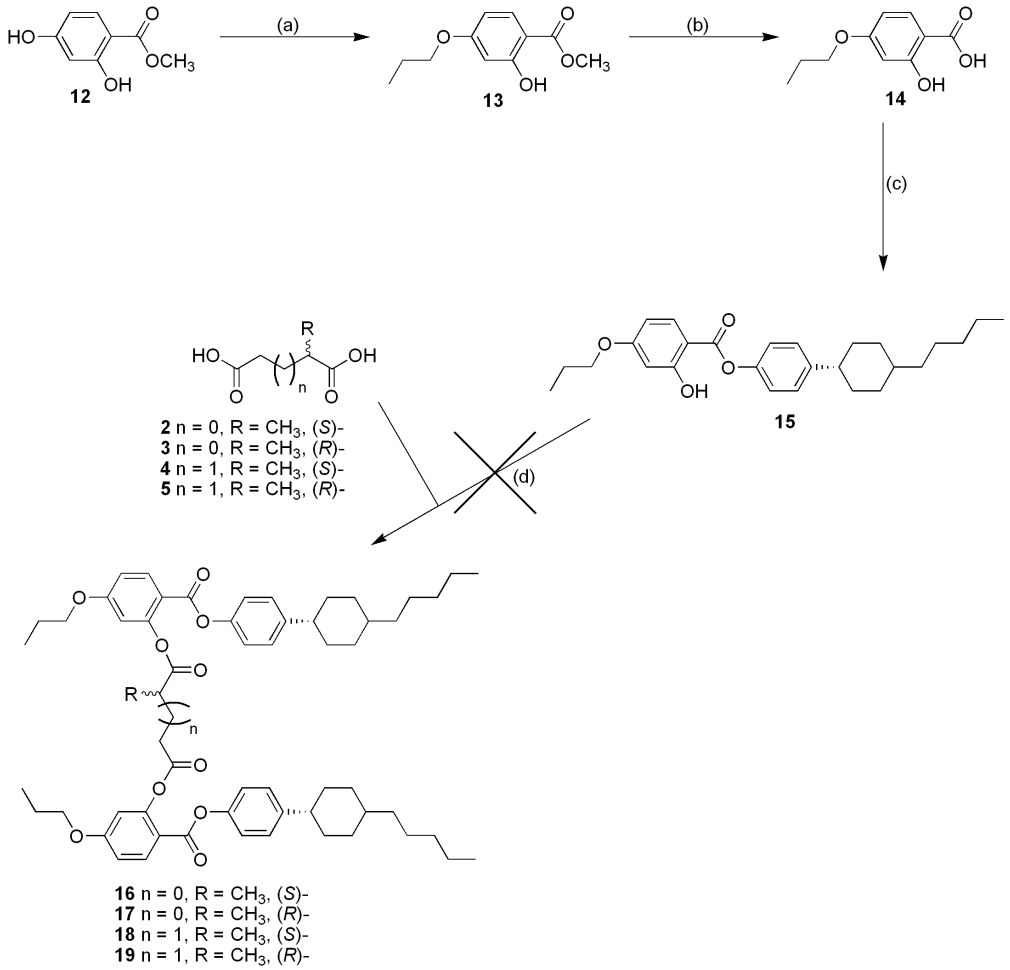

Scheme 5.2: *Synthetic pathway 2 for the synthesis of dimers* **16 – 19**.

Synthesis of methyl 2-hydroxy-4-propoxybenzoate (13)

Methyl 2,4-dihydroxybenzoate (**12**, 20.0 g, 0.12 mol), bromopropane (1 eq., 14.76 g, 0.12 mol) and potassium carbonate (2 eq., 33.17 g, 0.24 mol) were dissolved in acetone (500 ml) and heated under reflux for 4 days at 66 ° C. Upon completion of the reaction (TLC), the solution was filtered to remove any precipitated material, washed in acetone, and the solvent was removed *in vacuo* [3]. The crude product was purified by column chromatography over silica gel (hexane/DCM 1:1 v/v as eluent). The product was isolated as a colourless oil.

Yield: 21.29 g (85 %)

^{1}H NMR (400 MHz, $CDCl_3$): δ 10.87 (1H, s, OH), 7.61 (1H, dd J = 7.0, 2.4, ArH), 6.31 – 6.33 (2H, m, 2 x ArH) 3.82 (2H, t, OCH_2), 3.80 (3H, s, OCH_3) 1.71 (2H, sext, CH_2) 0.93 (3H, t, CH_3) ppm.

IR (neat) $\tilde{\nu}_{max}$: 3109, 2963, 2878, 1666, 1620, 1582, 1504, 1443, 1342, 1250, 1219, 1188, 1134, 1096, 1065, 995, 957, 833, 772, 733, 694, 640, 525 cm^{-1}.

MS m/z: 211.0971 $(M + H)^+$

Synthesis of 2-hydroxy-4-propoxybenzoic acid (14)

Compound **13** (18.00 g, 0.09 mol), and lithium hydroxide (3 eq., 6.15 g, 0.26 mol) were dissolved in 3:1 methanol – water (300:100 ml) and heated under reflux for approximately 45 hours at 70 ° C. Upon completion of the reaction (TLC), the solution was filtered to remove any precipitate and a solution of water/1 M HCl acid (1:1 v/v) was added [4]. The product precipitated from the reaction mixture and was the filtered off. The crude product was recrystallised from ethanol and isolated as colourless crystals.

Yield: 13.34 g (79 %)

^{1}H NMR (400 MHz, D_6-DMSO): δ 11.76 (1H, s, OH), 7.59 (1H, d, J = 8.9, ArH), 6.38 (1H, dd, J = 8.9, 2.4, ArH), 6.35 (1H, d, J = 2.4, ArH), 3.86 (2H, t, OCH_2), 1.62 (2H, sext, CH_2), 0.87 (3H, t, CH_3) ppm.

IR (neat) $\tilde{\nu}_{max}$: 3078, 2983, 2947, 2878, 2546, 1651, 1620, 1582, 1504, 1458, 1443, 1396, 1358, 1312, 1227, 1196, 1150, 1096, 1042, 1011, 972, 895, 856, 779, 694, 640, 602, 532 cm^{-1}.

MS m/z: 219.06 $(M + Na^+)$

Synthesis of 4-(4-pentylcyclohexyl)phenyl 2-hydroxy-4-propoxybenzoate (15)

Compound **14** (6.00 g, 0.03 mol), compound **1** (1 eq., 7.50 g, 0.03 mol), EDAC (1.1 eq., 6.40 g, 0.03 mol) and DMAP (0.2 eq., 0.70 g, 6.1 mmol) were dissolved in DCM (250 ml) and stirred for 21 hours at room temperature. Upon completion of the reaction (TLC), the solution was washed with water and dried over anhydrous magnesium sulphate. The drying agent was filtered off and the solvent removed *in vacuo* [5]. The crude product was purified by column chromatography over silica gel (DCM/hexane, 2:1 v/v as eluent). The product was recrystallised from ethanol as colourless, needle-like crystals.

Yield: 5.17 g (39 %)

^{1}H NMR (400 MHz, $CDCl_3$): δ 10.74 (1H, s, OH), 7.94 (1H, d, J = 8.9, ArH), 7.23 – 7.27 (2H, m, ArH) 7.09 (2H, dt, J = 8.5, 2.1, ArH), 6.51 (1H, dd, J = 8.9, 2.4, ArH) 6.47 (1H, d, J = 2.4, ArH), 3.97 (2H, t, OCH_2), 2.49 (1H, tt, ArHCy), 1.80 – 1.91 (6H, m, CH_2), 1.44 (2H, qd, CyH), 1.20 – 1.34 (9H, m, CH_2), 1.04 (4H, t, CH_3), 0.89 (3H, t, CH_3) ppm.

^{13}C NMR (100.6 MHz, $CDCl_3$): δ 169.00 (carboxylic acid), 165.78 (ArO), 164.41 (ArOH), 148.07 (ArO), 145.84 (Ar Cy), 131.65 (Ar CH), 127.86 (2 x Ar CH), 121.32 (2 x Ar CH), 112.82 (Ar next to carboxylic acid), 108.32 (Ar CH), 101.23 (Ar CH), 69.79 (CH_2O), 44.09 (Ar CH Cy), 37.33 (CH_2), 37.26 (Cy CH alkane), 34.39 (Cy CH_2), 33.54 (Cy CH_2), 32.19 (CH_2), 26.63 (CH_2), 22.69 (CH_2), 22.33 (CH_2), 14.06 (CH_3), 10.39 (CH_3) ppm.

IR (neat): $\tilde{\nu}_{max}$ 3140, 2916, 2847, 1667, 1628, 1582, 1504, 1466, 1396, 1350, 1250, 1196, 1126, 1072, 1042, 1011, 972, 903, 872, 810, 772, 718, 694, 656, 610, 540 cm^{-1}.

MS m/z: 425.27 $(M + H)^+$

UV: λ_{max} = 265.50 nm.

HPLC: > 99.0 % pure at 267 nm (eluted with 20% chloroform in acetonitrile).

5.3.4 Synthetic Pathway 3

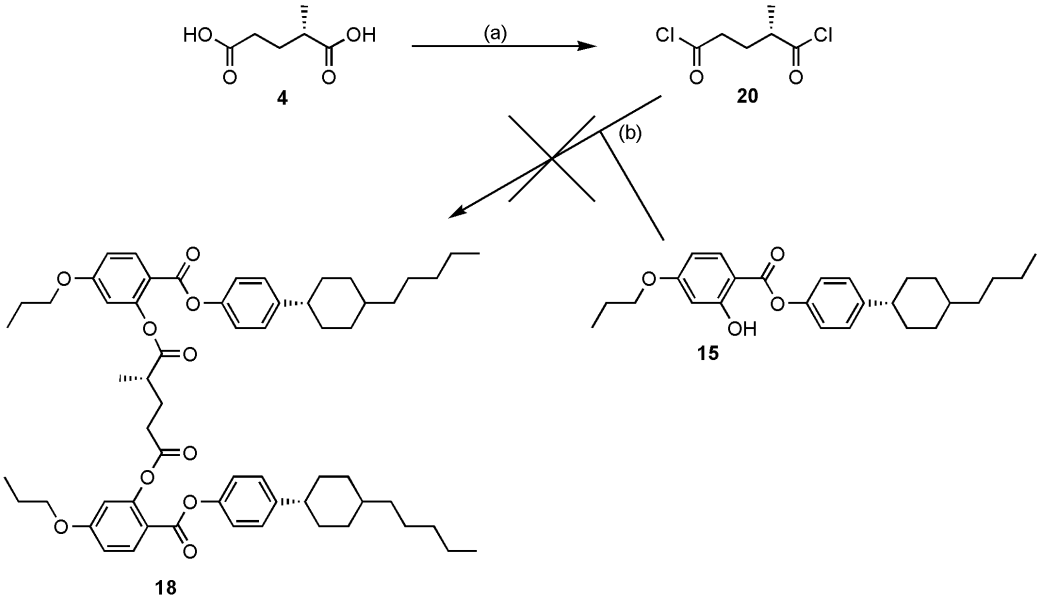

Scheme 5.3: *Attempted synthesis of compound* **18.**

Synthesis of (*S*)-2-methylpentanedioyl dichloride (20)

(*S*)-(+)-2-methylglutaric acid (0.15 g, 1.00 mmol) was dissolved in thionyl chloride (1 ml) and heated at 60 ° C for 5 hours. The solution was cooled, washed in toluene (10 ml x 3) and the solvent removed. The crude product was then washed with hexane (10 ml x 3) and the solvent removed. The acid chloride was used as soon as it was synthesised [6].

Yield: 0.14 g (77 %) wet.

5.3.5 Synthetic Pathway 4

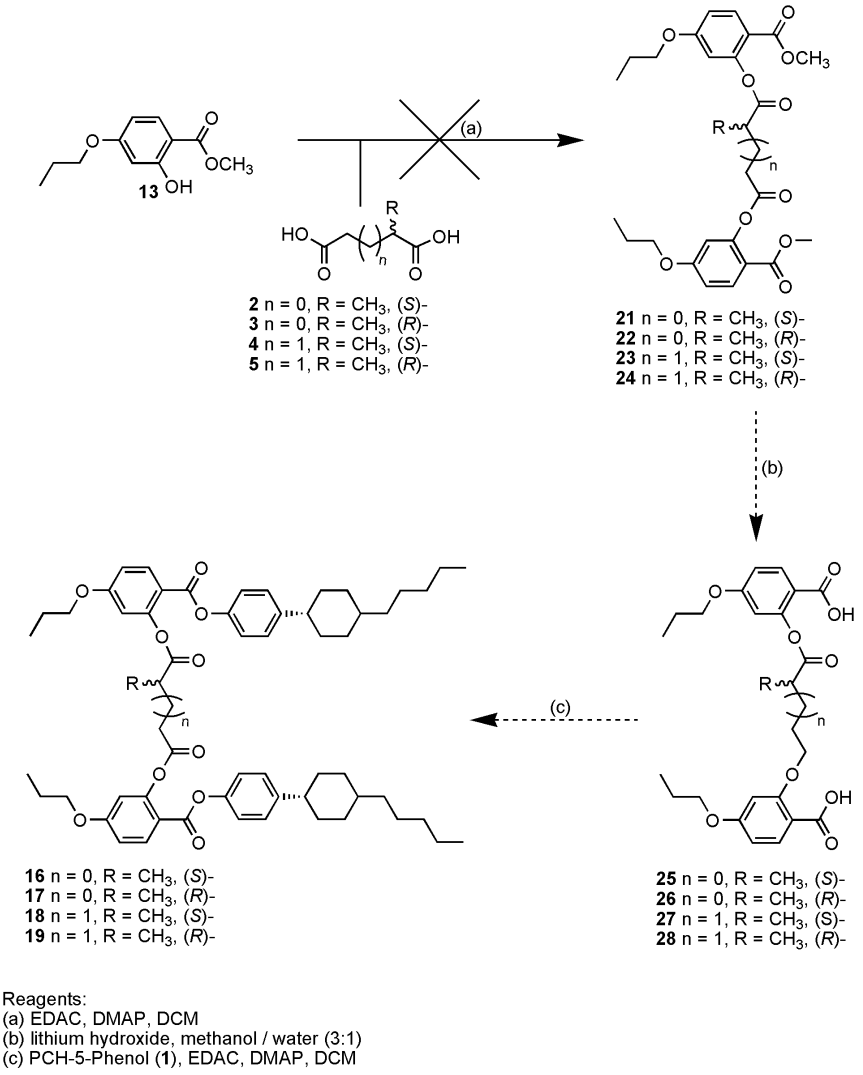

Scheme 5.4: *Synthetic pathway 4 for the synthesis of dimers* **16 – 19**.

5.3.5 Synthetic Pathway 5

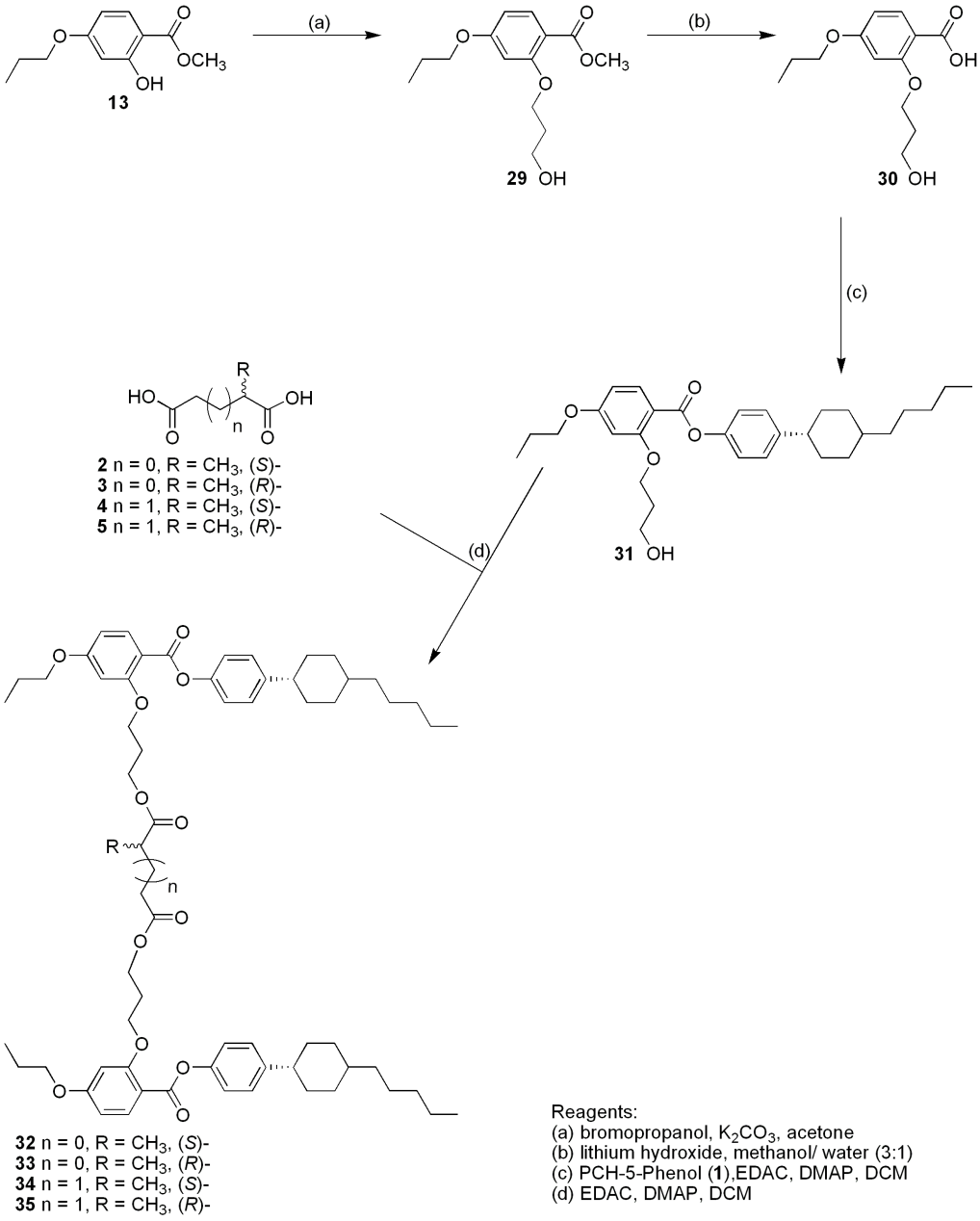

Scheme 5.5: *Synthetic pathway 5 for the synthesis of dimers* **32** – **35**.

Synthesis of methyl 2-(3-hydroxypropoxy)-4-propoxybenoate (29)

Potassium carbonate (2.2 eq., 10.12 g, 0.07 mol) was added to a solution of compound **13** (6.73 g, 0.03 mol) and 3-bromo-1-propanol (2 eq., 0.07 g, 0.07 mol) in acetone (250 ml). The reaction mixture was and heated under reflux for 3 days [3]. Upon completion of the reaction (TLC), the crude product was purified by column chromatography over silica gel (DCM to recover unreacted starting material and DCM/methanol 10:1 v/v to remove the product). The product was isolated as a colourless oil.

Yield: 8.33 g (97 %)

^{1}H NMR (400 MHz, $CDCl_3$): δ 7.86 (1H, d, ArH, J = 8.9), 6.43 – 6.47 (2H, m, ArH), 4.15 (2H, t, CH_2), 3.92 (2H, t, CH_2), 3.86 (2H, t, CH_2), 3.80 (3H, s, OCH_3), 3.50 (1H, t, OH), 2.01 – 2.10 (2H, m, CH_2), 1.78 (2H, sext, CH_2), 1.00 (3H, t, CH_3) ppm.

IR (neat): $\tilde{\nu}_{max}$ 3426, 2947, 2878, 1705, 1605, 1574, 1504, 1466, 1435, 1396, 1327, 1250, 1188, 1142, 1089, 1049, 964, 910, 833, 772, 633, 540 cm^{-1}.

MS m/z: 291.12 ($M^+ + Na^+$)

Synthesis of 2-(3-hydroxypropoxy)-4-propoxybenzoic acid (30)

The methodology used for the synthesis of **30** was similar to the preparation of compound **14**, except that the crude product was recrystallised from hexane/ethyl acetate (1:1 v/v) The following quantities were used: compound **29** (8.00g, 0.03 mol), and lithium hydroxide (3 eq., 2.14 g, 0.09 mol) were dissolved in 3:1 methanol/water (150:50 ml).

Yield: 2.56 g (34 %)

^{1}H NMR (400 MHz, $CDCl_3$): δ 8.07 (1H, d, J = 8.9, ArH), 6.58 (2H, dd, J = 8.9, 2.1, ArH), 6.51 (1H, d, J = 2.1, ArH), 4.31 (2H, t, CH_2), 3.96 (2H, t, CH_2), 3.90 (2H, t, CH_2), 2.13 (2H, quint, CH_2), 1.81 (2H, sext, CH_2), 1.03 (3H, t, CH_3) ppm.

IR (neat): $\tilde{\nu}_{max}$ 3441, 3302, 2940, 2878, 2615, 1690, 1605, 1574, 1504, 1420, 1396, 1327, 1234, 1188, 1126, 1080, 1026, 987, 910, 818, 772, 694, 648, 586 cm^{-1}.

MS m/z: 277.10 ($M^+ + Na^+$)

Synthesis of 4-(4-pentylcyclohexyl) phenyl 2-(3-hydroxypropoxy)-4-propoxybenzoate (31)

The methodology used for compound **31** was similar to the preparation of compound **15**, except that the reaction mixture was left for 5 days and the eluent for column chromatography was DCM / ethyl acetate 20:1 v/v. The following quantities were used: compound **30** (2.40 g, 9.44 mmol), compound **1** (1 eq., 2.33 g, 9.44 mmol), EDAC (1.2 eq., 2.17 g, 10.33 mmol) and DMAP (0.2 eq., 0.28 g, 2.27 mmol) were dissolved in DCM (100 ml).

Yield: 2.70 g (59 %)

^{1}H NMR (400 MHz, $CDCl_3$): δ 8.04 (1H, d, J = 8.9, ArH), 7.13 (2H, d, J = 8.5, 2 x ArH), 7.00 (2H, d, J = 8.5, 2 x ArH), 6.48 (1H, dd, J = 8.9, 2.4, ArH), 6.45 (1H, d, J = 2.4, ArH), 4.15 (2H, t, CH_2), 3.93 (2H, t, CH_2), 3.80 (2H, t, CH_2), 2.39 (1H, tt, CH Cy), 2.00 – 2.06 (2H, m, CH_2), 1.73 – 1.84 (2H, m, CH_2), 1.37 (1H, td, CH Cy), 1.11 – 1.27 (16H, m, 4 x CH_2, 4 x CH_2 Cy), 0.99 (3H, t, CH_3), 0.83 (3H, t, CH_3) ppm.

^{13}C NMR (100.6 MHz, $CDCl_3$): δ 164.66 (carboxylic acid), 163.77 (ArO), 161.28 (ArO), 148.74 (ArO), 144.83 (Ar Cy), 134.72 (Ar CH), 127.60 (2 x Ar CH), 121.57 (2 x Ar CH), 110.41 (Ar next to carboxylic acid), 105.58 (Ar CH), 99.65 (Ar CH), 69.79 (OCH_2), 68.51 (OCH_2), 61.88 ($HOCH_2$), 44.02 (Ar CH Cy), 37.37 (Cy CH alkane), 37.26 (CH_2), 34.40 (2 x CH_2 Cy), 33.58 (2 x CH_2 Cy), 32.18 (CH_2), 31.70 (CH_2), 26.62 (CH_2), 22.69 (CH_2), 22.38 (CH_2), 14.15 (CH_3), 10.35 (CH_3) ppm.

IR (neat): $\tilde{\nu}_{max}$ 3310, 2916, 2878, 2847, 1728, 1605, 1574, 1504, 1458, 1420, 1389, 1327, 1296, 1227, 1196, 1126, 1042, 1011, 964, 872, 818, 764, 725, 694, 664, 640, 602, 548 cm^{-1}.

MS m/z: 483.31 ($M^+ + H^+$)

UV: λ_{max} = 262.00 nm.

HPLC: = > 98.5 % pure at 262 nm (eluted with 20% chloroform in acetonitrile).

Synthesis of (*S*)-*Bis*-[4-(4-pentylcyclohexyl) phenyl 2-(3-hydroxypropoxy)-4-propoxybenzoate]-2-methylsuccinate (32)

Compound **31** (2.2 eq., 0.4 g, 0.83 mmol), compound, **2** (1 eq., 0.05 g, 0.38 mmol), EDAC (2.4 eq., 0.17 g, 0.9 mmol) and DMAP (0.2 eq., 0.01 g, 0.08 mmol) were dissolved in DCM (60 ml) and stirred for 5 days at room temperature. After completion of the reaction (TLC), the solution was washed with water and dried over anhydrous magnesium sulphate. The magnesium sulphate was filtered off and then the solvent removed. The crude product was purified by column chromatography over silica gel (DCM / ethyl acetate 20:1 v/v) and the product isolated as a viscous oil.

Yield: 0.09 g (22 %)

^{1}H NMR (400 MHz, $CDCl_3$): δ 7.95 (2H, d, J = 8.9, 2 x ArH), 7.14 (4H, d, J = 8.5, 4 x ArH), 7.00 (4H, dd, J = 8.5, 1.5, 4 x ArH), 6.46 (2H, dd, J = 8.9, 1.8, 2 x ArH), 6.42 (2H, d, J = 1.8, 2 x ArH), 4.23 (4H, q, 2 x OCH_2), 3.99 – 4.02 (4H, m, 2 x OCH_2), 3.90 (4H, td, 2 x OCH_2), 2.75 – 2.84 (1H, m, CH), 2.61 (1H, q, J = 8.2, CH), 2.39 (2H, tt, 2 x CH Cy), 2.29 (1H, dd, J = 16.5, 6.1, CH), 2.00 – 2.08 (4H, m, 2 x CH_2), 1.71 – 1.84 (4H, m, 2 x CH_2), 1.37 (2H, td, 2 x CH Cy), 1.13 – 1.27 (32H, m, 16 x CH_2), 1.09 (3H, d, J = 7.0, CH_3), 0.95 – 1.02 (6H, m, 2 x CH_3), 0.79 – 0.87 (6H, m, 2 x CH_3) ppm.

^{13}C NMR (100.6 MHz, $CDCl_3$): δ 175.05 (carboxylic acid next to chiral centre), 171.64 (carboxylic acid in spacer), 164.31 (2 x carboxylic acid next to aromatic ring), 163.95 (2 x ArO), 161.20 (2 x ArO), 148.95 (2 x ArO), 144.96 (2 x Ar Cy), 134.38 (2 x ArCH), 127.64 (4 x Ar CH), 121.49 (4 x Ar CH), 111.33 (2 x Ar next to carboxylic acid), 105.53 (2 x Ar CH), 100.24 (2 x Ar CH), 69.75 (2 x OCH_2), 65.07 (2 x OCH_2), 61.36 (d, 2 x OCH_2), 44.05 (2 x Ar CH Cy), 37.52 (CH_2 next to chiral centre), 37.34 (2 x CH_2), 37.25 (2 x Cy CH alkane), 35.74 (chiral CH), 34.37 (4 x CH_2 Cy), 33.55 (4 x CH_2 Cy), 32.17 (2 x CH_2), 28.52 (d, 2 x CH_2), 26.61 (2 x CH_2), 22.68 (2 x CH_2), 22.41 (2 x CH_2), 16.97 (chiral CH_3), 14.09 (2 x CH_3), 10.43 (2 x CH_3) ppm.

IR (neat) $\tilde{\nu}_{max}$: 2916, 2847, 1728, 1605, 1586, 1504, 1458, 1435, 1389, 1327, 1242, 1188, 1134, 1018, 972, 872, 833, 764, 694, 656, 617, 602, 540 cm^{-1}.

MS m/z: 1083.61 ($M^+ + Na^+$)

UV: λ_{max} = 259.50 nm.

HPLC: > 98.7 % pure at 259 nm (eluted with 20% chloroform in acetonitrile).

Synthesis of (*R*)-*Bis*-[4-(4-pentylcyclohexyl) phenyl 2-(3-hydroxypropoxy)-4-propoxybenzoate]-2-methylsuccinate (33)

The methodology used was similar to the preparation of **32**, except that the reaction was stirred for 20 days at room temperature and the eluent used was hexane/ethyl acetate (2:1 v/v). The following quantities were used: Compound **31** (2.2 eq., 0.4 g, 0.83 mmol), compound **3** (1 eq., 0.05 g, 0.38 mmol), EDAC (4.5 eq., 0.33g, 1.72 mmol) and DMAP (1.1 eq., 0.05 g, 0.41 mmol were dissolved in DCM (60 ml).

Yield: 0.01 g (3 %)

^{1}H NMR (400MHz, $CDCl_3$): δ 7.95 (2H, d, J = 8.9, 2 x ArH), 7.14 (4H, d, J = 8.5, 2 x ArH), 7.00 (4H, dd, J = 8.5, 1.5, 4 x ArH), 6.46 (2H, dd, J = 8.9, 1.8, 2 x ArH), 6.42 (2H, d, J = 1.8, 2 x ArH), 4.23 (4H, q, 2 x OCH_2), 3.99 – 4.03 (4H, m, 2 x OCH_2), 3.90 (4H, td, 2 x OCH_2), 2.75 –2.84 (1H, m, CH), 2.61 (1H, q, J = 8.2, CH), 2.39 (2H, tt, 2 x CH Cy), 2.29 (1H, dd, J = 16.5, 5.8, CH), 2.05 (4H, s, 2 x CH_2) 1.71 – 1.84 (4H, m, 2 x CH_2), 1.36 (2H, qd, 2 x CH Cy), 1.13 – 1.27 (32H, 16 x CH_2), 1.09 (3H, d, J = 7.0, CH_3), 0.95 – 1.00 (6H, m, 2 x CH_3), 0.83 (6H, t, 2 x CH_3) ppm.

^{13}C NMR (100.6 MHZ, $CDCl_3$): δ 175.13 (carboxylic acid next to chiral centre), 171.86 (carboxylic acid in spacer), 164.32 (2 x carboxylic acid next to aromatic ring), 161.20 (2 x ArO), 148.96 (2 x ArO), 145.00 (2 x Ar Cy), 134.43 (2 x Ar CH), 127.67 (4 x Ar CH), 121.51 (4 x Ar CH), 111.33 (2 x Ar next to carboxylic acid), 105.51 (2 x Ar CH), 100.24 (2 x Ar CH), 69.77 (2 x OCH_2), 65.13 (2 x OCH_2), 60.56 (d, 2 x OCH_2), 44.07 (2 x Ar CH Cy), 37.68 (CH_2 next to chiral spacer), 37.35 (2 x CH_2), 37.25 (2 x Cy CH alk), 35.80 (chiral CH), 34.39 (4 x CH_2 Cy), 33.57 (4 x CH_2 Cy), 32.18 (2 x CH_2), 28.56 (d, 2 x CH_2), 26.62 (2 x CH_2), 22.69 (2 x CH_2), 22.44 (2 x CH_2), 16.99 (chiral CH_3), 14.10 (2 x CH_3), 10.45 (2 x CH_3) ppm.

IR (neat) $\tilde{\nu}_{max}$: 2970, 2924, 2855, 1728, 1605, 1574, 1504, 1458, 1373, 1342, 1234, 1196, 1165, 1026, 964, 856, 764, 625, 540, 517 cm^{-1}.

MS m/z: 1083.61 ($M^+ + Na^+$)

UV: λ_{max} = 259.50 nm.

HPLC: > 98.3 % pure at 259 nm (eluted with 20% chloroform in acetonitrile).

Synthesis of (*S*)-*Bis*-[4-(4-pentylcyclohexyl) phenyl 2-(3-hydroxypropoxy)-4-propoxybenzoate]-2-methylpentanedioate (34)

The methodology used was similar to the preparation of **32**, except that the reaction was stirred for 19 days at room temperature and the eluent used was DCM/ethyl acetate (20:1 v/v). The following quantities were used: Compound **31** (2.2 eq., 0.4 g, 0.83 mmol), compound **4** (1 eq., 0.06 g, 0.38 mmol), EDAC (2.4 eq., 0.17 g, 0.9 mmol) and DMAP (0.2 eq., 0.01 g, 0.08 mmol) were dissolved in DCM (60 ml).

Yield: 0.09 g (22 %)

^{1}H NMR (400 MHz, $CDCl_3$): δ 8.00 (2H, d, J = 8.9, 2 x ArH), 7.20 (4H, m, 4 x ArH), 7.05 (4H, m, 4 x ArH), 6.51 (2H, dd, J = 8.9, 2.1, 2 x ArH), 6.47 (2H, d, J = 2.1, 2 x ArH), 4.27 (4H, q, 2 x OCH_2), 4.07 4H, td, 2 x OCH_2), 3.95 (4H, t, 2 x OCH_2), 2.39 – 2.48 (4H, m, 2 x CH Cy, 2 x CH), 2.33 (1H, t, J = 7.6, CH), 2.23 – 2.28 (2H, m, 2 x CH), 2.07 – 2.15 (4H, m, 2 x CH_2), 1.78- 1.90 (4H, m, 2 x CH_2), 1.42 (2H, td, 2 x CH Cy), 1.18 – 1.33 (32H, m, 16 x CH_2), 1.10 (3H, d, J = 7.0, CH_3), 1.00 – 1.05 (6H, m, 2 x CH_3), 0.84 – 0.92 (6H, m , 2 x CH_3) ppm.

^{13}C NMR (100.6 MHz, $CDCl_3$): δ 175.77 (carboxylic acid next to chiral centre), 172.90 (carboxylic acid in spacer), 164.32 (2 x carboxylic acid next to aromatic ring), 163.96 (2 x ArO), 161.21 (2 x ArO), 148.96 (2 x ArO), 145.00 (2 x Ar Cy), 134.44 (2 x Ar CH), 127.67 (4 x Ar CH), 121.51 (4 x Ar CH), 111.36 (2 x Ar next to carboxylic acid), 105.50 (2 x Ar CH), 100.25 (2 x Ar CH), 69.78 (2 x OCH_2), 65.13 (2 x OCH_2), 61.19 (2 x OCH_2), 44.06 (2 x Ar CH Cy), 38.68 (chiral CH), 37.36 (2 x CH_2), 37.26 (2 x Cy CH alk), 34.39 (4 x CH_2 Cy), 33.57 (4 x CH_2 Cy), 32.20 (2 x CH_2), 31.75 (CH_2 in spacer), 28.59 (CH_2 next to chiral centre), 28.45 (2 x CH_2), 26.63 (2 x CH_2), 22.70 (2 x CH_2), 22.43 (2 x CH_2), 17.02 (chiral CH_3), 14.11 (2 x CH_3), 10.45 (2 x CH_3) ppm.

IR (neat) $\widetilde{\nu}_{max}$: 2916, 2847, 1728, 1605, 1574, 1504, 1458, 1435, 1389, 1327, 1296, 1242, 1188, 1126, 1034, 1018, 972, 872, 833, 764, 694, 633, 602, 540 cm^{-1}.

MS m/z: 1097.63 ($M^+ + Na^+$)

UV: λ_{max} = 259.50 nm.

HPLC: > 98.0 % pure at 259 nm (eluted with 20% chloroform in acetonitrile).

Synthesis of (*R*)-*Bis*-[4-(4-pentylcyclohexyl) phenyl 2-(3-hydroxypropoxy)-4-propoxybenzoate]-2-methylpentanedioate (35)

The methodology used for the synthesis of **35** was similar to the preparation of **32**, except that the reaction was stirred for 23 days at room temperature and the eluent used was hexane/ethyl acetate (2:1 v/v). The following quantities were used: Compound **31** (2.2 eq., 0.4 g, 0.83 mmol), compound **5** (1 eq., 0.06 g, 0.38 mmol), EDAC (2.4 eq., 0.17 g, 0.9 mmol) and DMAP (0.2 eq., 0.01 g, 0.08 mmol) were dissolved in DCM (60 ml).

Yield: 0.04 g (9 %)

^{1}H NMR (400 MHZ, $CDCl_3$): δ 7.96 (2H, d, *J* = 8.9, 2 x ArH), 7.15 (4H, m, 4 x ArH), 7.00 (4H, m, 4 x ArH), 6.46 (2H, dd, *J* = 8.9, 2.1, 2 x ArH), 6.42 (2H, d, *J* = 2.1, 2 x ArH), 4.22 (4H, q, 2 x OCH_2), 4.02 (4H, td, 2 x OCH_2), 3.91 (4H, t, 2 x OCH_2), 2.34 – 2.43 (4H, m, 2 x CH Cy, 2 x CH), 2.28 (1H, t, *J* = 7.6, CH), 2.18 – 2.24 (2H, m, 2 x CH), 2.03 – 2.10 (4H, m, 2 x CH_2), 1.72 – 1.89 (4H, m, 2 x CH_2), 1.36 (2H, qd, 2 x CH Cy), 1.13 – 1.27 (32H, m, 16 x CH_2), 1.05 (3H, d, *J* = 7.0, CH_3), 0.96 – 1.00 (6H, m, 2 x CH_3), 0.83 (6H, t, 2 x CH_3) ppm.

^{13}C NMR (100.6 MHz, $CDCl_3$): δ 175.77 (carboxylic acid next to chiral spacer), 172.91 (carboxylic acid in spacer), 164.33 (2 x carboxylic acid next to aromatic ring), 163.97 (2 x ArO), 161.21 (2 x ArO), 148.97 (2 x ArO), 145.01 (2 x Ar Cy), 134.44 (2 x Ar CH), 127.67 (4 x Ar CH), 121.51 (4 x Ar CH), 111.38 (2 x Ar next to carboxylic acid), 105.51 (2 x Ar CH), 100.27 (2 x Ar CH), 69.79 (2 x OCH_2), 65.15 (2 x OCH_2), 61.21 (2 x OCH_2), 44.07 (Ar CH Cy), 38.69 (chiral CH), 37.36 (2 x CH_2), 37.27 (2 x Cy CH alk), 34.39 (4 x CH_2 Cy), 33.58 (4 x CH_2 Cy), 32.20 (2 x CH_2), 31.76 (CH_2 in spacer), 28.57 (d, CH_2 next to chiral centre), 28.46 (2 x CH_2), 26.63 (2 x CH_2), 22.70 (2 x CH_2), 22.44 (2 x CH_2), 17.02 (chiral CH_3), 14.11 (2 x CH_3), 10.45 (2 x CH_3) ppm.

IR (neat) $\widetilde{\nu}_{max}$: 2916, 2847, 1728, 1605, 1574, 1504, 1458, 1435, 1389, 1327, 1296, 1242, 1188, 1126, 1034, 1018, 980, 872, 826, 764, 725, 694, 656, 602, 540 cm^{-1}.

MS m/z: 1097.63 ($M^+ + Na^+$)

UV: λ_{max} = 259.50 nm.

HPLC: > 97.0 % pure at 259 nm (eluted with 20% chloroform in acetonitrile).

5.4 Experimental Methods

5.4.1 Contact Studies

Contact studies are a qualitative method used to investigate mesophase behaviour in a binary mixture over the full concentration range, particularly to determine helical twist sense of a target material. Additionally, it is possible to investigate pitch variation of the helical macrostructure, and to determine if any other mesophase behaviour can be induced by doping a nematic liquid crystal with a chiral dopant. The dopant does not have to be a liquid crystal itself but it must be miscible in the host.

For binary mixtures, it was hoped that the helical twisting power of the synthesised materials would reduce the pitch length with increasing concentration in the host to a point where blue phases would be observed.

A small amount of a chiral compound was placed on the slide and covered with a coverslip and an achiral nematic liquid crystal host (E7, available from Merck) added around the chiral compound by capillary flow, as depicted in Figure 5.1.

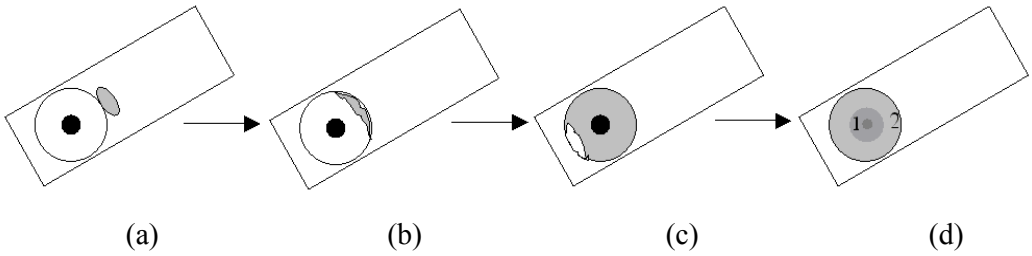

Figure 5.1: *Preparation of contact slides:* (a) *shows the chiral dopant on a microscope slide; (b) shows the presence of the achiral compound under the coverslip as it begins to flow via capillary action; (c) shows the achiral compound almost fully surrounding the chiral dopant;* (d) *Shows the chiral dopant surrounded by the nematic host. At point 1 the concentration of chiral dopant is the highest and so chirality is at the strongest. At point 2 the concentration of chiral dopant is the lowest and so chirality is at the weakest.*

There is therefore, a concentration gradient going from the centre outwards, i.e. from 1 to 2.

As the chiral dopant dissolved into the host mixture a concentration gradient formed. Depending on the helical twisting power of the dopant, rapid changes to the pitch were observed in the host mixture. If the helical twisting power is large then blue phases could be induced. Figure 5.2 shows typical pitch changes that are observed in a contact preparation. The pitch is tightening as the concentration increases (top to bottom in the figure). After the initial mixing at room temperature the mixture was heated to the isotropic liquid and examined on cooling slowly into the liquid crystal mesophase.

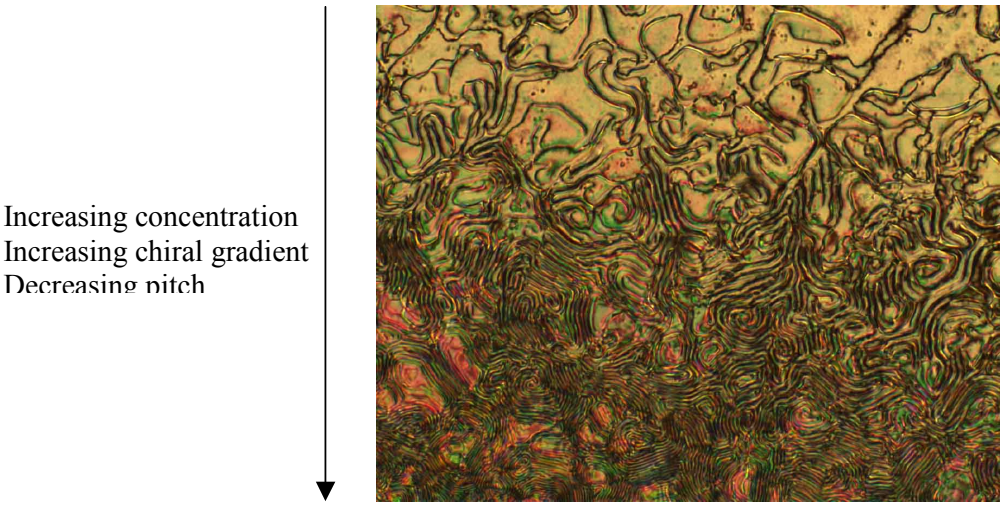

Figure 5.2: *Optical micrograph showing a chiral gradient produced by the addition of a chiral liquid crystal to an achiral nematic host (compound* **9** *in* E7 *at 55.0 °C, magnification x 100).*

5.4.2 Mixture Work

Phase diagrams and the phase rule are quantitative methods used to investigate mesophase behaviour for binary mixtures over specific concentration ranges. As with the contact studies, these experiments can be used to investigate the variation of the pitch length as a function of concentration, and to determine if any additional mesophase behaviour can be induced by doping a nematic liquid crystal with a chiral dopant.

In order to prepare binary mixtures, a chiral compound and an achiral compound (E7) were thoroughly mixed before being place on a microscope slide and covered with a coverslip. A number of concentrations were prepared in order to determine which mixture ratio of dopant-to-host would provide a blue phase with the widest temperature range. However, due to the low yields of the H-shaped dimers, there was insufficient material available to complete extensive studies on binary phase diagrams.

5.4.3 Pitch Measurements and Helical Twisting Power Studies

Grandjean-Cano wedges were used to determine the helical pitch (twist) in chiral nematic liquid crystals [7, 8, 9]. Due to its shape, the wedge cell increases in thickness from the thinnest part, to the edge, which is the thickest. When a chiral nematic compound is put in the wedge cell planar alignment of the helical structure occurs. The size of the wedge cell gap determines how many disclination lines of the chiral nematic material are observed (number of half pitches from top to bottom), and the distance between them can be used to determine the pitch length. At the narrowest point of the wedge, only a single twist might be present, whereas at the edge of the wedge, the number of twists could be found. An illustration of this structure is shown in Figure 5.3. The number of twists present must be an integral number and as a result of this disclinations that are formed [8]. These disclinations show up as straight lines going across the wedge cell. The lines can generally be seen with the naked eye. A number of techniques can be used to measure the distance between the lines. Callipers give an electronic reading, but have a large error for very small measurements. Small distances can more accurately be measured using a polarising optical microscope, either with a graticule or camera attached to a monitor, which then allows the distance between the lines to be measured using a ruler, and subsequently calibrated to give the distance.

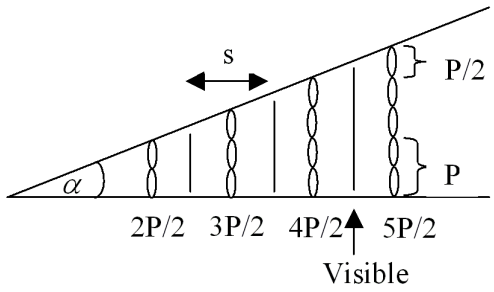

Figure 5.3: *Illustration of chiral nematic compound in a Cano Wedge* (based on Fig 5.17 from [8])

The value of the pitch can be determined by the equation shown in Equation 5.1 below, where P is the pitch, s is the distance between the lines, and α is the angle of the wedge [10].

$$P = 2s \tan\alpha \qquad \textbf{(Equation 5.1 [19])}$$

In order to prepare one mixture, a chiral compound (dopant) was thoroughly mixed with an achiral compound (host). Usually three or more of these mixtures were made up of different concentrations. Confirmation of the miscibility between the dopant and host was determined by examining the sample prior to filling the wedge by observation in the polarising microscope. Wedge cells, with a $\tan\alpha$ value of 0.0092, were then filled with the mixtures *via* capillary flow and the cells left overnight to allow the mixtures to settle. The distances between the disclination lines that appeared in the cells were subsequently measured. For each mixture, the pitch value was determined. The lower the concentration of the chiral compound the smaller the number twists, for the same thickness in a Cano wedge. This means the value of s is larger.

Once the pitch values for each mixture have been calculated, a graph of pitch against reciprocal concentration was plotted. A line of best fit gives the gradient, and the reciprocal of this, multiplied by one hundred, gives the helical twisting power for the compound (Equation 5.2).

$$\text{Helical twisting power} / \text{“m}^{-1} = \frac{1}{\text{gradient}} \times 100 \qquad \textbf{(Equation 5.2)}$$

5.5 References

[1] K. Ishikiriyama, A Boller and B. Wunderlich, *J. of Thermal. Analysis*, 1997, **50**, 547.

[2] D. L. Thomsen III, P. Keller, J. Naciri, R. Pink, H. Jeon, D. Shenoy, B. R. Ratna, *Macromolecules*, 2001, **34**, 5868.

[3] A. Yoshizawa, H. Iwamochi, S. Segawa and M. Sato, *Liq. Cryst.*, 2007, **34**, 1039.

[4] J. M. Khurana, S. Chauhan, and G. Bansal, *Monatshefte fuer Chemie*, 2004, **135**, 83.

[5] M. Sato, A. Yoshizawa and F. Ogasawara, *Mol. Cryst. and Liq. Cryst*., 2007, **475**, 99.

[6] K. Hiratina, K. Kasuga, T. Hirose, K. Taguchi and K. Fujiwara, *Bull. Chem. Soc. Jpn.,* 1992, **65**, 2381.

[7] Edt. H-S. Kitzerow and C. Bahr, *Chirality in Liquid Crystals*, Springer-Verlag, New York, 2001, p 34.

[8] I. Dierking, *Textures of Liquid Crystals*, Wiley VCH, Germany, 2003, p 66, 67.

[9] E. P. Raynes, *Liq. Cryst*., 2007, **34**, 697.

[10] A.I. Stipetic, *Hallcrest Reports*, 1999, p 5, 7, 9, 10, 14.

6 EXPERIMENTAL DISCUSSION

6.1 Synthetic Pathway 1

Synthetic pathway 1, as shown in Scheme 5.1 (p48), outlines the synthesis of the linear dimers. The one-step synthesis involved a room temperature esterification of PCH-5-phenol (**1**) and a flexible chiral dicarboxylic acid; [(*S*)-(-)-methylsuccinic acid (**2**), (*R*)-(+)-methylsuccinic acid (**3**), (*S*)-(+)-2-methylglutaric acid (**4**), (*R*)-(–)-2-methylglutaric acid (**5**) and (*S*)-(+)-phenylsuccinic (**6**)].

The chiral dimers (compounds **7** – **11**) were isolated in good yields (typically 51 % - 82 %). ^{1}H NMR, ^{13}C NMR, infrared spectroscopy, mass spectrometry and elemental analysis confirmed the structures of the compounds. Elemental analysis showed the dimers to be greater than 99.5 % chemically pure.

6.2 Synthetic Pathway 2

The aim of synthetic pathway 2 (Scheme 5.2, p53) was to synthesise H-shaped liquid crystal dimers from mesogenic monomers reacted with the dicarboxylic acids; [(*S*)-(–)-methylsuccinic acid (**2**), (*R*)-(+)-methylsuccinic acid (**3**), (*S*)-(+)-2-methylglutaric acid (**4**), (*R*)-(–)-2-methylglutaric acid (**5**) and (*S*)-(+)-phenylsuccinic (**6**)].

The three-step synthesis of the monomer was achieved without major difficulties. The alkylation of methyl 2,4-dihydroxybenzoate, **12**, with bromopropane was successful and methyl 2-hydroxy-4-propoxybenzoate, **13**, was isolated in good yield (85 %). The deprotection of compound **13** was successful and the analogous acid, **14**, was isolated in good yield (79 %). ^{1}H NMR, infrared spectroscopy and mass spectrometry confirmed the structures of both materials. The esterification of acid, **14**, with PCH-5-phenol was successful and the ester **15** was isolated in low yield (39 %). ^{1}H NMR, ^{13}C NMR, IR, and mass spectrometry confirmed the structure of **15**. The purity was determined by HPLC (267 nm) with the material having a chemical purity of greater than 99.0 %.

The dimerisation stage proved problematic. Esterification reactions of the compound **15** with the chiral diacids (compounds **2** – **4**) were not successful and no product was isolated. In order to encourage the reaction of compound **19** (from compound **4**), the reaction mixture was heated and for a longer period of time. This did not appear to have an affect on the production of a dimer.

It was thought that the ring structure in compound **15** was too sterically hindering to allow the addition of the dicarboxylic acid-DMAP intermediate into the aromatic ring environment, to synthesize the laterally appended systems **16** – **19**. The esterification reaction is thought to proceed *via* a mechanism similar to that suggested by Steglich for esterification reactions using DCC and DMAP [1, 2]. The suggested mechanism is adjusted for esterification reactions using EDAC and DMAP. Although EDAC molecules can cyclise, see Figure 6.1, in this case it was proposed that the linear analogue of EDAC is the reacting species. The suggested mechanism can be seen in Figure 6.2.

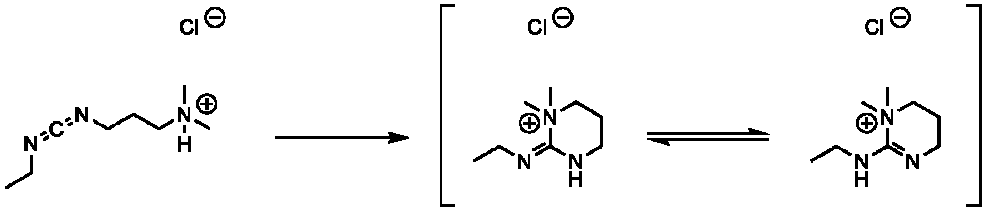

Figure 6.1: *Illustration showing the linear analogue and cyclic tautomers of EDAC.*

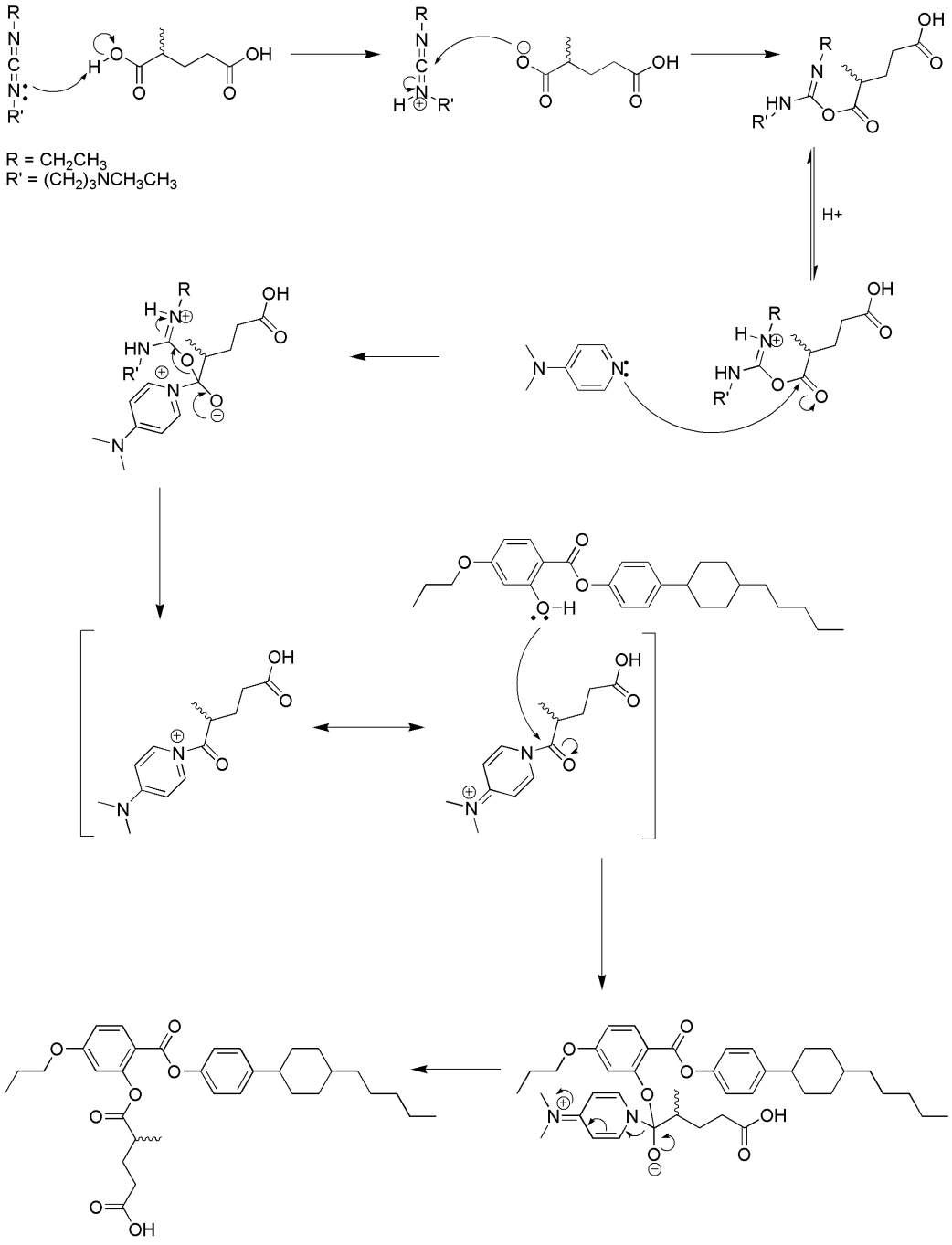

Figure 6.2: *Illustration showing suggested Steglich esterification reaction, amended using EDAC and DMAP for dimers* **16 – 19** [1, 2].

It is suggested in the mechanism that the dicarboxylic acid is deprotonated by EDAC, which then attaches to the imine, creating an EDAC-dicarboxylic acid intermediate. EDAC is then deprotonated by DMAP, producing a DMAP-

carboxylic acid intermediate that undergoes resonance with two canonical forms. As a consequence, it is possible that the system is intramolecularly H-bonded between the acid and the amide moieties, see Figure 6.3 (top), the reaction then takes place at only one of the acid moieties resulting in the mono-product being formed and not the dimer. Additionally, the suggested mechanism shows that the DMAP-acid intermediate is very sterically hindered, see the space-filling model in Figure 6.3 (bottom). The carbonyl is situated between a bulky benzene ring and a carboxylic acid with a methyl side group, plus with the potential for H-bonding, the intermediate cannot position close enough to the ring system of the mesogenic unit for reaction to take place. As a result, the dicarboxylic acid cannot couple to compound **15** and dimerisation does not occur.

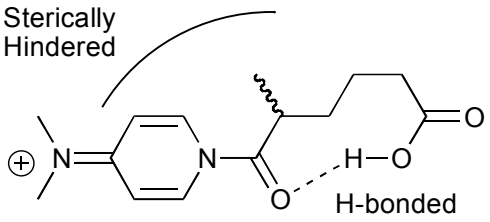

(a)

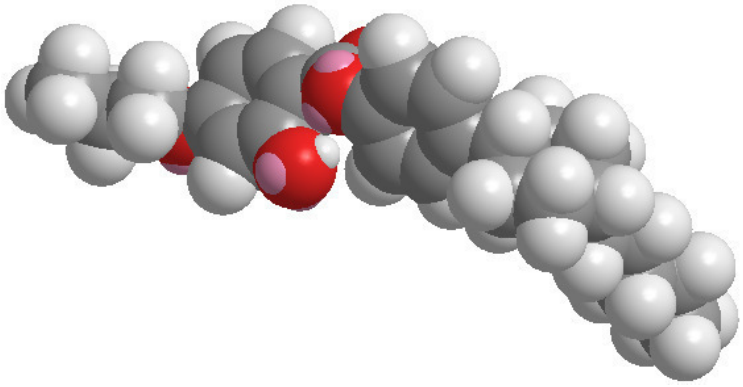

(b)

Figure 6.3: *Illustration showing (a) intramolecular hydrogen bonding of the DMAP-acid intermediate;* (b) *the 3-dimensional energy minimization space-filling model of compound* **15**.

In order to encourage dimerisation to occur the solvent was changed from DCM to THF. The esterification of compound **16** in this case did not proceed and no

product was isolated, indicating that the reaction was not susceptible to solvent changes.

6.3 Synthetic Pathway 3 (Scheme 5.3, p56)

As the standard esterification reaction of compound **15** with the chiral spacers (compounds **2** – **4**) did not yield products, it was decided to use an activated acid chloride in place of the dicarboxylic acids. Chloride is a better leaving group than hydroxyl, and so it was hoped that the acid chlorides would provide a more reactive attacking species for the reaction with compound **15**, and encourage the addition of the spacer to the mesogen to take place.

The acid chloride derivative of compound **3** was successfully synthesized and compound **20** was isolated with a good yield of 77 %. However, the reaction of compound **15** with compound **20** did not yield any product. Furthermore, increasing the temperature of the reaction mixture did not have an effect on dimerisation.

As well as effect of steric hindrance and H-bonding in the reactive intermediate as previously discussed, it was also thought that hydrogen bonding between the hydroxyl group in the 2-position of the benzene ring and the oxygen group of the carboxylic acid in the 1-position of the benzene ring occurs for compound **15**, preventing the addition of the chiral spacers to the hydroxyl group. The intramolecular hydrogen bonding creates a 6-membered ring, as demonstrated in Figure 6.4, deactivating the hydrogen atom of the hydroxyl group. Due to the strength of hydrogen bonds and the stability of the 6-membered rings disrupting this system to allow the introduction of a sterically hindered group onto the hydroxyl group through an esterification reaction was not achievable, which is contrary to the report by Sato, Yoshizawa and Ogasawara [3].

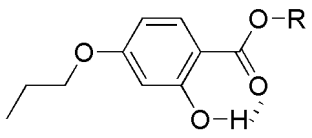

Figure 6.4: *Illustration of the potential intramolecular hydrogen bonding that is believed to occur in* **16 – 19**, *preventing dimerisation from taking place.*

6.4 Synthetic Pathway 4 (Scheme 5.4, p57)

In order to confirm the occurrence of intramolecular hydrogen bonding in compound **15**, the attempted coupling of methyl 2-hydroxy-4-propoxybenzoate, **13**, to the chiral spacers, prior to the addition of PCH-5-Phenol (**1**), was carried out. No product was isolated during the reaction either. This suggests the intramolecular bonding occurs in the monomer, but also in the diacids. Substitution at the hydroxyl group of phenolic moieties can generally be carried out, as shown in the synthesis of T-shaped dimers [3]. This inability of the diacid to attach to compound **13** or **15** implies that the choice of moiety used in the reaction to couple to the phenolic compound plays an important part in allowing the substitution to proceed.

6.5 Synthetic Pathway 5 (Scheme 5.5, p58)

In order to remove the affect of steric hindrance and prevent intramolecular hydrogen bonding, a propanol spacer was attached to the hydroxyl group of compound **13**, onto which the chiral spacer could be added.

The three-step synthesis of the monomer occurred without difficulties. The alkoxylation of compound **13** was successful and compound **29** was isolated in very good yield (97 %). ^{1}H NMR, infrared spectroscopy and mass spectrometry confirmed the structures of the compound. In order to join the alkoxy spacer onto the hydroxyl group on the benzene ring, a Williamson etherification reaction was required rather than an esterification. Firstly, the hydroxyl group of the phenolic moiety was deprotonated. The negatively charged oxygen was then reacted with the bromopropanol, as seen in Figure 6.5. The presence of the alkoxy chain on the ring meant the sterically hindered chiral spacers (**2** – **4**) did not have to directly attack the crowded hydroxyl group of the phenol moiety in a hindered environment, but could attach to the end of the alkoxy chain, where steric hindrance would not be a problem (Figure 6.6). The alcohol derivative retains the presence of the hydroxyl group at the end of the chain to allow the addition of the dicarboxylic chiral spacers, through the DMAP-dicarboxylic acid intermediate. The addition of an extra chain was predicted to affect the properties of the materials, but by keeping the spacer unit short the overall flexibility of the molecular structure would not be increased dramatically, unlike it would be if a

using a longer spacer chain were used, which is often common practice with liquid crystal polymers and dendrimers [4, 5, 6].

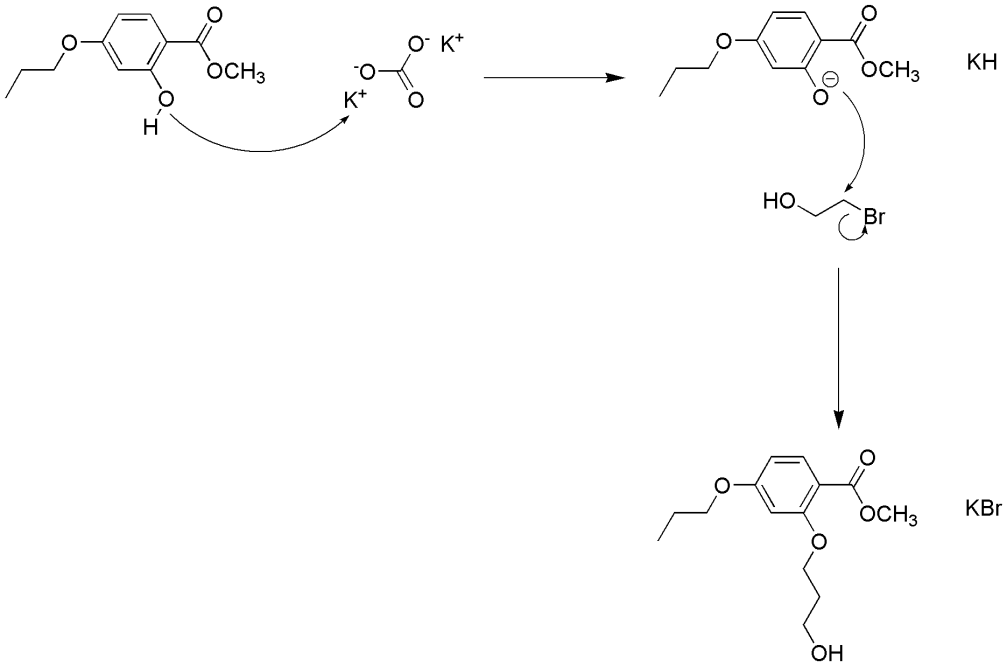

Figure 6.5: *Illustration showing the mechanism of the Williamson reaction used to attach an alkoxy chain to compound* **13** *to produce compound* **29**.

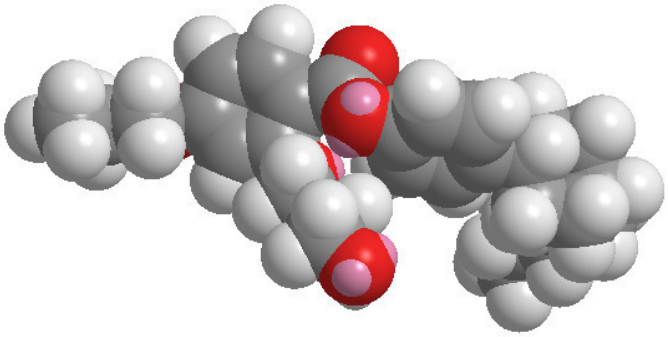

Figure 6.6: *Illustration showing the 3-dimensional energy minimization space-filling models of compound* **31.**

The deprotection of compound **29** was successful and compound **30** was isolated, but in relatively poor yield (34 %). It is thought that hydrogen bonding between compound **30** and the water in the acid solution work-up occurred, resulting in a large proportion of compound **30** staying in solution and not forming a precipitate. ^{1}H NMR, infrared spectroscopy and mass spectrometry confirmed the structures of the compound. The esterification of compound **30** with PCH-5-

phenol (**1**) was successful and compound **31** was isolated in good yield (59 %). ^{1}H NMR, ^{13}C NMR, IR, and mass spectrometry confirmed the structure of compound **31**. Purity was determined by HPLC (262 nm), and the compound was shown to have greater than 98.5 % chemical purity.

Dimerisation of compound **31** with the chiral spacers spacer [(*S*)-(–)-methylsuccinic acid (**2**), (*R*)-(+)-methylsuccinic acid (**3**), (*S*)-(+)-2-methylglutaric acid (**4**), (*R*)-(–)-2-methylglutaric acid (**5**) and (*S*)-(+)-phenylsuccinic (**6**)] was accomplished. The esterification of compound **31** with compound **2** was successful and compound **32** was isolated, but in relatively low yield (22 %). Purity was determined by HPLC (259 nm) and the material was shown to be greater than 98.7 % pure. The esterification of compound **31** with compound **3** was successful and compound **33** was isolated in very low yield (3 %). Purity was determined by HPLC (259 nm) and the compound was shown to be greater than 98.3 % pure. The esterification of compound **31** with compound **4** was successful and compound **34** was isolated in low yield (22 %). Purity was determined by HPLC (259 nm) and the compound was shown to be greater than 98.0 % pure. The esterification of compound **31** with compound **5** was successful and compound **35** was isolated in low yield (9 %). Purity was determined by HPLC (259 nm) and the compound was shown to be greater than 97.0 % pure. ^{1}H NMR, ^{13}C NMR, IR, and mass spectrometry confirmed the structure of the dimers. ^{1}H NMR spectra of the dimers can be seen in the Appendices.

6.6 References

[1] B. P. Mundy, M. G. Ellerd and F. G. Favaloro, *Named Reactions and Reagents in Organic Synthesis,* John Wiley and Sons, Inc, New Jersey, Second Edition, 2005, p 248.

[2] Organic Chemistry Portal, *Name Reactions,* accessed September 2010, http://www.organic-chemistry.org/namedreactions/steglich-esterification.shtm

[3] M. Sato, A. Yoshizawa and F. Ogasawara, *Mol. Cryst. and Liq. Cryst.*, 2007, **475**, 99.

[4] J.W. Goodby, I.M. Saez, S.J. Cowling, J.S. Gasowska, R.A. MacDonald, S. Sia, P. Watson, K.J. Toyne, M. Hird, R.A. Lewis, S.-E. Lee, and V. Vaschenko, *Liq. Cryst.*, 2009, **36**, 567.

[5] I.M. Saez and J.W. Goodby, *J. Mater. Chem.,* 2005, **15**, 26.

[6] I.M. Saez and J.W. Goodby in *Liquid Crystalline Functional Assemblies and their Supramolecular Structures, Structure and Bonding,* Series Ed. D.M.P. Mingos, Vol. Ed T. Kato, Springer-Verlag, Berlin Heidelberg, 2008, **128**, 1.

7 RESULTS AND DISCUSSION

7.1 Mesophase Identification and Transition Temperatures

The mesophase behaviour and transition temperatures of all the target compounds were evaluated using polarised optical microscopy and differential scanning calorimetry (DSC).

7.1.1 Linear Dimers

Each of the linear dimers exhibited liquid crystalline behaviour, except for compound **11**. The melting points and transition temperatures are given in Table 7.1. Interestingly, compounds **7** and **8** exhibited enantiotropic phases while compounds **9** and **10** exhibited monotropic phases.

Compound	Transition temperatures / ^{o}C [Enthalpy values / kJ mol^{-1}]					
	Cr		B		Iso	Recrystallisation
7	•	105.0 [20.7]	•	136.7 [16.4]	•	79.3 [18.9]
8	•	102.8 [16.5]	•	137.6 [14.2]	•	76.5 [16.0]
9	•	84.0 [31.7]	**(** •	66.9 **)** [11.3]	•	59.0 [(a)] [2.6]
10	•	84.7 [33.8]	**(** •	67.5 **)** [12.7]	•	58.7 [(b)] [3.2]
11	•	81.6 [22.2]		– –	•	52.9 [(c)] [8.5]

(a) Crystal-crystal transition observed after the compound recrystallised (51.9 ^{o}C, [11.9 kJ mol^{-1}]); (b) Crystal-crystal transition observed after the compound recrystallised (50.1 ^{o}C, [7.8 kJ mol^{-1}]); (c) Recrystallisation occurred upon heating (56.1 ^{o}C, [1.1 kJ mol^{-1}]).

Table 7.1: *Table of transitions temperatures (^{o}C) and enthalpies of transition ([kJ mol^{-1}]) of the linear chiral dimers,* **7** *to* **11**. *Temperatures in brackets denote monotropic phases.*

Both sets of compounds (**7** and **8** and **9** and **10**) exhibited mesophases that were characterized as crystal B phases. The crystal B phase belongs to the crystal smectic group, which has more ordering than the smectic counterparts [1, 2, 3]. This crystalline phase has hexagonal ordering, as shown in Figure 7.1, with long range positional ordering in three dimensions. Although there is an absence of liquid-like ordering, the diffuse motions of the molecules define the phase as an "anisotropic plastic crystal" [1, 2, 3]. The molecules in the crystal B phase are thus arranged in layers with their long axes orthogonal to the planes of the layers. In the planes of the layers plane the positional ordering is long range, and the molecules are undergoing rapid and diffuse motion about their long axes [1], see Figure 7.2. Out of the plane the crystal B phase can have various long range stacking arrangements of the layers, ie ABAB, ABCABC, and random. Due to the long range ordering, the crystal B phase typically exhibits defect textures more closely aligned with the solid state rather than the quasi-liquid state of the nematic phase, and as a consequence lancets and mosaic textures are usually observed.

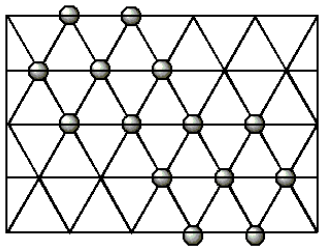

Figure 7.1: *Illustration showing the plan view of a crystal B phase*.

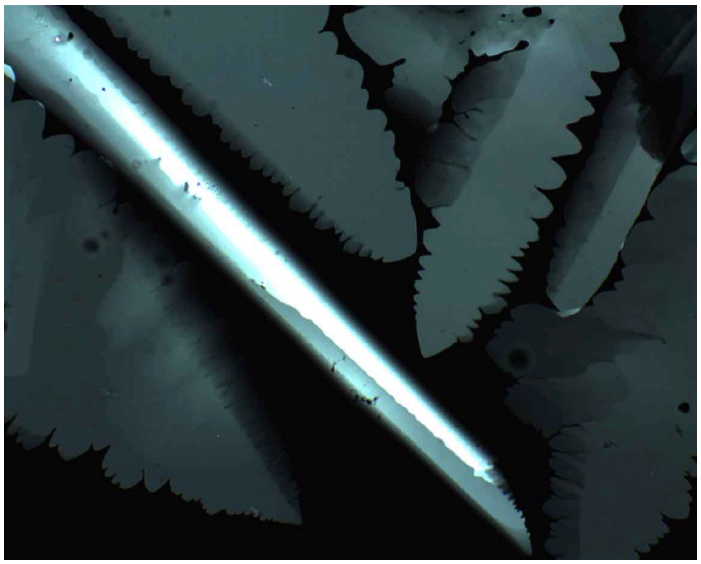

(a)

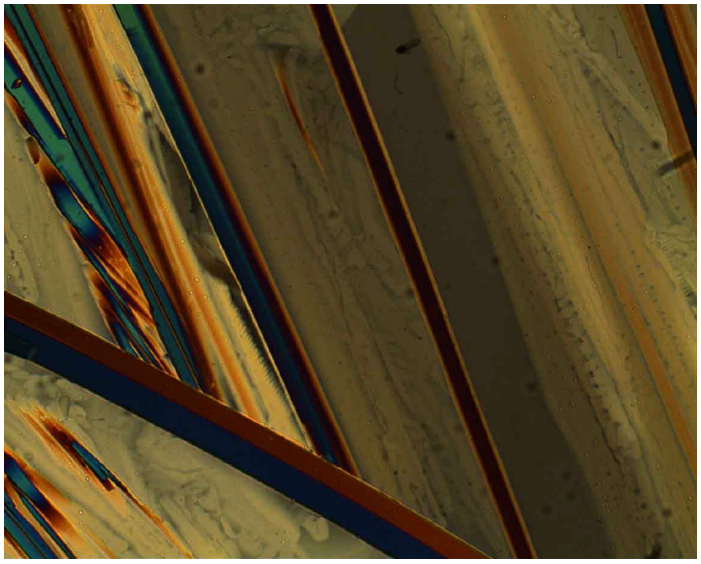

(b)

Figure 7.2: *Polarised optical micrographs illustrating the typical texture of a crystal B phase: (a) dendrites and mosaic texture (Iso – B transition of compound* **9** *at 70 °C); (b) the lancet texture (crystal B phase of compound* **10** *at 65 °C).*

It can be seen from Table 7.1, the transition temperatures of compounds **7** and **8** are very similar. The two compounds are enantiomers with the only difference being the stereochemistry of the chiral methyl group attached to the succinic spacer (Figure 7.3). The stereochemistry should not affect the transition

temperatures of a material for the same enantiopurity, thus the small difference in the temperatures of the melting point and Iso – B phase transition can be attributed to differences in the optical purities of the two enantiomers.

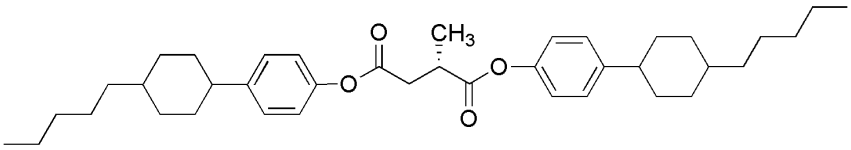

(a)

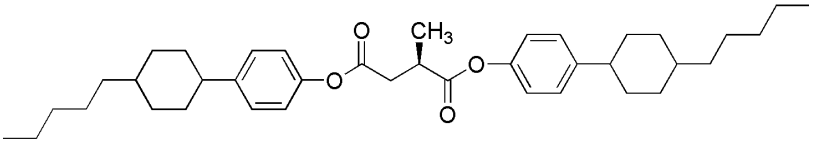

(b)

Figure 7.3: *Illustration showing the structures of* (a) *compound* **7**; (b) *compound* **8**.

The mesophases of compounds **7** and **8** were characterised using polarised optical microscopy. The textures observed displayed the mosaic texture and lancets associated with the crystal B phase, but unusually the lancets exhibited striations running along the length of the lancets (Figure 7.4). The striations could be due to the orientation of the molecules, for example, the twisted stereochemical structures of the molecules could cause the molecules to align in such away that their orientations differ slightly every few layers. This would produce layers defects of slightly different sizes, leading to the different coloured stripes observed. Conversely, the formation of stripes in mosaic textures is the signature of the formation of the more ordered phase E phase, however, no enthalpy was observed in the DSC for a phase transition between B and E phases.

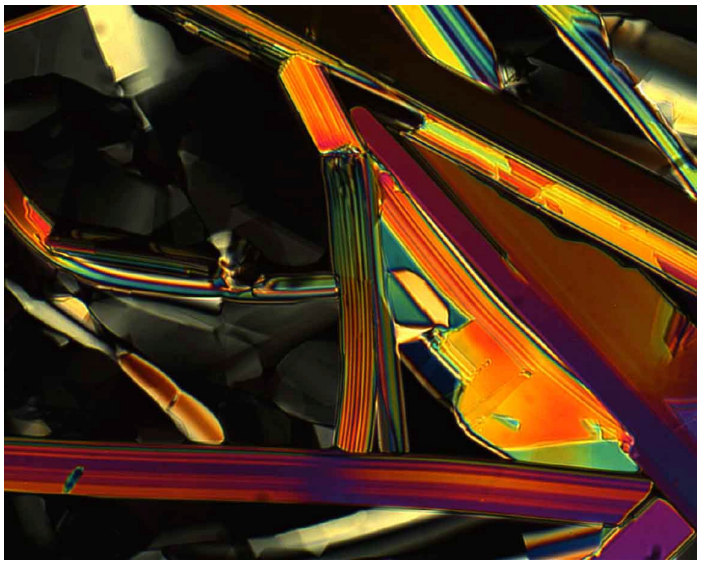

(a)

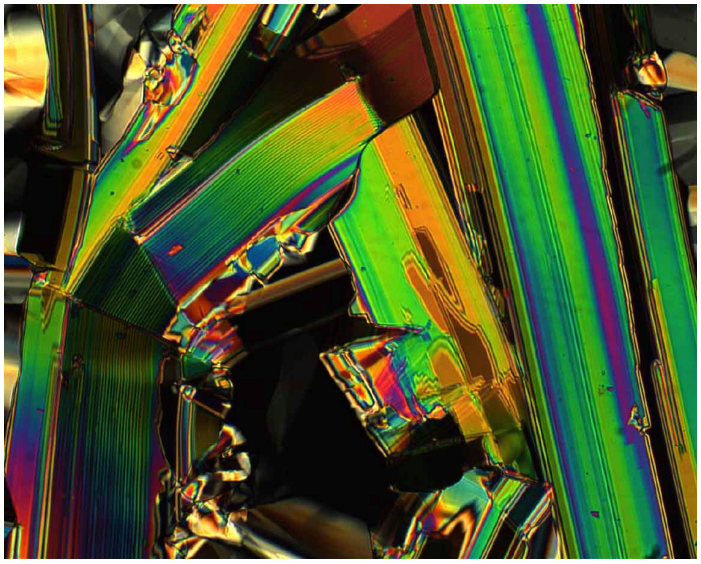

(b)

Figure 7.4: *Polarised optical micrographs showing the crystal B phase of* (a) *compound* **7** *at 135.0 °C (Magnification x 100);* (b) *compound* **8** *at 137.0 °C (Magnification x 100).*

It can be seen from in Table 7.1, compounds **9** and **10** have similar transition temperatures. The two are enantiomers (see Figure 7.5), and so the difference in transition temperatures can be ascribed to differences in enantiopurity. For example, the starting material **4** had an optical purity of 98.6 % by GC, whereas

compound **5** had an optical purity of 99.3 % by GC. The higher enantiopurity leads to a higher melting point of the spacer system.

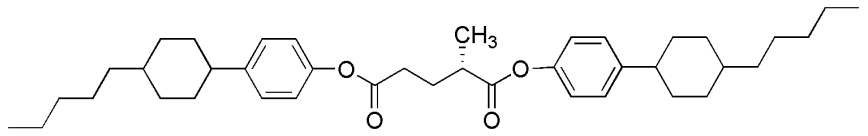

(a)

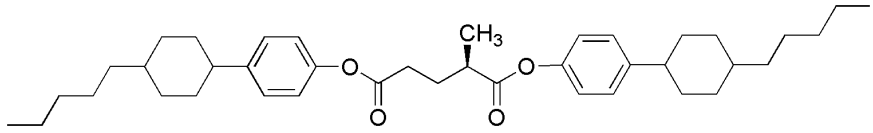

(b)

Figure 7.5: *Illustration showing the structures of* (a) *compound* **9**; (b) *compound* **10**.

Classic crystal B phases were observed for compounds **9** and **10** using polarised optical microscopy (Figure 7.6). Distinct mosaic textures can be seen at the Iso – B transition, with dendrites and lancets being observed in the formation of the B phase. An observation seen in compounds **9** and **10**, and not exhibited in compounds **7** and **8**, was a crystal – crystal transition. Upon cooling from the crystal B phase, a crystal phase was observed before undergoing a transition to a second crystal phase. This crystal – crystal transition was confirmed by pausing the temperature decrease at the phase transition. Once the nucleation process had started, the transition continued to occur without further cooling, indicating a crystal-crystal transition rather than a liquid crystal – crystal transition.

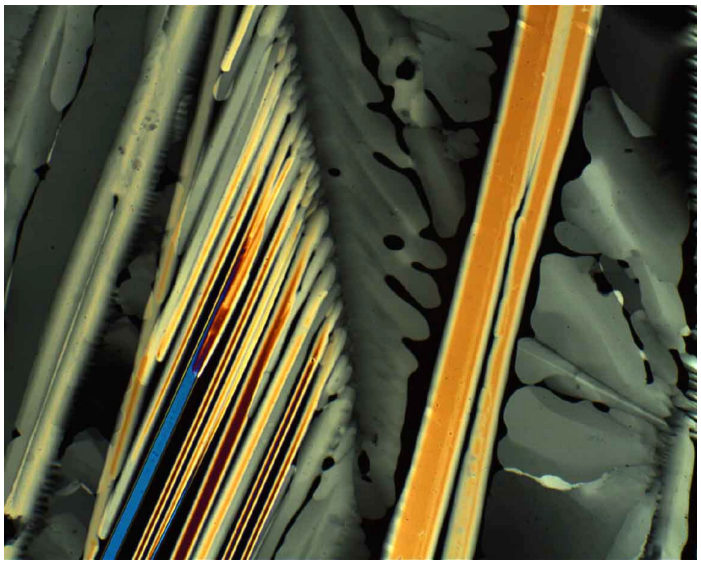

(a)

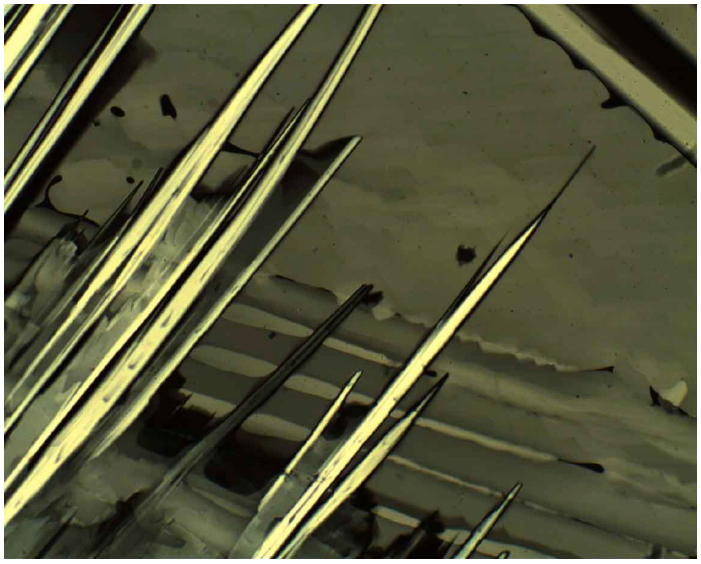

(b)

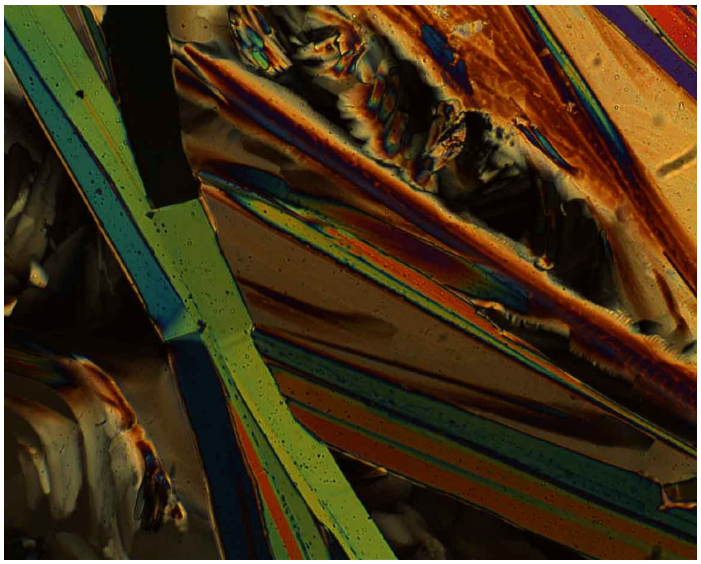

(c)

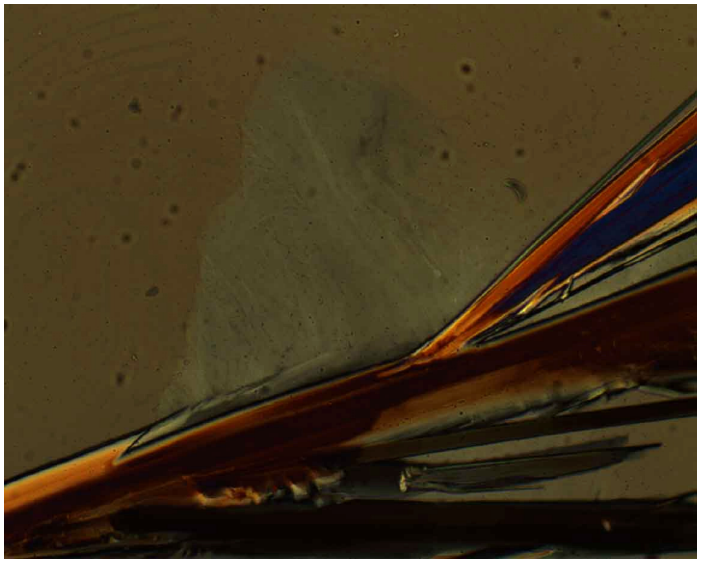

(d)

Plate 7.6: *Polarised optical micrographs showing* (a) *the isotropic – crystal B phase transition of* **9** *at 70.0 ^{o}C (Magnification x 100);* (b) *the phase transition of* **9** *at 66.0 ^{0}C (Magnification x 100);* (c) *the crystal B phase of* **10** *at 68.0 ^{o}C (Magnification x 100);* (d) *the second crystals phase of* **10** *at 63.0 ^{o}C (Magnification x 100).*

It was found that the transition temperatures of the glutaric acid based compounds (**9** and **10**) were lower than the succinic compounds (**7** and **8**). Extending the chiral spacer by one methylene group (glutaric acids with respect

to succinic acids) reduced the melting point of the compounds slightly, but decreased the Iso – B transition by over 69 ^{o}C. Additionally, the increase of the spacer chain from four carbons to five carbons produced a change from enantiotropic phases to monotropic phases. Monotropic phases are usually seen in liquid crystals due to substantial supercooling before undergoing recrystallisation. Thus a drop in clearing point demonstrates that even though recrystallisation temperature has fallen, which is due to kinetic effects, the reduction in the Iso – B phase, which is thermodynamic, is real and thus the B phase is substantially destabilised [1].

The difference in transition temperatures between the succinic acid dimers (compounds **7** and **8**) and glutaric acid dimers (compounds **9** and **10**) is due to the odd-even effect. Compounds **7** and **8** have a relatively linear and rigid structure in comparison to compounds **9** and **10** (see Figure 7.7). Having a more linear configuration, results in better packing between molecules, with stronger interactions holding them together. As a result, more energy is needed to enter a less ordered phase and so the transition temperatures are higher [1]. The additional carbon in compounds **9** and **10** make them more flexible and bent in structure [1]. This disrupts the packing of the molecules, which suppresses the liquid crystal behaviour and lowers the melting points of the materials [4].

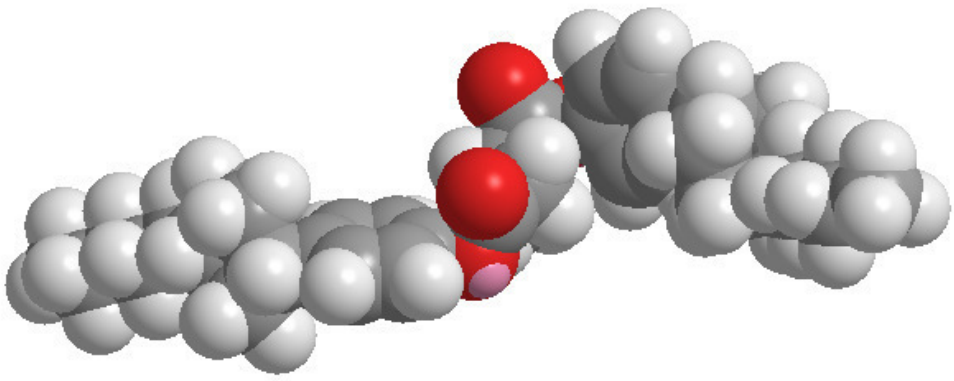

(a)

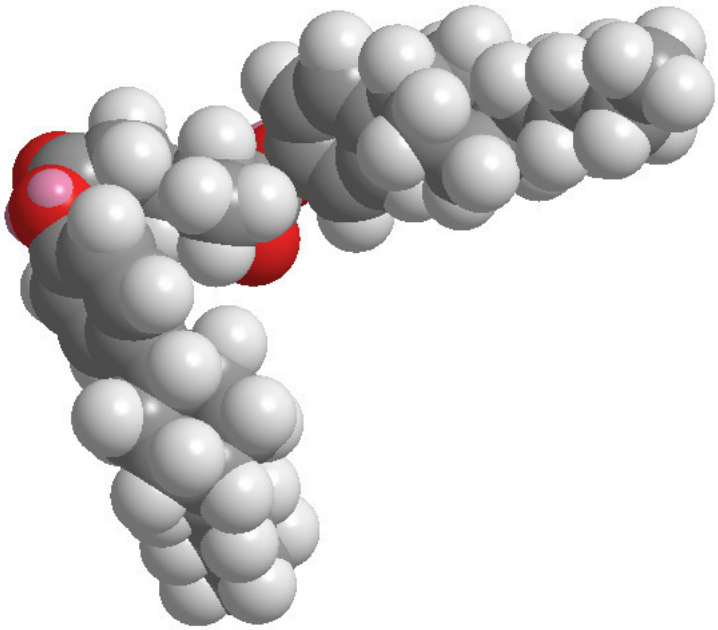

(b)

Figure 7.7: *Illustration showing the 3-dimensional energy minimization space-filling models of (a) compounds* **7***; (b) compound* **10.**

Compound **11** did not show any liquid crystal phases by polarised optical microscopy or DSC. Interestingly, it was found to recrystallise upon heating. Although mesophases were observed for compounds **7** and **8**, which have the same spacer length as compound **11**, compound **11** was not mesomorphic. This implies that the lateral benzene moiety present at the stereogenic centre in compound **11** (Figure 7.8) is the cause of the lack in liquid crystal behaviour. It is thought that this is due to the size and position of the benzene moiety prevents the dimer molecules from packing efficiently.

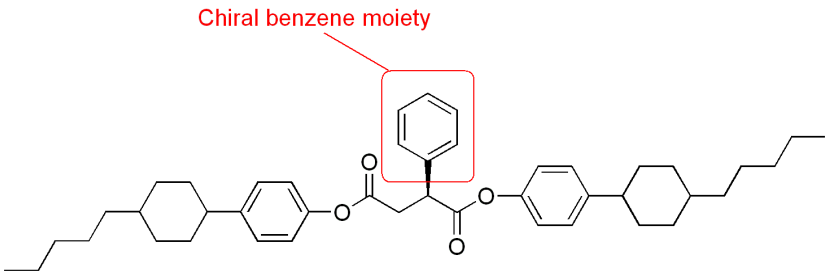

Figure 7.8: *Illustration showing the structure of compound* **11***, displaying the presence and position of the chiral benzene moiety.*

The structure of compound **11** was drawn in a 3-dimensional modelling programme and a MM2 minimization of the compound was obtained (see Figure 7.9). MM2 minimization routines perform a local energy minimization of a material at absolute zero in order to produce a 3-dimensional structure of a material, where angles of the bonds in the compound are in the lowest energy state.

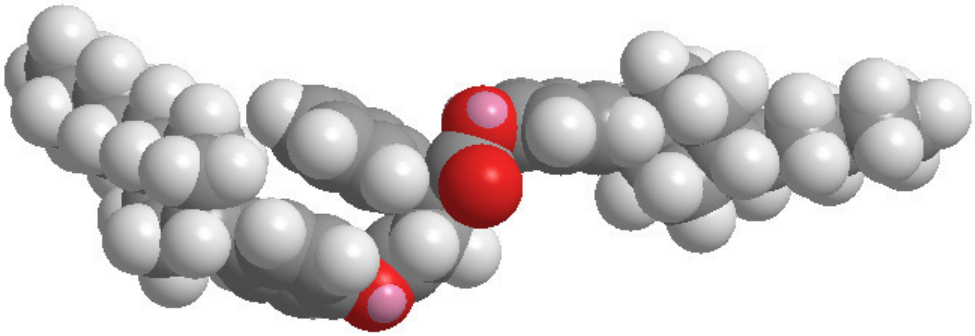

Figure 7.9: *Illustration showing the 3-dimensional energy minimization space-filling model of compound* **11.**

As seen in Figure 7.9, the benzene moiety is orientated perpendicular to the spacer chain, which itself is almost perpendicular to the two PCH-5-phenol moieties. Due to this, when the molecules of compound **11** interact laterally, the benzene moiety prevents the molecules from positioning close enough to form molecular ensembles that might support the formation of mesophases [1]. Another reason that no liquid crystal phases were seen may be due to the effect of the size of a lateral substituent on the depression of T_{N-1}. There is a direct relationship between the two [1] and as the benzene moiety is large, there would be a significant depression of the nematic phase stability. The polarity of a material can offset the depression of smectic phases caused by the size of a moiety, by improving the lamellar packing [1]. The benzene moiety, however, is non-polar and it is therefore not surprising that it depresses phase stability to such an extent that no liquid crystal phases can form, whereas in comparison the lateral methyl moiety in **7** and **8** is small enough to support crystal B mesophase formation.

As compound **11** did not show a liquid crystal phase and was found to be not soluble in the host liquid crystals used, no further analysis work was carried out on the dimer.

Not one of the linear dimers exhibited a blue phase. This is possibly due to the lack of frustrated structures for the compounds. The stereogenic centres of the dimers are located at the centre of the structure, isolating the potential chiral interactions of the molecule from its neighbours. In order to allow for the transfer of chiral interactions between the molecules in order to create the frustration required for the formation of a blue phase, the chirality may need to be situated in the terminal chains where the potential interactions are greater. Nevertheless, further work, including calculations on helical twisting powers and contact preparations, was subsequently carried out in order to investigate the frustration and chiral transfer ability of the compounds.

7.1.2 H-Shaped Dimers

The mesomorphic materials **15**, possessing a lateral hydroxy groups, and **31** possessing a hydroxypropoxy side chain were prepared as intermediates for the preparation of H-shaped dimers. Unfortunately it was not possible to prepare dimers from compound **15**, but data recording its properties are given below. Therefore it is worthy to note that both **15** and **31** were found to exhibit nematic phases, see Table 7.2.

Compound	Transition temperatures / ^{o}C Enthalpy values / kJ mol^{-1}]					
	Cr		N		Iso	Recrystallisation
15	•	105.3 [33.9]	•	173.8 [0.7]	•	66.0 [17.5]
31	•	91.0 [40.4]	**(** •	59.8 **)** [0.3]	•	58.0 [14.44]

Table 7.2: *Table of transitions temperatures (^{o}C) and enthalpies of transition ([kJ mol^{-1}]) of the mesogenic compounds,* **15** *and* **31**. *Temperatures in brackets denote monotropic phases*.

For compound **15** the nematic phase was characterised by polarised optical microscopy, for which typical *schlieren* defect textures showing two- and four-brush singularities were observed (see Figure 7.10).

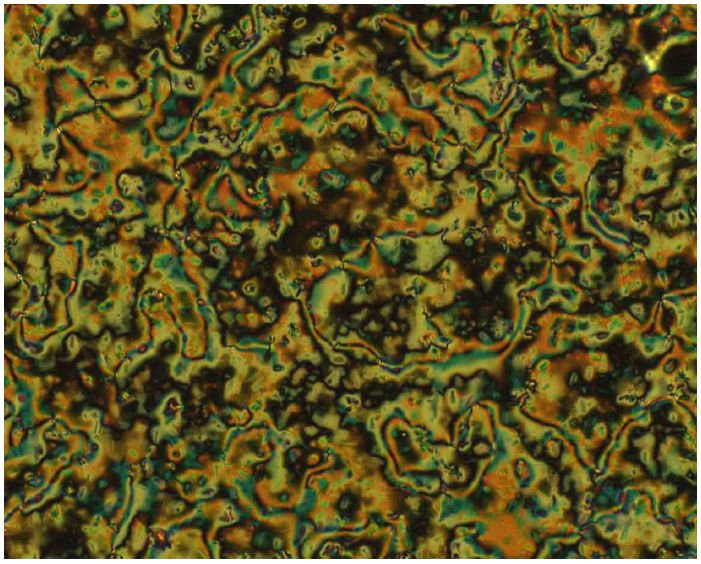

(a)

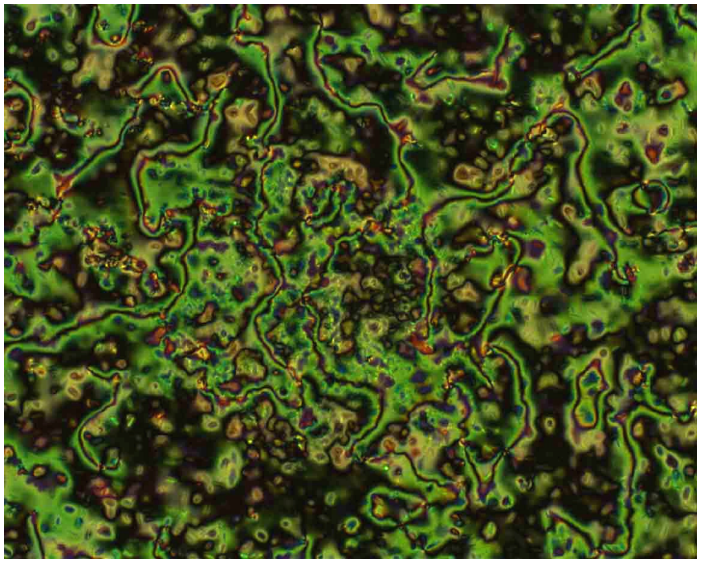

(b)

Figure 7.10*: Polarised optical micrograph showing the nematic phase of* **15** *at* (a) *167.3 °C (Magnification x 100);* (b) *169.8 °C (Magnification x 100).*

Similarly the nematic phase of compound **31** was characterised by polarised optical microscopy, for which typical *schlieren* textures were observed (see

Figure 7.11). Compound **31** exhibited a lower melting point than compound **15** but more significantly the nematic to isotropic liquid transition was depressed such that it became monotropic (transition at 59.8 ^{o}C) The addition of a small lateral side group (Figure 7.12) had caused a 115 ^{o}C reduction in the nematic phase stability. The large lateral alkyl group appears to prevent the lateral interactions between the molecules (see Figure 7.13). This leads to a reduction in of the phase transition temperature [1, 5].

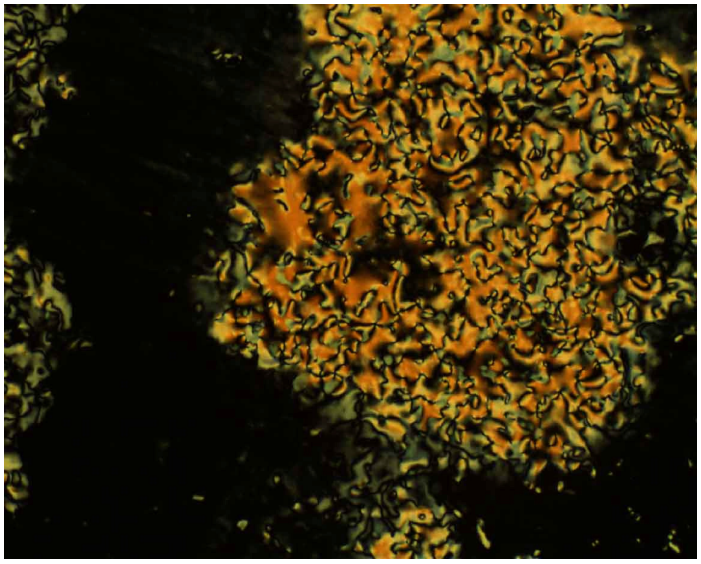

Figure 7.11: *Polarised optical micrograph showing the nematic phase of* **31** *at 61.0 ^{o}C (Magnification x 100).*

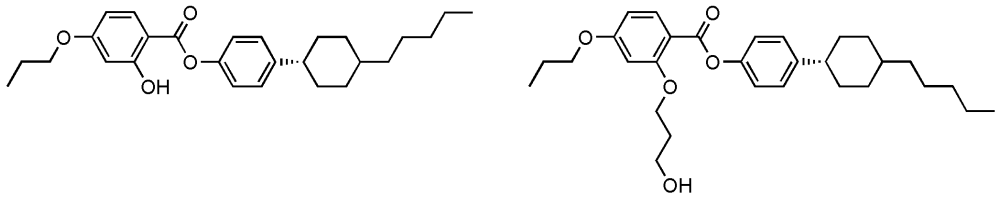

15 **31**

(a) (b)

Figure 7.12: *Illustration showing the structural differences between compounds* **15** *and* **31**.

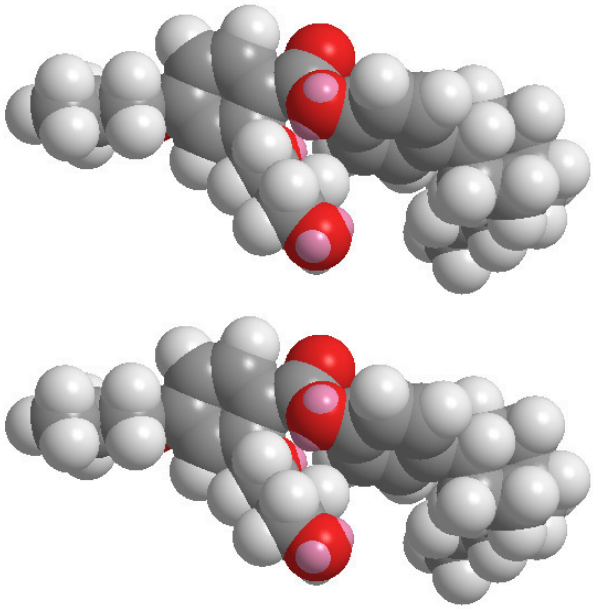

Figure 7.13: *Illustration showing the three-dimensional energy minimization space-filling model of side-side interactions between two molecules of compound* **31**.

H-shaped compounds **32** to **35** were examined by polarised optical microscopy. The transition temperatures and enthalpies of transitions are given in Table 7.3.

Compound	Transition temperatures / ^{o}C [Enthalpy values / kJ mol^{-1}]					
	Cr		N*		Iso	Glass Transition
32	•	66.3 [44.8]	**(** •	17.0 **)** [0.5]	•	– 8.7
33	•	N/A N/A	**(** •	11.5 **)** [0.2]	•	– 9.6
34	•	64.6 [43.4]	**(** •	11.9 **)** [0.6]	•	– 6.6
35	•	57.0 [31.9]	**(** •	12.4 **)** [0.5]	•	– 8.3

Table 7.3: *Table of transitions temperatures (^{o}C) and enthalpies of transition ([kJ mol^{-1}]) of the H-shaped chiral dimers,* **32** *to* **35**. *Temperatures in brackets denote monotropic phases.*

It should be mentioned that melting points were only observed on the first heat and that on every subsequent cycle only a glass transition, T_g, was observed for both pairs of enantiomers.

Compounds **32** and **33** both exhibited monotropic chiral nematic phases below room temperature. The textures of the phases were not well defined and were similar to the grainy texture usually observed in polymer systems. The pitch of the (*S*)-enantiomer (compound **32**) was in the visible spectrum and a blue colour of the chiral nematic was noted. Rotation of the polariser confirmed a left-handed helix. A photomicrograph of the nematic phase of compound **32** is shown in Figure 7.14. The (*R*)-enantiomer (compound **33**) exhibited a pitch beyond the visible and it was difficult to observe any texture. There is a noticeable transition temperature difference between compound **32** and **33**. It is believed that compound **33** contained a trace amount of solvent, which meant the melting point could not be determined by DSC and the phase transition is lower that expected. Isolation and purification of compound **33** was problematic. Purification by column chromatography was not successful and preparative HPLC had to be used as an alternative. This method proved successful, but a very low yield of compound **33** was obtained. The majority of this amount went for the DSC study. After structure and phase confirmation, along with the DSC study, there was insufficient of compound remaining for DSC analysis. Microscopy studies suggested a melting point of approximately 70 ^{o}C and a chiral nematic phase transition of around 17 ^{o}C.

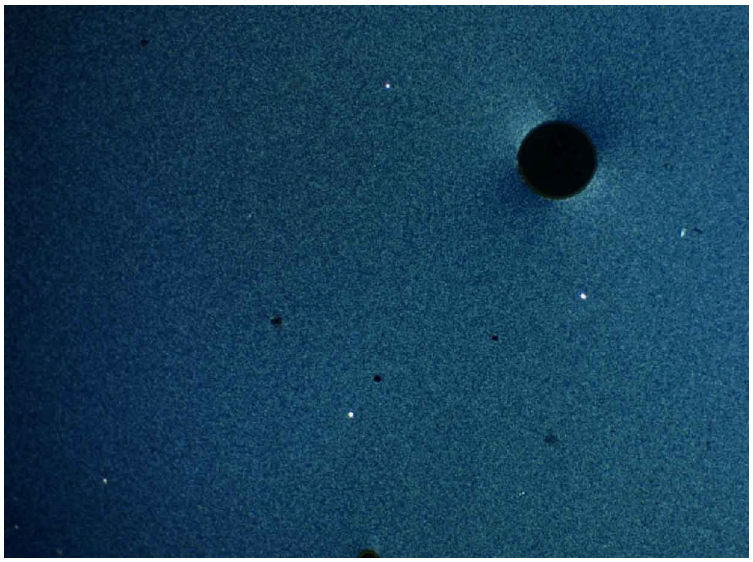

Figure 7.14: *Polarised optical micrograph showing the chiral nematic phase of* **32** *at 0.0 °C (Magnification x 100).*

Compounds **34** and **35** also exhibited monotropic chiral nematic phases below room temperature with the similar grainy texture observed in compounds **32** and **33**. As with compounds **32** and **33**, the pitch of the (*S*)-enantiomer (compound **34**) was in the visible spectrum and the blue colour of the chiral nematic was noted. Rotation of the polariser confirmed a left-handed helix. A photomicrograph of the nematic phase of compound **34** is shown in Figure 7.15. The (*R*)-enantiomer (compound **35**) exhibited a pitch beyond the visible and it was difficult to observe any texture. The small difference in the temperatures of the Iso – N* phase transition is attributed to differences in the optical purities of the (*S*)- and (*R*)-enantiomers of the glutaric acid based spacers. A longer spacer has the effect of lowering the clearing pint compared to compounds **32** and **33**. As seen with the linear dimers, increasing the length of the spacer increases the flexibility, while decreasing the linearity of the compounds. The interactions holding the molecules become weaker, and the movement away from the *trans*-conformation of the structure disrupts the packing of the molecules.

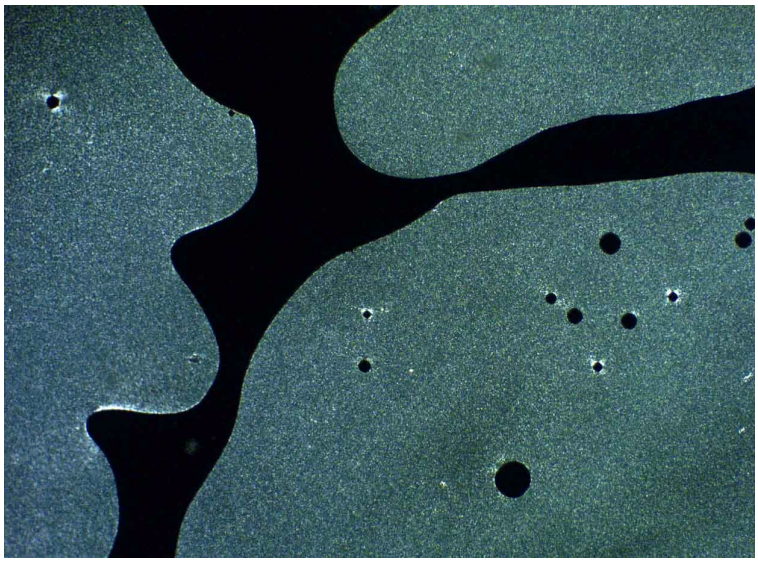

Figure 7.15: *Polarised optical micrograph showing the chiral nematic phase of* **34** *at 10.0 °C (Magnification x 100).*

All four H-shaped dimers exhibited monotropic chiral nematic phases. It appears that the lateral attachment of monomers with a spacer exhibits monotropic behaviour [6]. Not one of the dimers appeared to exhibit a conventional blue phase. It is thought that the isolation of the chiral group at the centre of the dimer prevents chiral amplification or transfer between the molecules, resulting in a lack of the formation of a frustrated structure required to observe blue phases. When the monomers are attached through one lateral group and one terminal group, with the chirality positioned in a terminal chain, both chiral nematic and blue phases are observed [7]. Sato *et. al.* synthesized T-shaped dimers with a terminal chiral chain (see Figure 7.16). As seen in Table 7.4 these dimers exhibit both low temperature chiral nematic phases and low temperature blue phases, with a wide temperature range. This work suggests that if the H-shaped dimers contained chiral groups in the terminal chains, then it may be possible to observed blue phases. Contact preparations were subsequently carried out discover if the dimers could be used as chiral dopants.

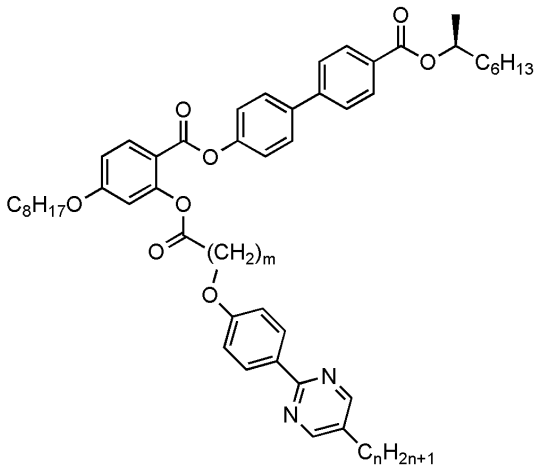

Figure 7.16: *Illustration showing the chiral T-shaped dimmer synthesizes by Sato et. al.* [7].

Compound	Transition Temperatures / °C							
	Glass		N*		BP		Iso	mp
T-1(10,8)	•	-25	•	15	•	28	•	63
T-1(9,8)	•	-23	•	19	•	28	•	45
T-1(8,8)	•	-19	•	28	•	32	•	68
T-1(10,6)	•	-22	•	14	•	25	•	40

Table 7.4: *Table showing the phase transitions of the T-shaped dimers* [8].

7.2 Mixture Work

7.2.1 Contact Studies

7.2.1.1 Linear Dimers

Compounds **7** and **8** did not mix quickly into the nematic host E7 at room temperature. However a strong concentration gradient was produced upon heating. Figures 7.17 and 7.18 show the optical textures observed in the contact mixtures for compounds **7** and **8** in E7. Chiral nematic fingerprint textures are evident and the pitch decreases as the concentration of the dopant increases. Pseudo-focal conic textures are observed at the highest concentration but no blue phases were found.

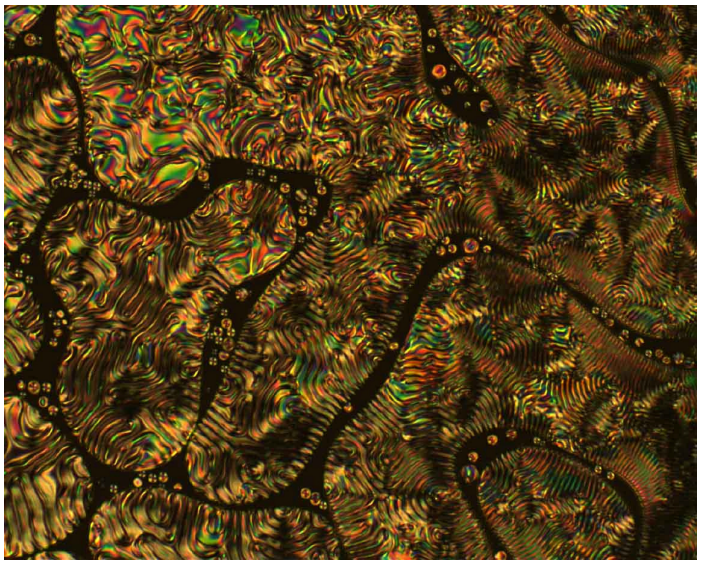

(a)

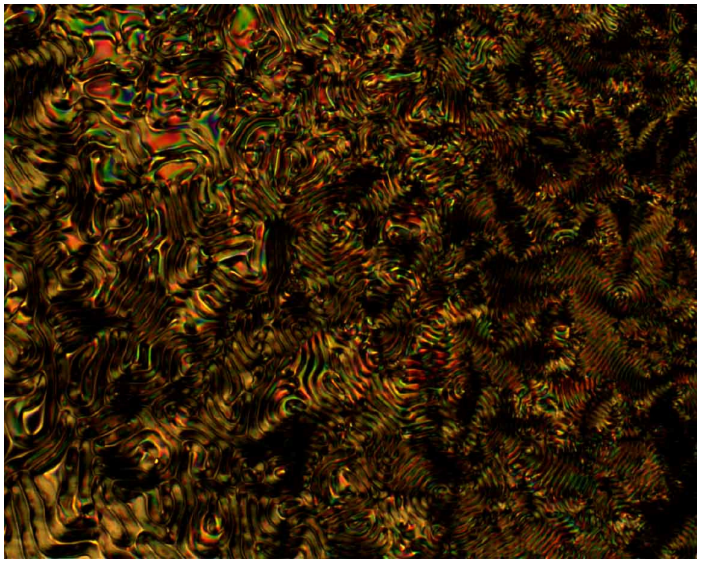

(b)

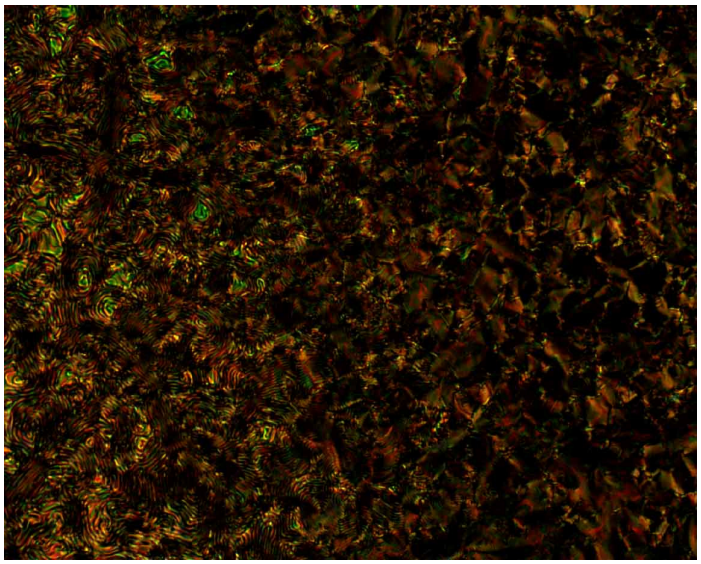

(c)

Figure 7.17: *Polarised optical micrographs showing (a) the nematic and induced chiral nematic phases at 58.5 ^{o}C; (b) the chiral gradient formed at 57.0 ^{o}C; (c) focal-conics formed due to high chirality, observed at 53.6 ^{o}C (compound* **7** *in* E7*, magnification x 100).*

The nematic to isotropic liquid transition was found to increase with increasing concentration of dopant. This is due to the higher clearing point of the dopant with respect to the host and the possibly that the chiral dopant would have formed a nematic phase (at a higher temperature than E7) had the crystal B phase stability been lower with respect to the nematic phase. The large pitch change observed in the mixtures of compounds **7** and **8** indicates reasonable chirality transfer from the dopants to the host. However, the chirality transfer is not strong enough to induce blue phases.

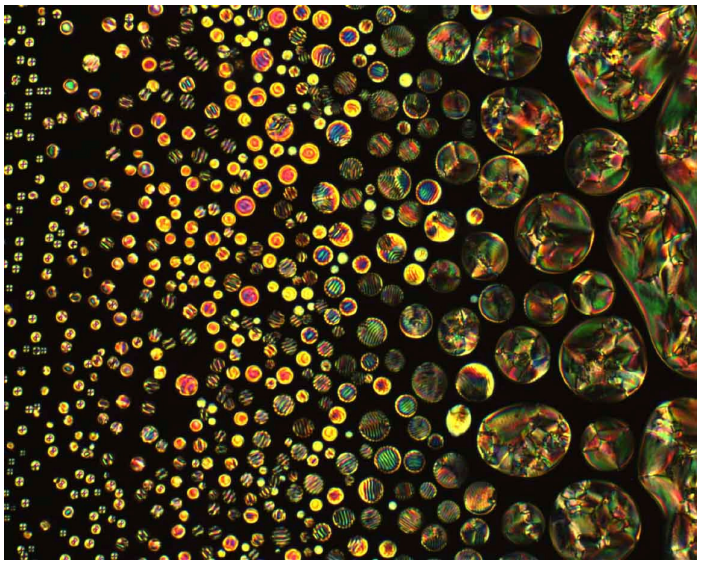

(a)

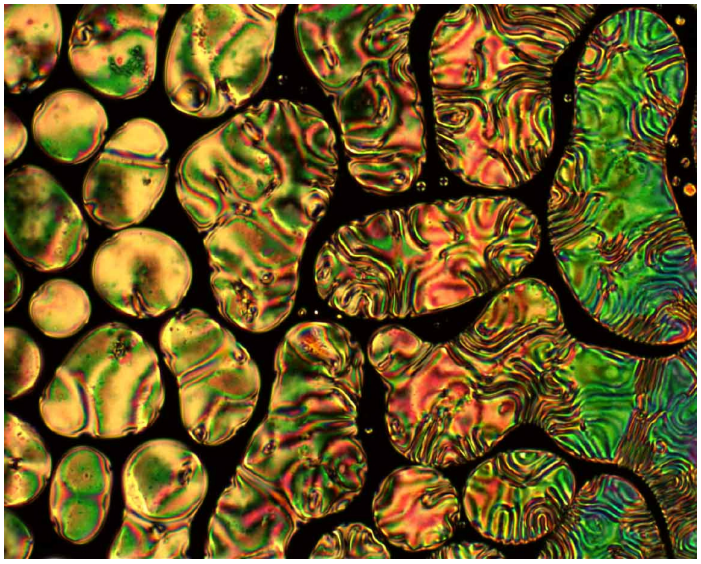

(b)

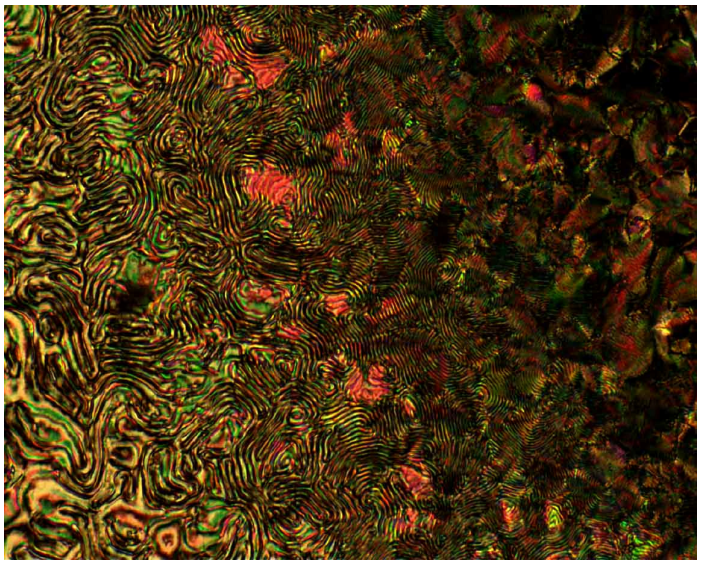

(c)

Figure 7.18: *Polarised optical micrographs showing (a) the nematic and induced chiral nematic phases forming as droplets at 60.0 ^{o}C; (b) the classic fingerprint texture of the chiral nematic phase forming in droplets at 58.4 ^{o}C; (c) the chiral gradient formed at 53.0 ^{o}C (compound* **8** *in* E7*, magnification x 100).*

Compounds **9** and **10** showed a similar behaviour to compound **7** and **8** and did not mix quickly into the nematic host E7 at room temperature. A rapid pitch change, however, was observed in the chiral nemetic fingerprint texture, indicating reasonable chirality transfer from the dopants to the host. As before, the pitch was found to decrease as the concentration of the dopant increased. Pseudo-focal conic textures are observed at the highest concentration, indicating a tight pitch. The pseudo-focal conic textures were more obvious in compounds **9** and **10**, than compounds **7** and **8**, indicating a tighter pitch, due to the additional methylene group. However, no blue phases were observed in the contact mixtures. Polarised optical micrographs of the contact studies for compounds **9** and **10** can been seen in Figures 7.19 and 7.20.

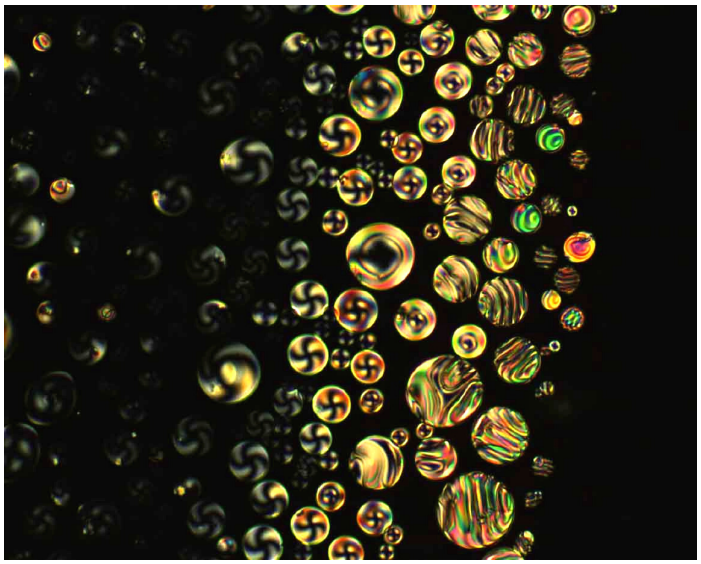

(a)

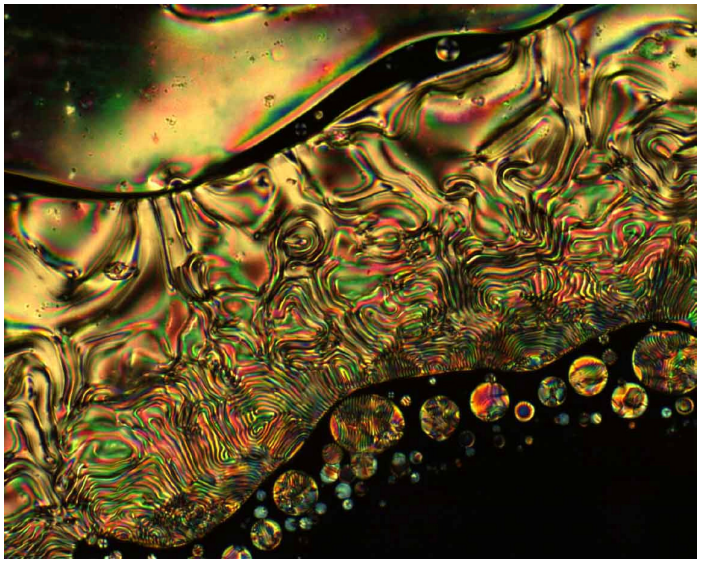

(b)

Figure 7.19: *Polarised optical micrographs showing (a) the nematic and induced chiral nematic phases forming as droplets at 59.1 ^{o}C; (b) the chiral gradient formed at 57.5 ^{o}C (compound* **9** *in* E7*, magnification x 100).*

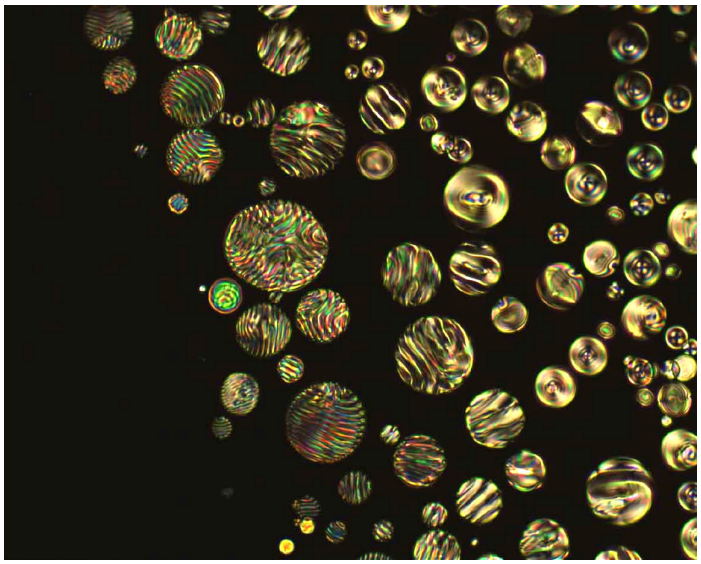

(a)

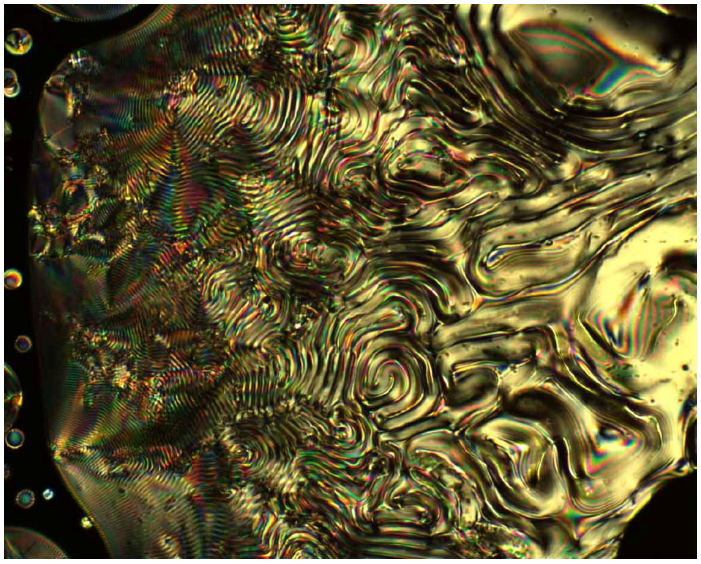

(b)

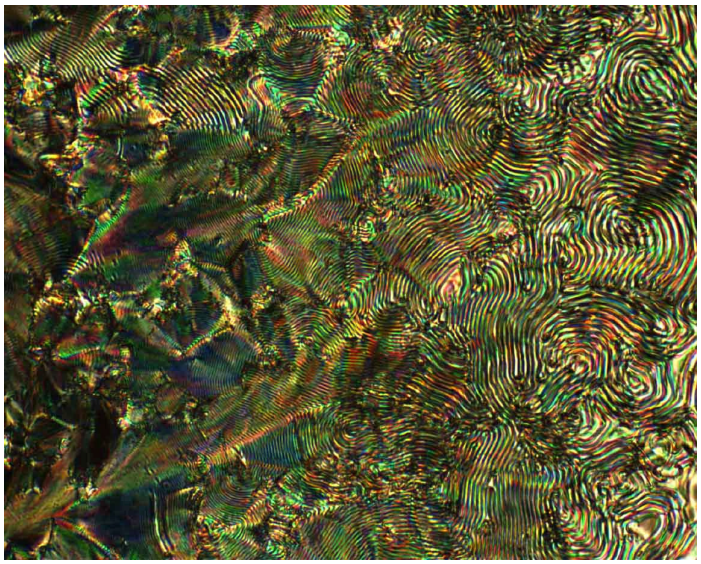

(c)

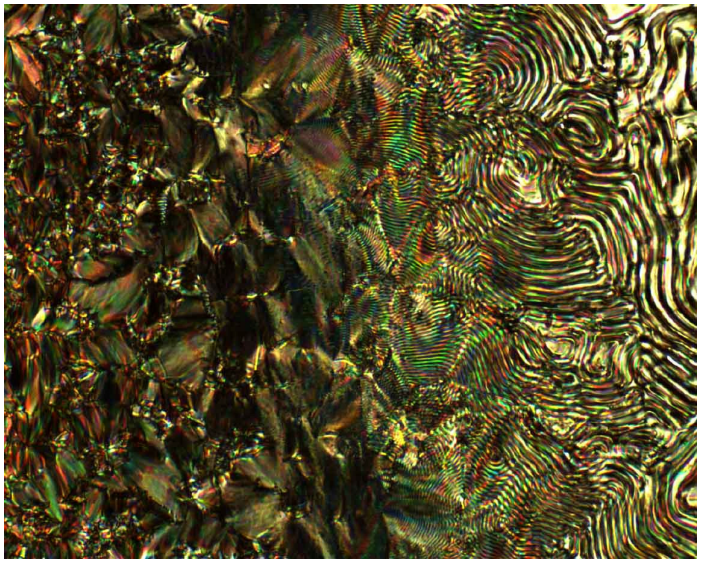

(d)

Figure 7.20: *Polarised optical micrographs showing (a) the nematic and induced chiral nematic phases forming as droplets at 59.5 ^{o}C; (b) the chiral gradient formed at 58.0 ^{o}C; (c) the chiral gradient formed at 55.5 ^{o}C; (d) the chiral gradient formed at 54.0 ^{o}C (compound* **10** *in* E7*, magnification x 100).*

The mixtures containing the dimers indicated that they are fairly strong dopants, but are not strong enough to produce blue phases. It is though that the chirality is isolated between the mesogens, restricting the chirality transfer between molecules.

7.2.1.2 H-Shaped Dimers

The initial attempts at producing a chiral gradient for compounds **32** to **35** with E7 were not successful due to the high viscosity of the dimers. Heating the mixtures to the isotropic liquid produced a chiral nematic fingerprint texture with a chiral gradient. The chiral nematic phase was observed in the mixtures at a much lower temperatures than the linear dimers due to the low clearing points of the H-shaped dimers. In all the mixtures, the gradient was not as pronounced as for the linear dimers. The mixtures showed distinct gradient boundaries at low temperatures between regions of high dopant concentration and low dopant concentration. This shows that dimers could not dissolve fully in E7. Even at higher temperatures, the effect of viscosity was evident. At 48.0 ^{o}C, compound **32** showed regions where the fingerprint texture existed in different directions. Due to the viscosity of the mixture, the molecules find it difficult to orientate in the same direction throughout the mixture. Figure 7.21 shows a selection of polarised optical micrographs from the contact work of the H-shaped dimers.

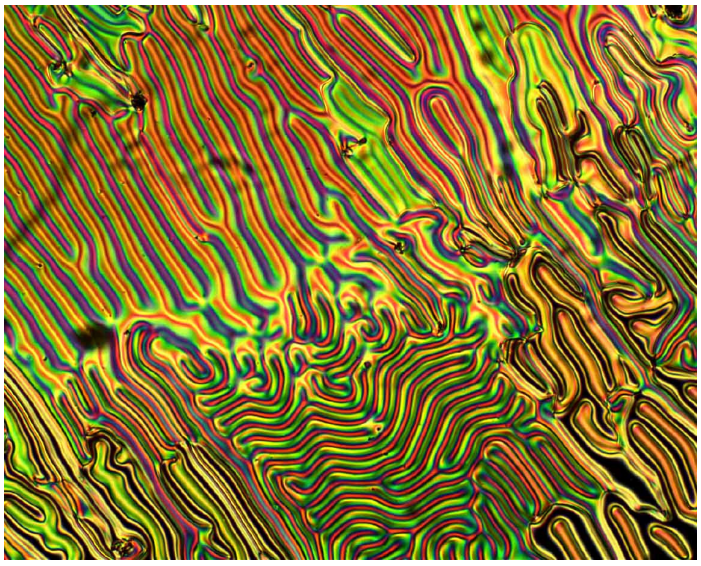

(a)

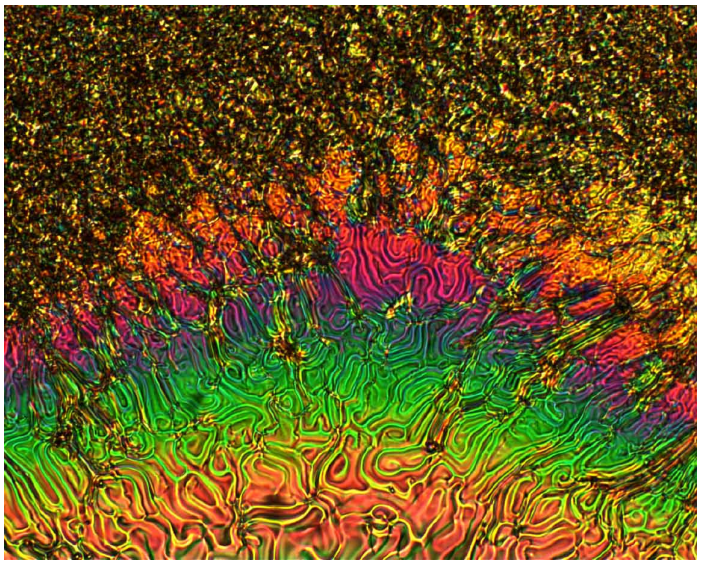

(b)

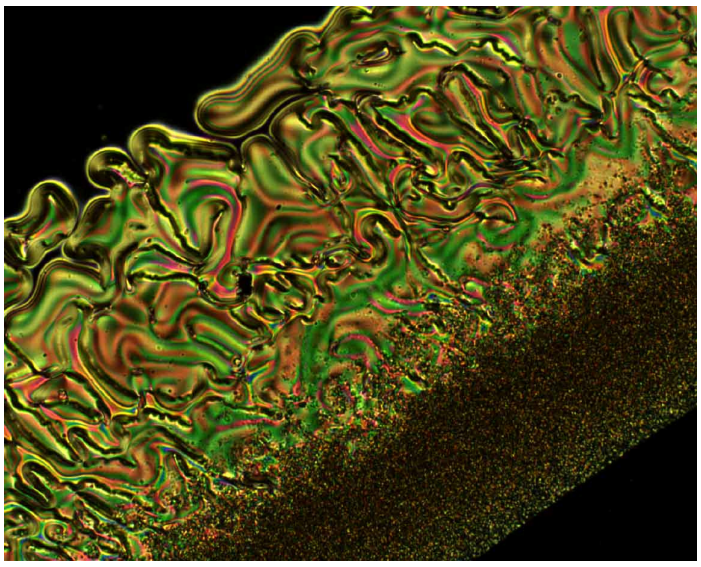

(c)

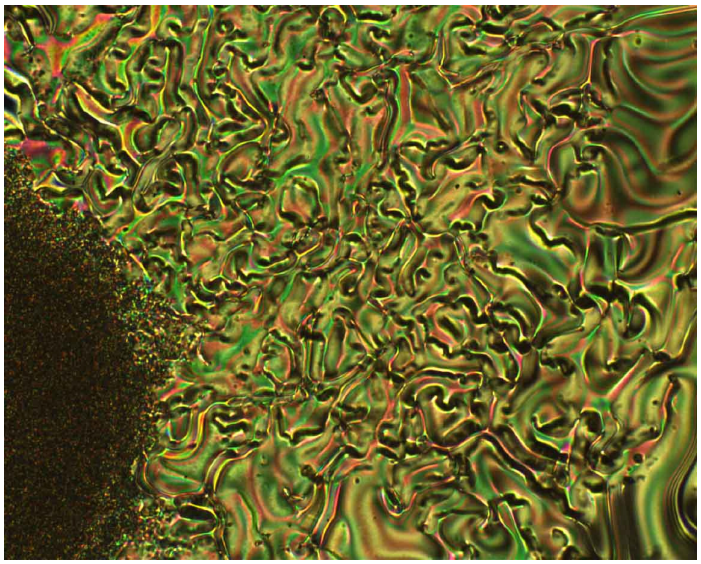

(d)

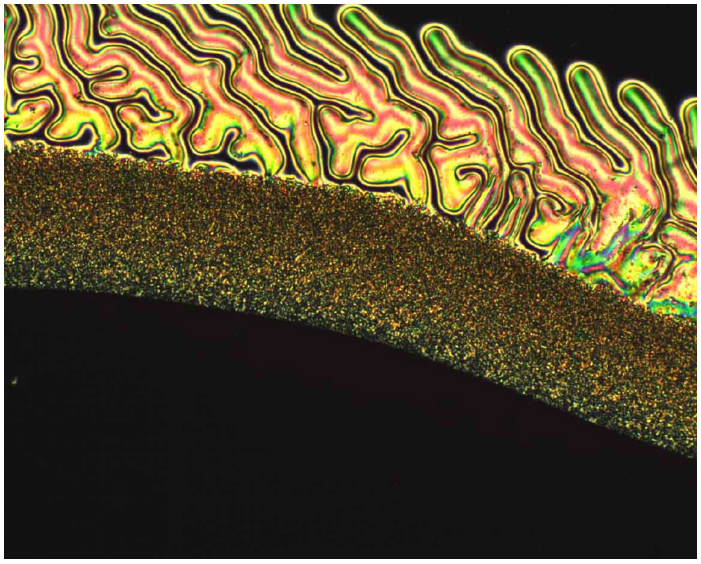

(e)

Figure 7.21: *Polarised optical micrograph showing (a) the chiral nematic phase of compound* **32** *at 48.0 ^{o}C; (b) the chiral gradient seen in compound* **32** *at 27.0 ^{o}C; (c) the chiral gradient seen in compound* **34** *at 27.7 ^{o}C; (d) the chiral gradient seen in compound* **34** *at 27.5 ^{o}C; (e) the chiral gradient seen in compound* **35** *at 27.7 ^{o}C (Magnification x 100).*

The contact preparations indicate that the H-shaped dimers are poorer dopants than the linear dimers. As with the linear dimers, no blue phases were found.

7.2.2 Pitch Measurements and Helical Twisting Power Studies

7.2.2.1 Linear Dimers

Each of the dimers was doped into E7 at concentrations of 0.25, 1.00 and 4.00 % w/w. The exact concentrations for each mixture were determined as this was crucial for the calculation of the induced pitch. The concentrations of the prepared mixtures are shown in Table 7.5.

Compound	Exact Concentration / % w/w
7	0.25
	0.99
	3.84
8	0.25
	0.99
	3.85
9	0.25
	0.99
	3.84
10	0.25
	1.00
	3.98

Table 7.5: *Table showing the exact mixture concentrations of the linear dimers in E7 for the pitch measurement studies.*

Each of the prepared mixtures was examined by polarised optical microscopy to ensure the mixtures were homogenous. The 0.25 % w/w mixtures exhibited long pitches and as a result conventional nematic textures were observed (see Figure 7.22).

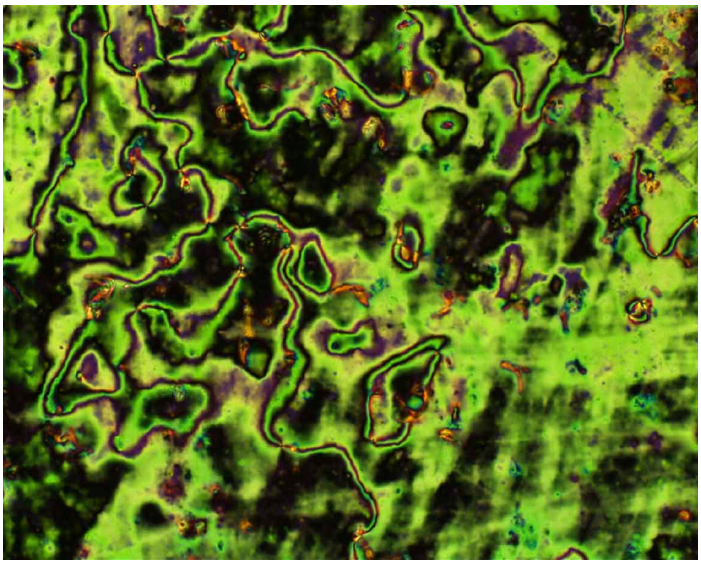

Figure 7.22: *Polarised optical micrograph showing the nematic texture of compound* **9** *at a concentration of 0.25 % w/w (Magnification x100, 57.6 °C).*

An increase in concentration shortened the pitch of the mixture and the chiral nematic fingerprint texture was observed for the 4 % w/w mixtures (see Figure 7.23)

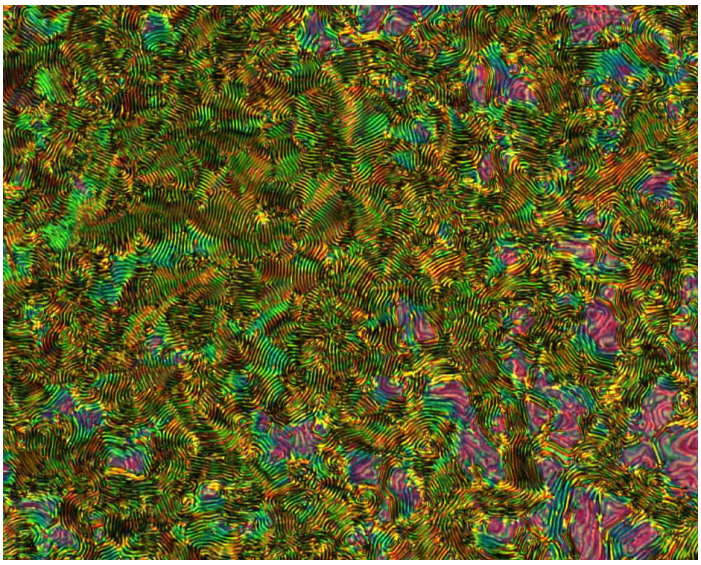

Figure 7.23: *Polarised optical micrograph showing the nematic texture of compound* **9** *at a concentration of 4.00 % w/w (Magnification x100, 55.0 °C).*

The mixtures were filled into Cano Wedge cells at room temperature and left to settle overnight. In some cases the disclination lines had not settled to become

straight or parallel. In these cases the cells were gently warmed until the disclination lines straightened. The wedge cells containing 0.25 % w/w, 1.00 % w/w and 4.00 % w/w of compound **7** are shown in Figure 7.24. All the mixtures are shown at a magnification of 100. Where possible a graticule was used to determine the distance between the disclination lines, but for larger distances it was determined using digital callipers. The distance between the disclination lines and the calculated pitch are shown in Table 7.6, including the errors, which takes into account the possible 5 % error of the wedge cells.

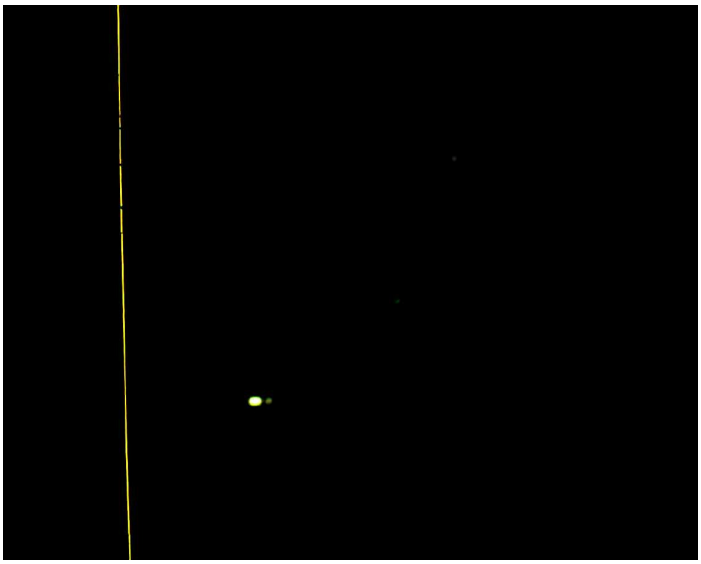

(a)

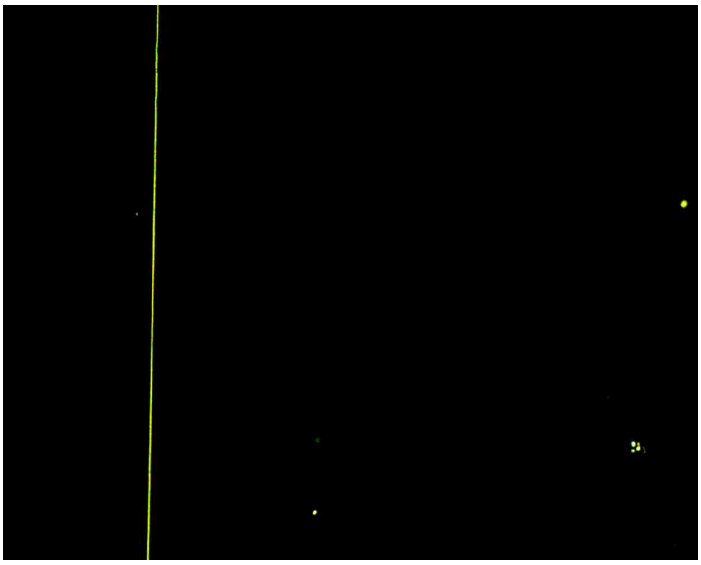

(b)

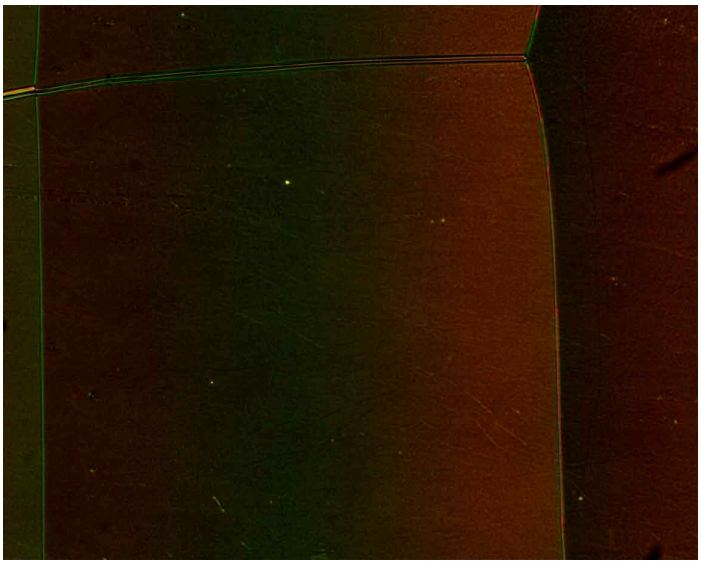

(c)

Figure 7.24: *Polarising optical micrographs showing the wedge cells of compound* **7** *at concentrations of (a) 0.25 % w/w; (b) 0.99 % w/w; (c) 3.84 % w/w (Magnification x 100).*

Compound	Mixture Concentration / % w/w	Line Width (*s*) / mm	Pitch / μm	Pitch Error / μm
7	0.25	6.75	124.20	± 6.21
	0.99	2.28	41.95	± 2.10
	3.84	0.58	10.70	± 0.54
8	0.25	7.76	142.78	± 7.14
	0.99	1.72	31.69	± 1.58
	3.85	0.98	8.00	± 0.90
9	0.25	6.30	115.92	± 5.80
	0.99	1.79	32.86	± 1.64
	3.84	0.58	10.68	± 0.53
10	0.25	7.00	128.80	± 6.44
	1.00	1.80	33.12	± 1.66
	3.98	0.42	7.78	± 0.39

Table 7.6: *Table showing the measured distance between the disclinations lines and the calculated pitch for each linear dimer.*

The calculated pitch was plotted against the reciprocal of the concentration. A linear fit of the data gave the gradient, which was used to determine the helical twisting power for each compound. The results for the mixtures of compounds **7** to **10** are shown in Figure 7.25. The calculated helical twisting powers are given in Table 7.7.

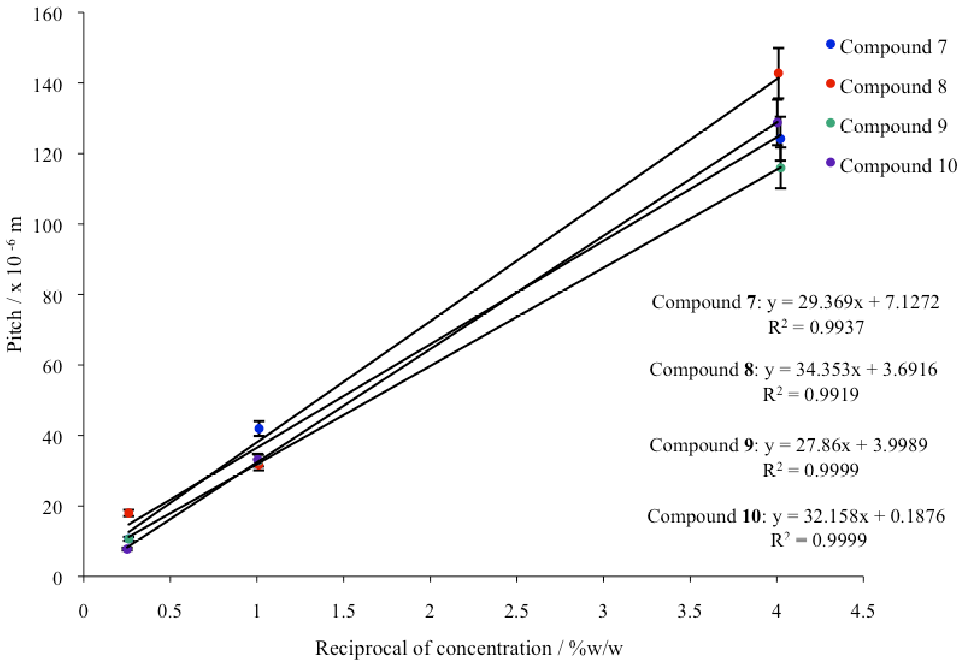

Figure 7.25: *A Graph to show how pitch varies with respect to concentration of chiral dopants in a non-chiral host,* E7 *(with associated error bars representing the 5 % error of the wedge cells).*

Compound	Helical Twisting Power / μm^{-1}	Error
7	3.4	± 0.2
8	2.9	± 0.2
9	3.6	± 0.2
10	3.1	± 0.2

Table 7.7: *Table showing the helical twisting powers for the linear chiral liquid crystal dimers* **7** – **10**.

The results show that increasing the spacer length increases the helical twisting powers of the dimers. The linearity of compounds **9** and **10** result in a slight increase in the frustration of the compounds. This was demonstrated previously in Figure 7.7 *via* three-dimensional modelling. This result differs from a known blue phase exhibiting dimer [4]. Investigations into binaphthyl liquid crystals of different spacer lengths (Figure 7.26) showed that the helical twisting powers of the odd-spacer length dimers are much smaller than the even length spacers, as recorded in Table 7.8. For these compounds blue phases were observed for the dimers with an odd number of methylene groups, whereas the even dimers only exhibited smectic A and chiral nematic phases. It was thought that blue phases appeared in the odd dimers due to the smaller twist elastic constant with respect to even dimers [4, 8].

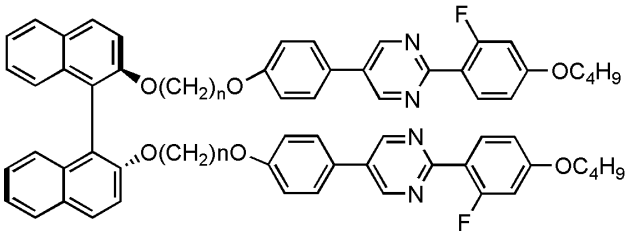

Figure 7.26: *Illustration showing the structure of the binaphthyl dimer* [4]

n	Transition Temperatures / °C							Pitch / μm
	SmA		N*		BP		Iso	
6	•	63	•	113			•	8.4
7	•	94			•	103	•	21.9
8	•	105	•	124			•	8.5
9	•	116			•	120	•	N/A
10	•	108	•	122			•	8.2
11	•	127			•	127	•	N/A
12	•	135	•				•	16.1

Table 7.8: *Table showing the phase transitions and pitch lengths for binaphthyl dimers with odd and even spacer length* [4].

Compounds **7** and **9** were found to have higher helical twisting powers than compounds **8** and **10**. However, this is not due to the relative optical purities of the dicarboxylic acids producing higher helical twisting powers, because compounds **8** and **10** had higher optical purities than compounds **7** and **9**. The observed difference may be due to the stereochemistry and shapes of the compounds which affect the lateral interactions between the molecules, and hence the pitch.

The low values of the helical twisting powers for compounds **7** to **10** explain why blue phase did not occur in the linear dimers. In order to observe a blue phase a high helical twisting power, generally of between 8 and 9 "m^{-1} is required [9]. This equates to a relatively small pitch. It is not unusual to observe the absence of a blue phase in liquid crystals that also exhibit a chiral nematic phase with a pitch of over 1 μm.

7.2.2.2 H-shaped Dimers

As with the linear dimers several mixtures of different concentrations were prepared Target concentrations of 0.50 % w/w, 1.00 % w/w and 4.00 % w/w were prepared, with the exact concentrations used shown in Table 7.9. Unfortunately, there was insufficient quantity of compound **33** to prepare the mixtures for Cano wedge cells. There was also insufficient quantity of compound **35** to prepare all three mixtures for the wedge cells, so only the 0.50 % w/w and 1.00 % w/w mixtures were prepared.

Compound	Exact Concentration / % w/w
32	0.50
	0.99
	3.99
34	0.50
	1.00
	3.95
35	0.50
	1.00

Table 7.9: *Table showing the exact mixture concentrations of the H-shaped dimers in E7 for the pitch measurement studies.*

The mixtures were filled into Cano wedge cells, but the high viscosity of the dopant meant that it was not possible to obtain straight disclination lines at room temperature over several days. The wedge cells were then gently heated and left to anneal at an elevated temperature overnight. Figure 7.27 shows examples of the disclination lines observed for compound **32**. The distance between the disclination lines was measured using digital calliper. The measurements and the calculated pitch are shown in Table 7.10.

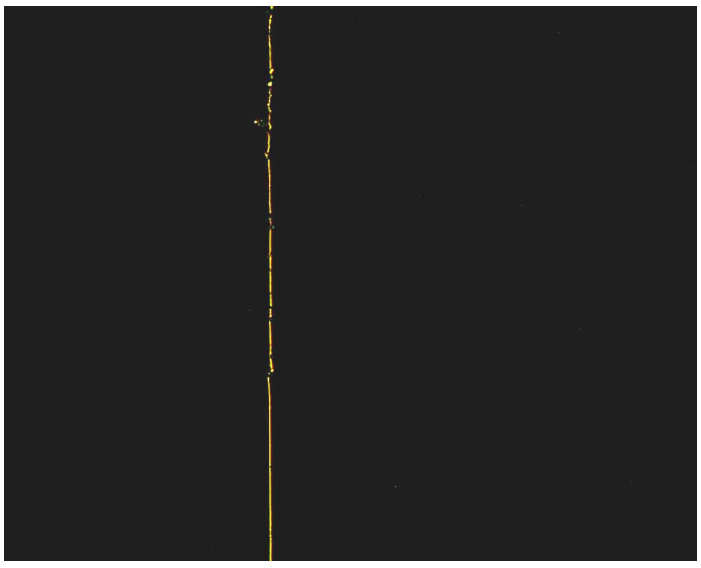

(a)

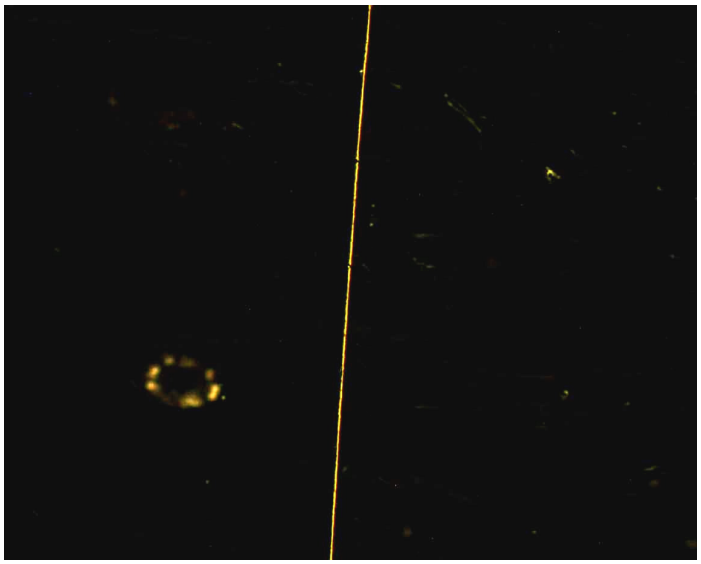

(b)

(c)

Figure7.27: *Polarising optical micrographs showing the Cano wedge cell of compound* **32** *at concentrations of (a) 0.50 % w/w; (b) 0.99 % w/w; (c) 3.99 % w/w (Magnification x 100).*

Compound	Mixture Concentration / % w/w	Line Width (*s*) / mm	Pitch / μm	Pitch Error / μm
32	0.50	15.23	280.23	± 14.01
	0.99	7.75	142.60	± 7.13
	3.99	2.68	49.31	± 2.47
34	0.50	12.99	239.02	± 11.95
	1.00	16.08	295.87	± 14.79
	3.95	4.28	78.75	± 3.94
35	0.50	N/A	N/A	N/A
	1.00	14.86	273.42	± 13.67

Table 7.10: *Table showing the distance between the disclination lines and the pitch measurements for compounds* **32**, **34** *and* **35**.

The pitch results determined for compounds proved to be erroneous. The 0.5 % w/w mixture for compound **35** did not provide any measurable results, even after heating the mixture gently. The 1.00 % w/w mixture for compound **34** showed a higher value for *s*, and so larger pitch, than for the 0.25 % w/w. This relationship should have been the reverse. Due to this, it was decided to leave the wedge cells to settle for a longer period of time. During this time, the disclination lines were found to drift over time. When the distances between the disclination lines were measured a second time days later they were found to be different from the first measurement. The value of *s* for 1.00% w/w, for example, change dramatically and decreased by 10.3 mm, becoming similar to the value of *s* for the 4.00 w/w mixture. It is believed that if wedge cells were measured for a third time, different results would be determined again. It is thought that constant conformational changes are occurring in the mixtures, altering the pitch or possible cluster formation depending on equilibration time, cooling rate and concentration. On this occasion, a value for 0.5 % w/w mixture for compound **35** was obtained. The second set of measurements and the calculated pitch are shown in Table 7.11.

Compound	Mixture Concentration / % w/w	Line Width (*s*) / mm	Pitch / μm	Pitch Error / μm
32	0.50	15.51	285.38	± 14.27
	0.99	6.93	127.51	± 6.38
	3.99	2.61	48.02	± 2.40
34	0.50	15.71	280.97	± 14.05
	1.00	5.78	106.35	± 5.32
	3.95	4.45	81.88	± 4.09
35	0.50	15.54	285.94	± 14.00
	1.00	14.99	275.82	± 13.79

Table 7.11: *Table showing the second set of measurements for the distance between the disclination lines and the pitch measurements for compounds* **32**, **34** *and* **35**.

The helical twisting powers of the dimers were calculated from the results obtained and are shown in Table 7.12. Compound **35** has been omitted from the table. As only two data points were present for analysis, it was hoped that a third value could be determined using the line of best fit from the graph of compound **34** as a guide. Due to the uncertainty of the measurements of compound **34**, this was not carried out.

Compound	Helical Twisting Power / μm^{-1} 1st measurement	Helical Twisting Power / μm^{-1} 2nd measurement
32	0.75	0.73
34	1.19	0.86

Table 7.12: *Table showing the calculated helical twisting powers for the first and second measurements of the wedge cells.*

The helical twisting powers of compounds **32** and **34** were found to be much lower than the helical twisting powers for the linear dimers. Modelling suggests that the chiral centres in the linear dimers are more exposed to neighbouring molecules than the chiral centre in the H-shaped dimers. In the H-shaped dimers

the chiral centre is almost concealed between the large flexible mesogens, and so it has very little effect in transferring the effects of chirality (Figure 7.28). It is also thought that the flexible alkyl spacers that had to be added during the synthesis in order to successfully produce the dimers may have had an affect. The alkyl spacers provided even more flexibility to the H-shaped dimers, so the effect of the chiral centre is less likely to participate in chirality transfer than if the alkyl spacers were not present. Higher helical twisting powers could be obtained if the mesogens were longer or if they possessed chiral groups.

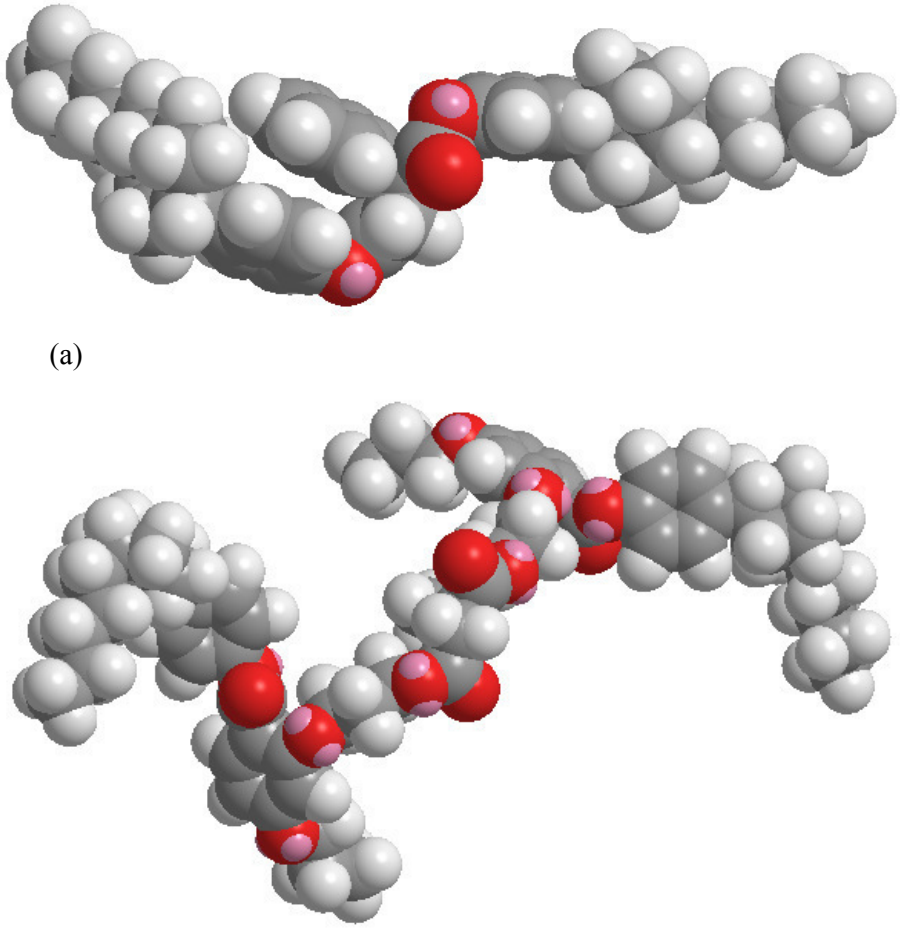

(a)

(b)

Figure 7.28: *Illustrations comparing the three-dimensional models of* (a) *compound* **7** *and* (b) *compound* **32.**

7.3 References

[1] P.J. Collings and M. Hird, *Introduction to Liquid Crystals,* Taylor and Francis Ltd, London, 1998, p 4, 10, 50, 61, 62, 71, 72, 76.

[2] G. W. Gray and J. W. Goodby, *Smectic Liquid Crystals – Textures and Structures*, Leonard Hill, Glasgow and London, 1984, p 136.

[3] J. W. Goodby, *J. Mater. Chem*., 1991, **1**, 307.

[4] J. Rokunohe and A. Yoshizawa, *J. Mater. Chem*., 2005, **15**, 275.

[5] H. Stegemeyer, Liquid Crystals, Springer, Germany, 1994, p 27.

[6] T. Donaldson, H. Staesche, Z.B. Lu, P.A. Henderson, M.F. Achard and C.T. Imrie, *Liq. Cryst.,* 2010, **37**, 8, 1097.

[7] M. Sato, A. Yoshizawa and F. Ogasawara, *Mol. Cryst. Liq. Cryst.*, 2007, **475**, 99.

[8] A. E. Blatch, I. D Fletcher and G. R. Luckhurst, *J. Mater. Chem.,* 1997, **7**, 9.

[9] E. P. Raynes, *Liq. Cryst*., 2007, **34**, 697.

8 CONCLUSION

8.1 Conclusion

Four linear dimers exhibiting a crystal B phase were synthesized and isolated in good yield. The fifth dimer, composed of a chiral phenyl moiety, was isolated in low yield and did not show a liquid crystal phase. This was due to the effect of the size and position of the phenyl moiety on molecular packing. The linear dimers synthesized from the chiral glutaric acids showed lower phase transition temperatures than the dimers synthesized for the chiral succinic acids. The additional methylene group in the glutaric acid dimers causes the compounds to become more flexible and less linear. The interactions between the molecules are not as strong as the interactions between the more linear and more rigid molecules of the succinic acid dimers. As a result, the molecules cannot pack as efficiently, thereby lowering the phase temperatures and ranges. None of the linear dimers exhibited blue phases. It is thought that having the chiral group in the centre of the dimers isolates the chiral group and prevents chirality transfer to neighbouring molecules. In an attempt to induce a blue phase, contact preparations were carried out. A strong chiral gradient was seen across the mixtures and the pitch of the dimers was found to decrease as the concentration of the dopant increased. The large pitch change observed indicates a reasonable chirality transfer from the dopant to host, but as chiral nematic and not blue phases were observed, the chirality transfer was not strong enough to induce the formation of blue phases. Subsequent pitch measurements and helical twisting studies determined that the linear dimers had helical twisting powers much lower than helical twisting powers in blue phase compounds and so it is not surprising that blue phases were not observed for these systems.

The synthesis of H-shaped dimers from compound **15** was found not to be possible. It is though this is due to intramolecular hydrogen bonding occurring in the monomer, and also in the dicarboxylic acids. Another theory is that the sterically hindered dicarboxylic acids could not attack the hydroxyl moiety, which was also located in a sterically hindered position. Due to this the target structures of the H-shaped dimers had to be modified. An alkyl chain was

attached to the hydroxyl group to give compound **31**. Although both mesogens exhibited a nematic phase, the addition of the alkyl chain lowered the transition temperate of the phase dramatically. The size of the lateral alkyl chain prevented side-side interactions between the molecules of compound **31**. Dimerisation of compound **31** with the dicarboxylic acids was successful, leading to the synthesis of four H-shaped dimers, which were isolated in low yields. The dimers all exhibited chiral nematic phases, but they occurred below room temperature. As with the linear dimers, the odd-even effect was noticed in the H-shaped dimers. As the dimers did not exhibit blue phases, believed to be due to the chirality isolation, contact preparations were carried out to discover if the dimers could be used as chiral dopants to induce blue phases. Due to the viscosity of the compounds, initial attempts at producing a concentration gradient across the mixture was not achieved. Heating the mixtures to the isotropic liquid and allowing them to anneal produced a chiral gradient, which was not as pronounced as the chiral gradient seen in the linear dimers. Subsequent pitch measurements and helical twisting power studies were carried out. Due to the viscosity of the dimers, linear disclination lines could not be achieved. Heating the mixtures led to the formation of some straight lines, which however moved over time and an accurate value of the line widths, *s,* could not be determined. Initial measurements of the line widths suggest that the helical twisting powers of the H-shaped dimers are much lower than the linear dimers. It is believed that even though the H-shaped dimers have the potential to be more frustrated than the linear dimers, the larger mesogenic units isolates the chiral groups considerably and the required chiral transfer to adjacent molecules to produce the frustration of the blue phase is not possible.

Despite not observing a blue phase or inducing a blue phase, previous research along with the results of this project show that using dimers to produce blue phase liquid crystals is still a promising area of research and should be continued, with a few adjustments.

8.2 Future work

After reviewing the results of this project, there are a number of areas that could be investigated further.

8.2.1 Addition of a Second Chiral Centre

As the dimers are not frustrated enough due to the isolation of chirality at the centre of the dimers, the synthesis of H-shaped dimers with chiral terminal chains is proposed. It is thought that having the chiral group in the terminal chains allowing chiral transfer between the molecules. Upon dimerisation of the chiral monomers with dicarboxylic acids, a dimer with three points of chirality will be formed.

A number of different chiral chains could be used, including 2-methylbutan-1-ol. This four-carbon chain has a methyl group attached to the stereogenic centre in the middle of the chain. Taking into account the synthetic hurdles encountered in the previous synthesis of the H-shaped dimers, the reaction scheme in Scheme 8.1 is proposed.

Only the (*S*)-enantiomer of 2-methylbutan-1-ol is available to purchase (TCI and Aldrich). To investigate the effect of stereochemistry on transition phases (*S*)-(+)-3-methylbutan-2-ol and (*R*)-(–)-3-methylbutan-2-ol could be used. Theses are both available to purchase (Alfa Aesar). However, the highly branched structure (Figure 8.1) could have a negative impact on the liquid crystallinity of the dimers, but this would be one point of interest to investigate. Chiral pentane chains could be used in the synthesis also, but if the chains used are too long, the liquid crystallinity of the compound might be suppressed [1].

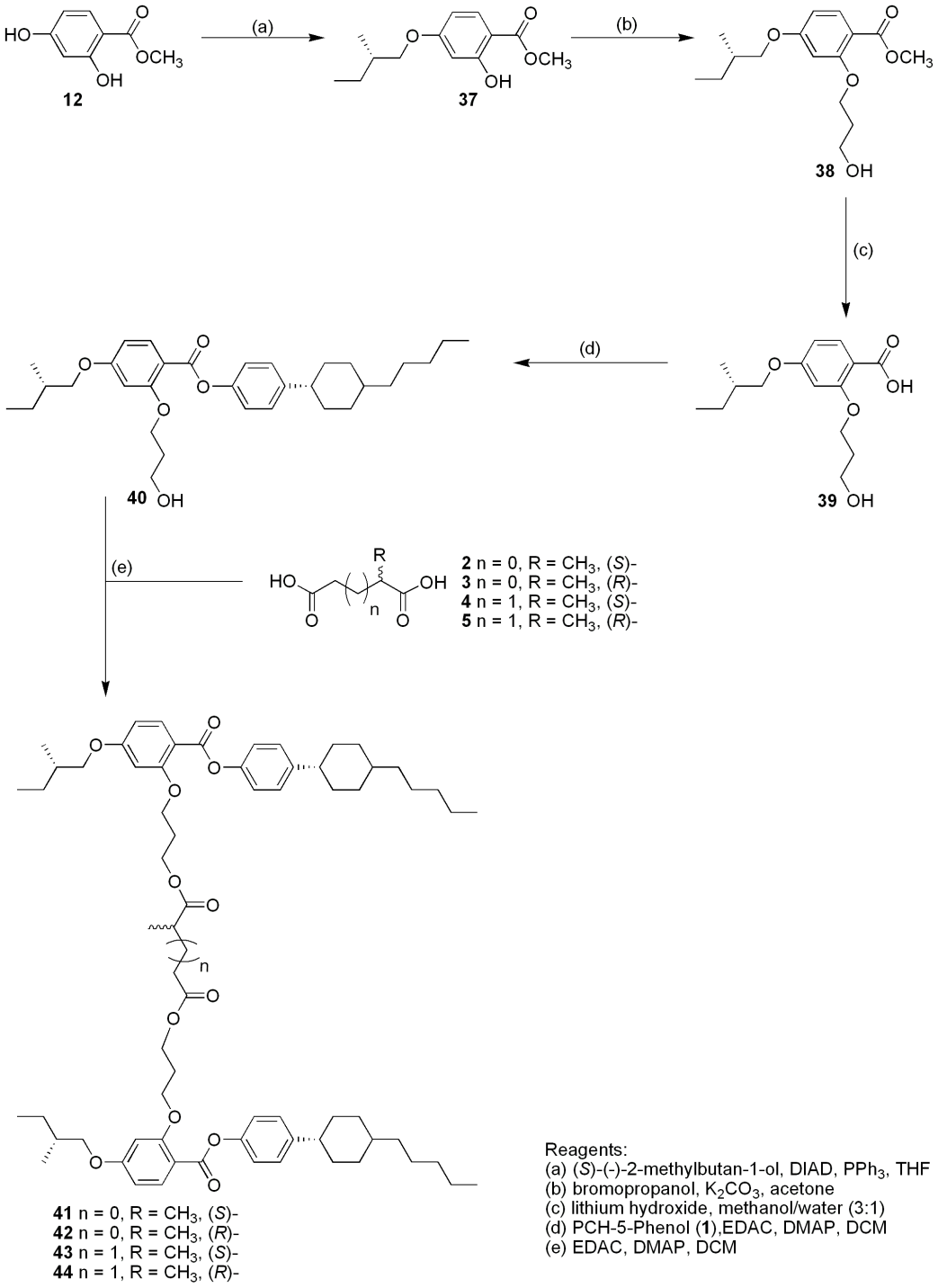

Scheme 8.1: *Reaction scheme 6 for the proposed synthesis of dimers* **41** – **44**.

Figure 8.1: *Illustration showing the structure of* (a) *(R)-(–)-3-methylbutan-2-ol;* (b) *(S)-(+)-3-methylbutan-2-ol;* (c) *the proposed dimer using 3-methylbutan-2-ol.*

8.2.2 The Effect of Using Different Length Terminal Chains and Chiral Spacers

In order to investigate the odd-even effect, dicarboxylic acids of different chain length could be used. The liquid crystal phases exhibited by the dimers would be affected by the increased flexibly of the chain and the deviation of the structure away from the preferred *trans*-conformation. Dicarboxylic acids of chains lengths from three carbons to nine carbons could be used.

Comparison of different length terminal chains would give an idea of how their flexibility affects liquid crystal phases. Terminal chain lengths of three carbons to seven carbons could be used to synthesize compounds, and the differences in phases and transition temperatures compared.

8.2.3 Addition of a Third Aromatic Ring

Despite the addition of a third aromatic ring to a monomer increasing the transition temperature of the nematic phase compared with a monomer with two aromatic rings [1], interesting phase results may be observed in dimers if the structure contained five or more aromatic rings. Work carried out outside this project has shown that compounds with this number of aromatic rings have exhibited blue phases [2, 3, 4]. It would be interesting to see if synthesizing H-shaped dimers with five or six aromatic rings would exhibit blue phases.

8.2.4 The Use of Miscible Host Liquid Crystals.

Due to the miscibility issues of E7 and the H-shaped dimers investigations into host liquid crystals could be examined. A number of different host liquid crystals, such as E9, could be mixed with the H-shaped dimers to find the host liquid crystal that best suits the dopant with respect to miscibility. It would also be interesting to discover if changing the host liquid crystal has an effect on the phases observed.

8.3 References

[1] P. J. Collings and M. Hird, *Introduction to Liquid Crystals*, Eds.: G. W Gray, J. W. Goodby and A. Fukuda, Taylor and Francis, London and New York, 1997, p 55, 61.

[2] A. Yoshzawa, Y. Kogawa, K. Kobayashi, Y. Takanishi and J. Yamamoto, *J. Mater. Chem.*, 2009, **19**, 5759.

[3] J. Rokunohe and A. Yoshizawa, *J. Mater. Chem*., 2005, **15**, 275.

[4] M. Sato, A. Yoshizawa and F. Ogasawara, *Mol. Cryst. and Liq. Cryst.*, 2007, 475, 99.

9 APPENDICES

9.1 ^{1}H NMR Spectra of Compounds 32 to 35

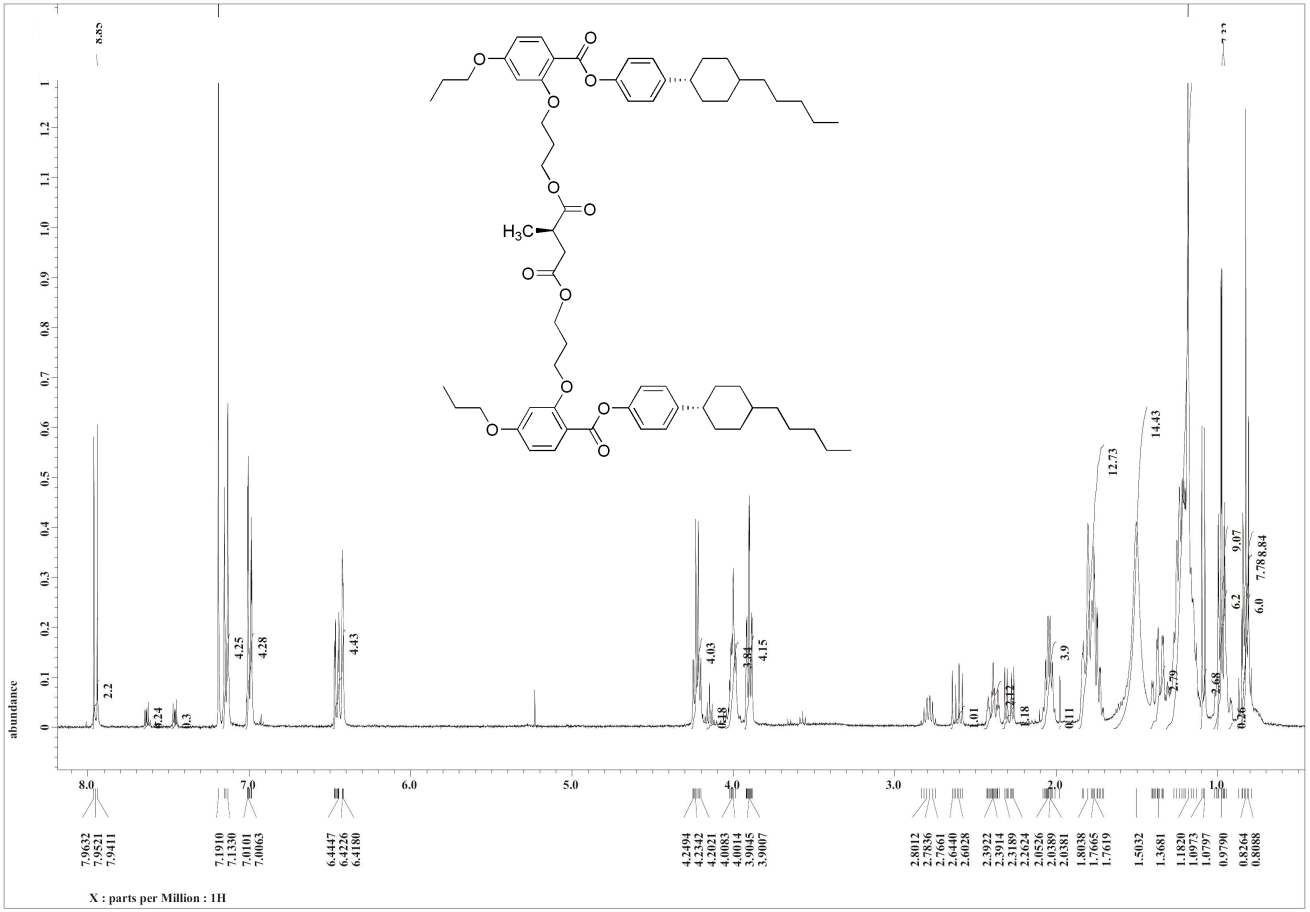

Figure 9.1: *^{1}H NMR spectrum of compound* **32** *(400 MHz, $CDCl_3$).*

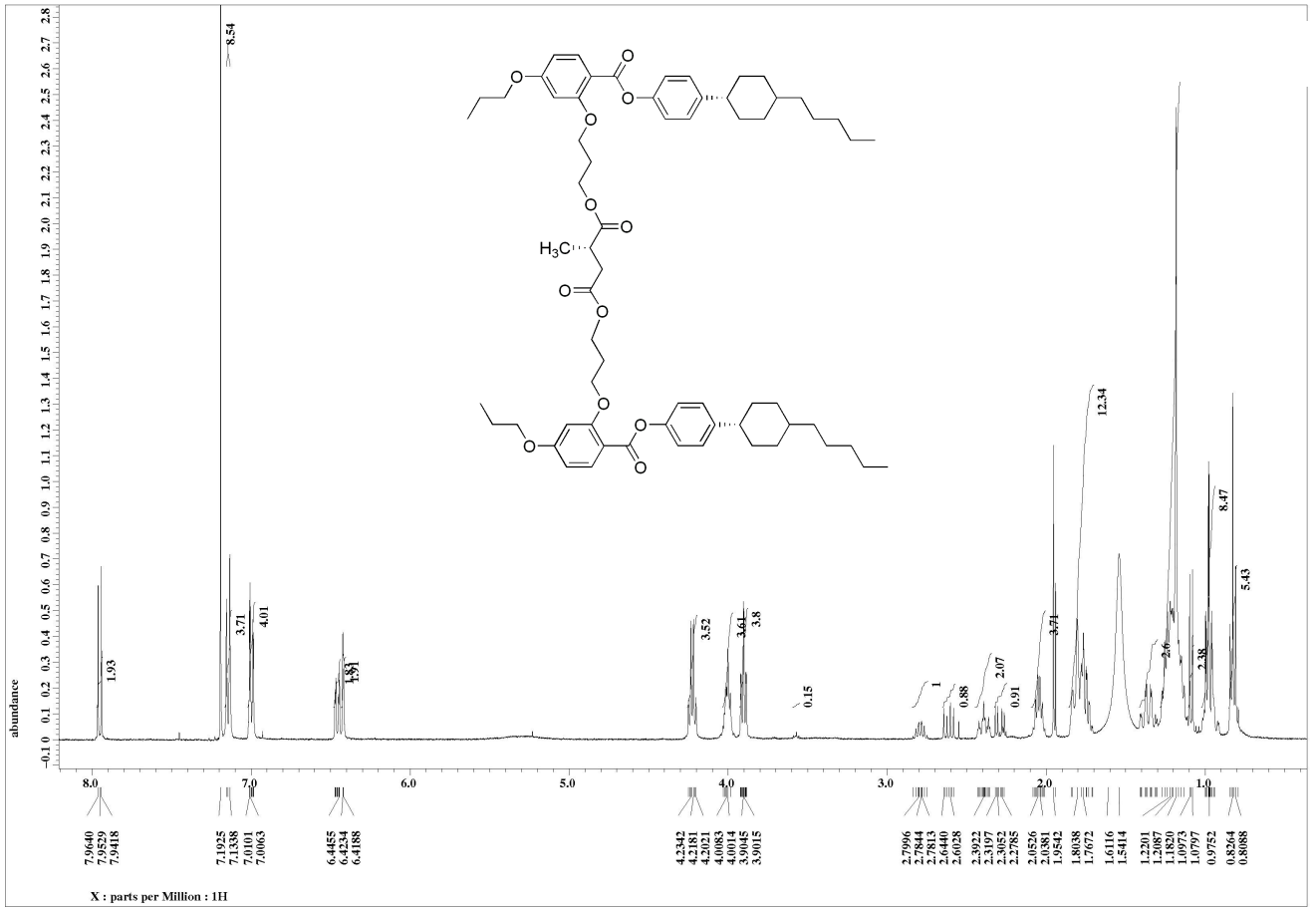

Figure 9.2: *^{1}H NMR spectrum of compound* **33** *(400 MHz, $CDCl_3$).*

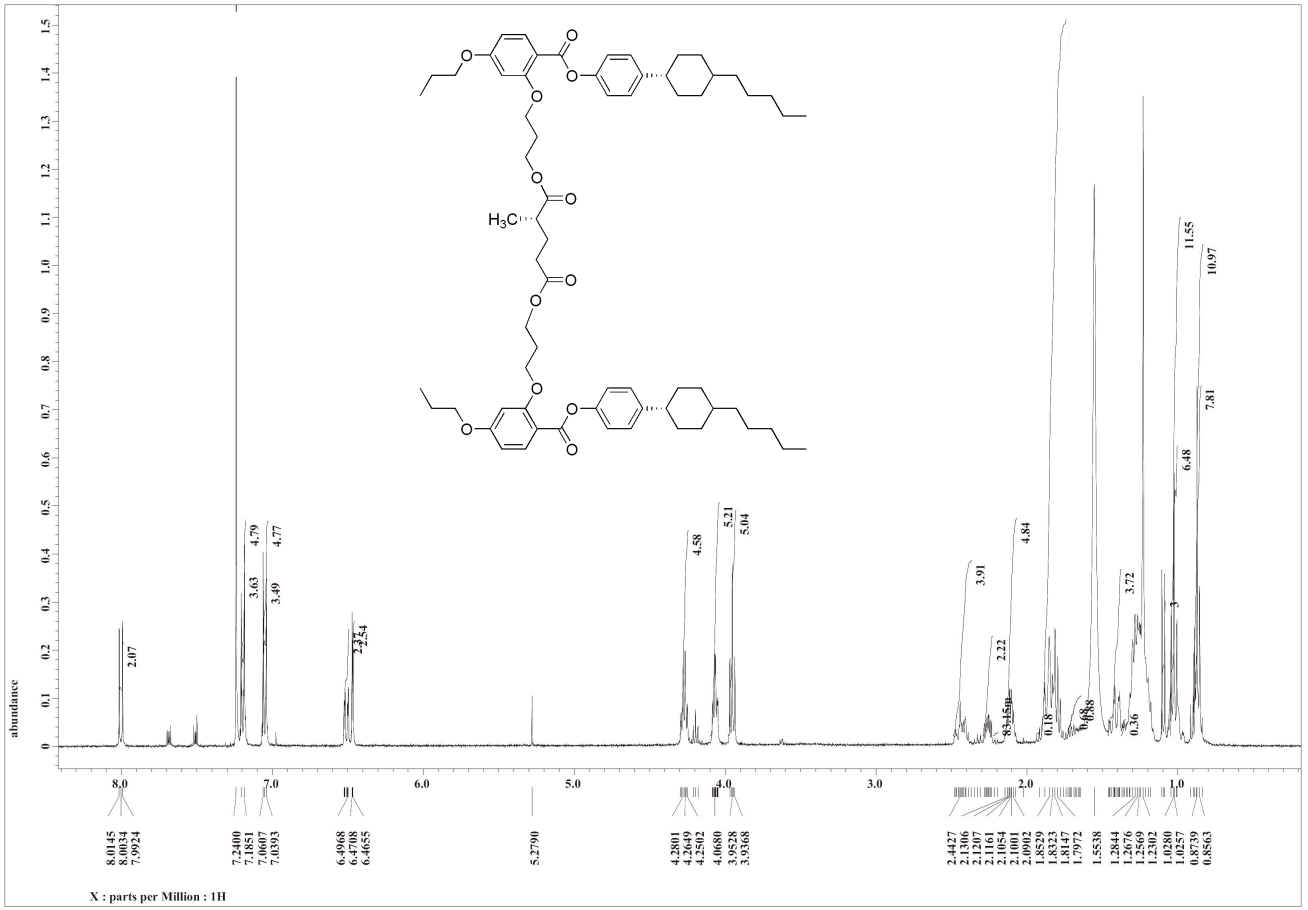

Figure 9.3: *^{1}H NMR spectrum of compound* **34** *(400 MHz, $CDCl_3$).*

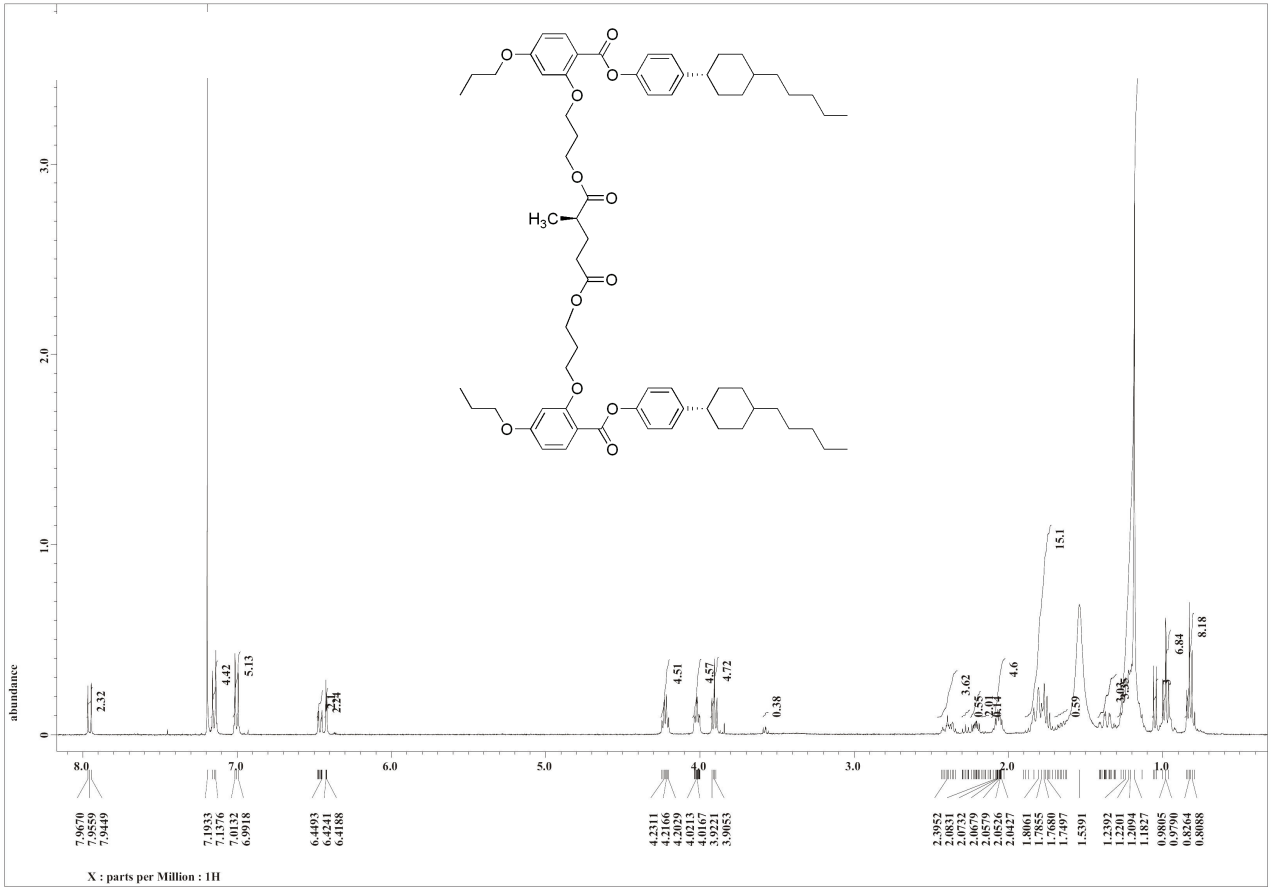

Figure 9.4: *^{1}H NMR spectrum of compound* **35** *(400 MHz, $CDCl_3$).*

9.2 Polarised Optical Micrographs of Compounds 7 to 10

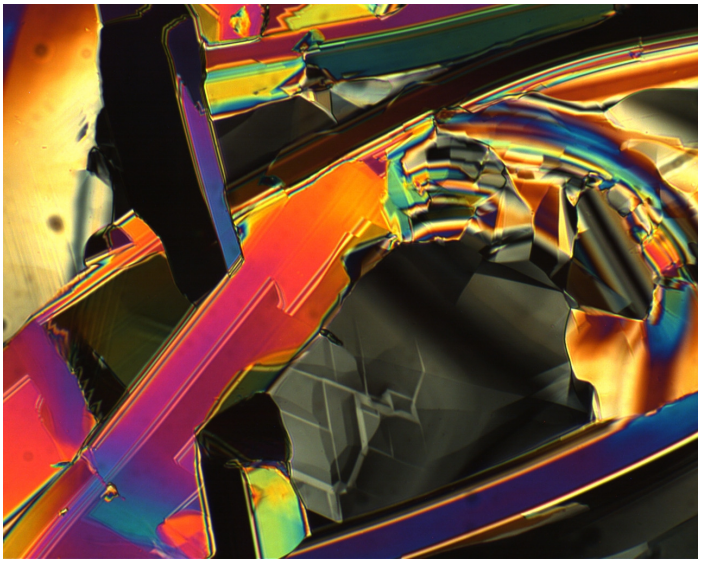

Figure 9.5: *Polarised optical micrograph showing the crystal B phase of compound* **7** *at 104 °C (Magnification x 100).*

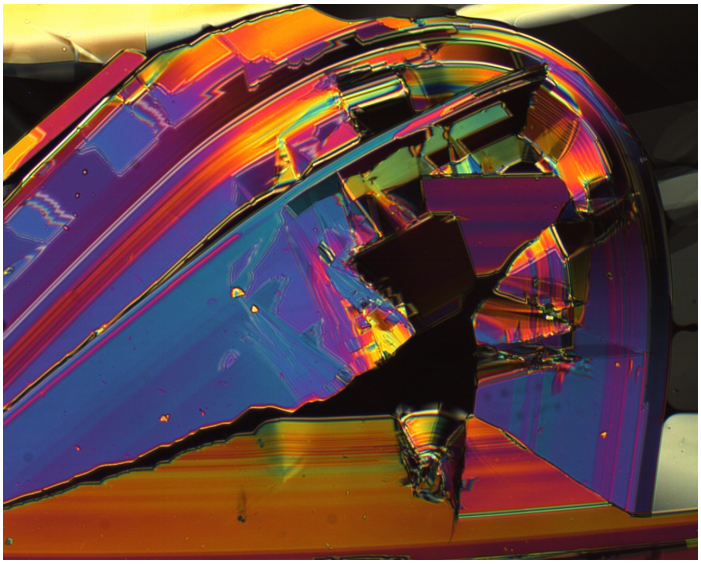

Figure 9.6: *Polarised optical micrograph showing the crystal B phase of compound* **8** *at 135 °C (Magnification x 100).*

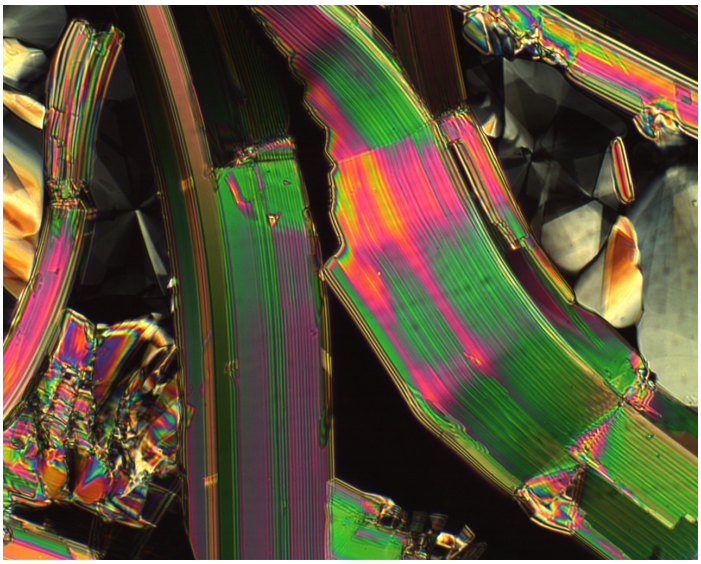

Figure 9.7: *Polarised optical micrograph showing the crystal B phase of compound* **8** *at 138 °C (Magnification x 100).*

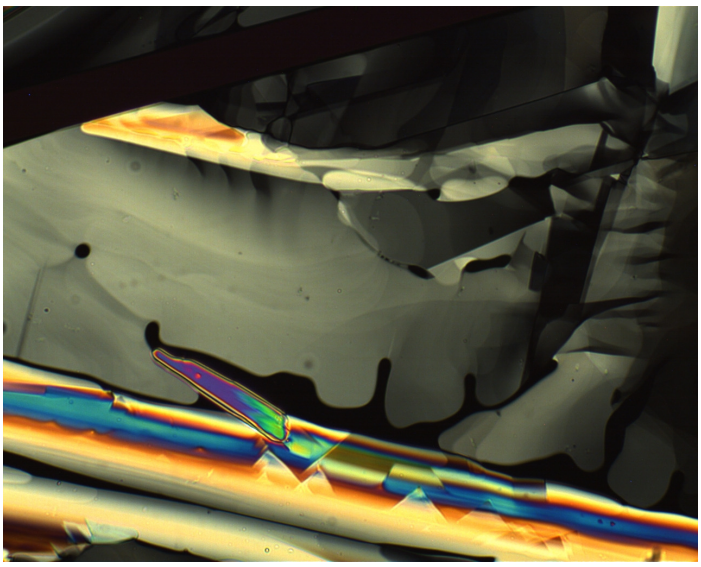

Figure 9.8: *Polarised optical micrograph showing the mosaic texture of the crystal B phase of compound* **8** *at 138 °C (Magnification x 100).*

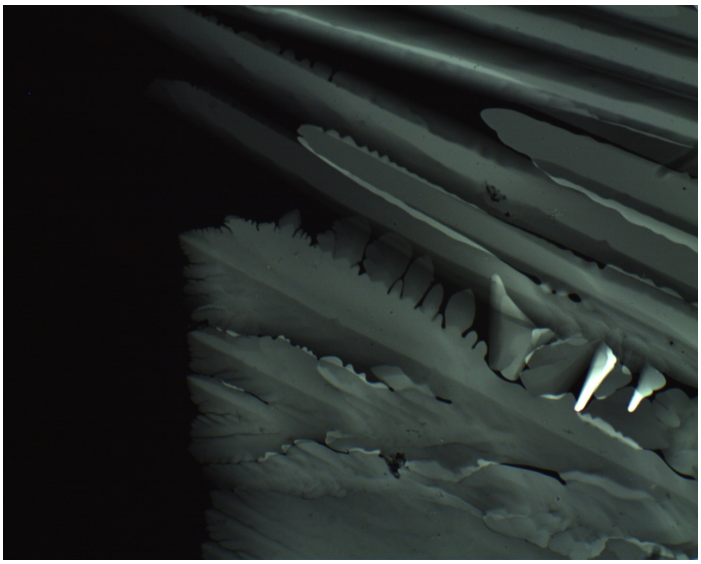

Figure 9.9: *Polarised optical micrograph showing the Iso – B phase transition of compound* **9** *at 104 °C (Magnification x 100).*

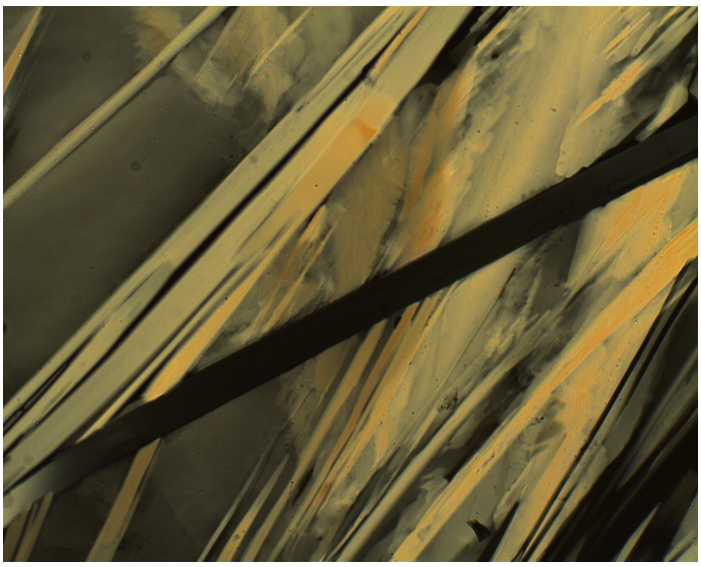

Figure 9.10: *Polarised optical micrograph showing the first crystal phase of compound* **9** *(Magnification x 100).*

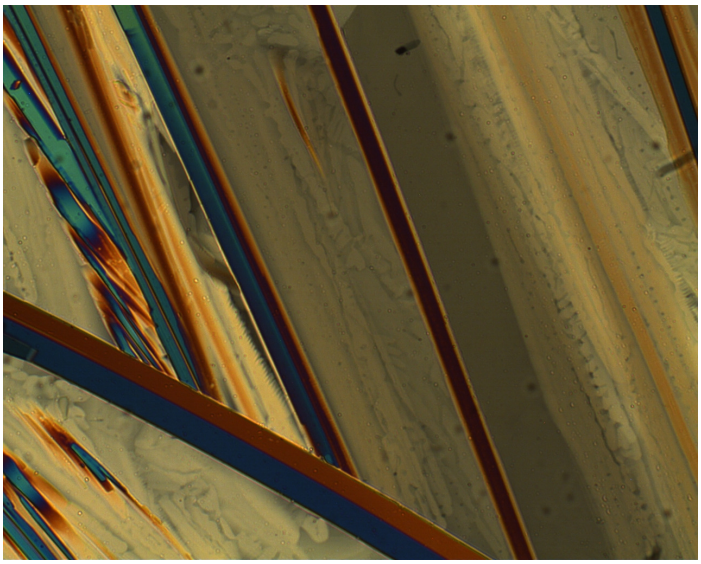

Figure 9.11: *Polarised optical micrograph showing the crystal B phase of compound* **10** *at 55 °C (Magnification x 100).*

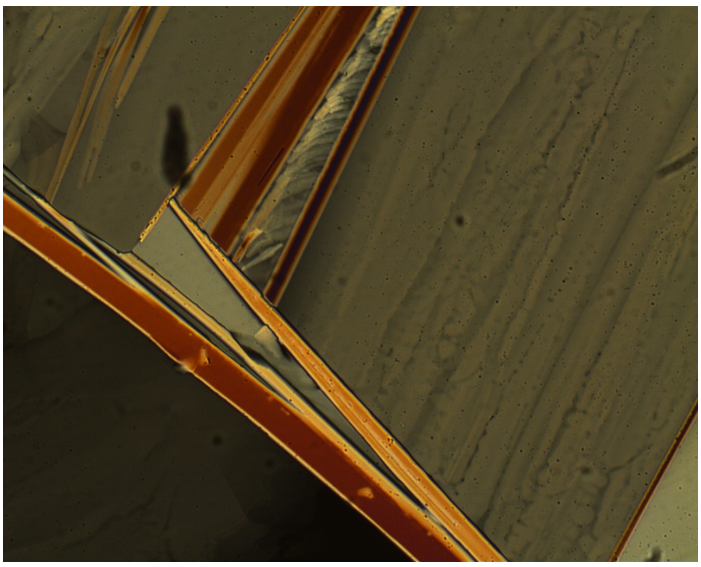

Figure 9.12: *Polarised optical micrograph showing the crystal B phase of compound* **10** *at 68 °C (Magnification x 100).*